All-optical control of fiber solitons

DISSERTATION

zur Erlangung des akademischen Grades

Dr. rer. nat.
im Fach Physik

eingereicht an der
Mathematisch-Naturwissenschaftlichen Fakultät
der Humboldt-Universität zu Berlin

von
Sabrina Pickartz

Präsidentin der Humboldt-Universität zu Berlin
Prof. Dr.-Ing. Dr. Sabine Kunst

Dekan der Mathematisch-Naturwissenschaftlichen Fakultät
Prof. Dr. Elmar Kulke

Gutachter: 1. Prof. Dr. Thomas Elsässer
2. Prof. Dr. Ulf Leonhardt
3. PD Dr. Uwe Bandelow

Tag der mündlichen Prüfung: 18.5.2018

Abstract

This work discusses the problem how to control an optical soliton propagating along a nonlinear fiber, which has been addressed by a great bulk of recent publications. The approach chosen here is to change soliton delay, duration and intensity in a simple, predictable manner by applying low-intensity velocity-matched dispersive light waves.

A new analytic theory of cross-phase modulation interactions of solitons with dispersive control waves is presented which combines quantum mechanical scattering theory, soliton perturbation theory and a multi-scale approach. This led to the following results, which could not be obtained by previous approaches, and not at all by mere numerical simulation: (1) The evolution of all soliton parameters is correctly predicted. In particular the possible amplitude enhancement of solitons is successfully quantified. The standard formulation of the soliton perturbation theory is not suitable for the given situation as it cannot predict soliton amplification. Therefore a modified soliton perturbation theory is proposed, which is of interest for many applications beyond cross-phase modulation interactions of optical pulses. (2) General ranges for control parameters are quantitatively determined, which ensure an effective interaction. (3) The derived theory allows a better understanding of numerical results. One example is the appearance of a caustic structure that was predicted using the analytical theory and only thereafter recognized in numerous previously reported numerical solutions. (4) The Raman effect is incorporated into the theory. The classical estimation of the Raman self-frequency shift is refined and expanded by a new relation for the amplitude loss arising with the Raman self-frequency shift. Furthermore, control pulses are identified which cancel soliton degradation due to Raman effect. In contrast to previously reported attempts with the interaction scheme under consideration, even parameter ranges are found which lead to a stable cancellation of the Raman effect. (5) New qualitative insights into the underlying process emerged. The prominent role of the self-steepening effect could be isolated. Though the pulse interaction is mediated by cross-phase modulation, the self-steepening effect causes an essential enhancement leading to much stronger changes in soliton parameters.

Only minimal assumptions are made, the use of specially prepared (e.g., dispersion managed) fibers is avoided. The only essential pre-requirement is the existence of at least one zero-dispersion wavelength in the fiber transparency window. The theory is widely applicable, not only to optical pulses. The theory was tested by ample direct numerical simulations. The presented work relies on several published papers and some new material which has not been published.

Zusammenfassung

Das Thema dieser Arbeit ist eine mögliche Steuerung eines optischen Solitons in nichtlinearen optischen Fasern. Es gelang, die interessierenden Solitonparameter wie Intensität, Dauer und Zeitverschiebung durch die Wechselwirkung mit einer dispersiven Welle geringer Intensität kontrollierbar zu modifizieren.

Es wird eine neue analytische Theorie vorgestellt für die Wechselwirkung zwischen Solitonen und dispersiven Wellen, die auf der Kreuzphasenmodulation in nichtlinearen Fasern beruht. Das vorgestellte Modell kombiniert quantenmechnische Streutheorie und Störungstheorie für Solitonen aus der nichtlinearen Optik. Damit wurden folgende Ergebnisse erzielt, die weder durch frühere Ansätze noch durch direkte numerische Simulation gewonnen wurden: (1) Die Entwicklung aller Solitonparameter wird korrekt vorhergesagt. Insbesondere wird die mögliche Verstärkung der Solitonamplitude erfolgreich bestimmt. Die Standardformulierung der Störungstheorie für Solitonen ist nicht in der Lage, die Solitonenverstärkung zu beschreiben. Die vorgestellte Erweiterung der Standard-Störungstheorie überwindet diese Schwierigkeit. Außerdem ist sie geeignet für Anwendungen, die über die Wechselwirkung von Pulsen durch Kreuzphasenmodulation hinausgehen. (2) Passende Intervalle der Kontrollparameter, die eine effektive Solitonmanipulation garantieren, können quantitativ bestimmt werden. (3) Die Modellgleichungen ermöglichen ein besseres Verständnis der numerischen Ergebnisse. Ein Beispiel ist das Auftreten von Kaustiken, welche hier analytisch vorhergesagt und erst im Anschluss in den vorhandenen numerischen Simulationsergebnissen wiedererkannt wurden. (4) Der Raman-Effekt wurde in die Modellbeschreibung eingebunden. Die klassische Abschätzung der Eigenfrequenzverschiebung des Solitons durch den Raman-Effekt wurde verbessert und erweitert durch eine neue Relation für den einhergehenden Amplitudenverlust. Weiterhin wurden solche Kontrollpulse bestimmt, die dieser Schwächung des Solitons entgegenwirken. Im Unterschied zu früheren Versuchen liefert die hier entwickelte Modellbeschreibung die passenden Parameterbereiche für eine stabile Auslöschung des Raman-Effektes. (5) Obwohl die Wechselwirkung selbst auf der Kreuzphasenmodulation basiert, spielt der „self-steepening“-Effekt, der die Bildung von optischen Schocks beschreibt, eine entscheidende Rolle für eine effiziente Veränderung der Solitonparameter.

Das Wechselwirkungsregime verlangt nur minimale Voraussetzungen, die einzige Bedingung an die Faser ist die Existenz wenigstens einer Wellenlänge mit Null-Dispersion im Transparenzfenster der optischen Faser. Die Theorie lässt sich auf weitere Systeme außerhalb der nichtlinearen Optik anwenden. Die Theorie wurde ausführlich durch numerische Simulation getestet. Die vorliegende Arbeit basiert auf mehreren Veröffentlichungen und einigem noch unveröffentlichten Material.

Contents

1 Introduction

Transmission of huge data volumes via optical fibers is meanwhile common, examples are the internet or wide area networks. The demands of this technology stimulated a great bulk of research in the field of fiber optics for several decades. In optical fibers information is encoded in a series of light pulses. To achieve high bitrates and yet faultless data transmission over long distances, stable ultra short pulses are desirable. In nonlinear fibers there exists a kind of pulse suggesting itself for this purpose: solitons, first observed in an optical fiber in 1980 [60], occur due to a fine balance between fiber nonlinearity and dispersion. They are localized and extremely stable in shape, thus ideal carriers of modern optical transmission technology [44]. Solitons lend themselves to a variety of applications. Examples are the generation of ultra-short pulses and pulse compression [7, 8], soliton switches [71], and soliton lasers [59].

Long-range transmission utilizes optical technology. Yet, signaling, switching and processing of information is mostly done by electronic devices. The conversion between optical and electrical signal costs energy and time, so the electronic components act as an "electrical bottleneck". The involved electronic devices are an obstacle to fully exhaust optical capabilities, i.e. to allow arbitrary signal formats and transmission protocols, and extremely high bitrates. Surely, since the dawn of optical data transmission also the development of electronic devices has been fast-paced. Still, it is an intriguing idea to replace electrical components by optical equivalents and thereby render a conversion between optical and electrical signals unnecessary. An early example is the introduction of an all-optical scheme for pulse regeneration in 1983 [42], which resulted in an all-optical transmission line. Though solitons are very robust even for extreme short pulse durations and high intensities, in a real fiber they are subject to fiber attenuation, dispersion leading to pulse broadening, and nonlinear distortion, all of which impair the quality of the signal. In soliton transmission systems only optical amplifiers are required to reshape a signal. They exploit the nonlinear optical effects of Raman gain. This was experimentally demonstrated in 1988 [58]. Many approaches to all-optical devices are investigated, e.g., all-optical switching [18] or optical signal-processing [87], and attempts towards "on chip" optical signal-processing are made [61].

It is widely argued that electrons might be replaced by photons and electronics by photonics on the next level of technology, e.g., in a futuristic optical computer. But unfortunately, each practical step in this direction happens to be extremely difficult. Traditional optoelectronic devices employ fundamental interactions of fields and particles, for instance one can effectively manipulate electrons and holes in semiconductor devices by applying an electric field. Storage and manipulation of photons is a different story. For one reason, photons do not interact with each other, only indirect coupling through an external nonlinear material is possible. Moreover, such indirect interactions are very weak. For instance, a nonlinear

contribution to the material refractive index, as created by the most extreme but still non-destructive optical pulse in a fiber, is 10^{-3} at most. As a result, two pulses at different frequencies, such as two optical solitons in a nonlinear fiber, just penetrate through each other without any changes. One has to apply either very long pulses or pulses with nearly identical frequencies and velocities. The latter can co-propagate long enough to be aware of each other, still their interaction requires a propagation distance of such length, that it hardly may serve for a future optical computer.

Despite of these difficulties, manipulation of photons by photons is a rapidly evolving and promising field. One recent achievement (2011) was the invention of an unusual regime of pulse interactions [23]. Using the so-called "optical event horizons" – the concept comes from an analogy between optical equations and the equations of general relativity – one can effectively modify an intense signal pulse by applying a much weaker control pulse, which is similar to the classical transistor scheme [54]. Apart from remote applications to future technologies, the proposed scheme immediately applies to pulse compression, generation of optical super-continua, and cancelling of the Raman self-frequency shift. The signal pulse, i.e. a soliton, can be strongly compressed or broadened. Therefore the interaction was proposed as a basic mechanism for all-optical switching [23]. During the compression process the soliton can reach a multiple of its initial peak power. This has possible applications to pulse compression up to a single-cycle regime, and it has been discussed in the context of extreme events like optical rogue waves [20]. Due to the similarity of the envelope pulse propagation equations in different systems, the concept of optical event horizons has also non-optical applications, e.g., in the theory of rogue water waves [24]. The induced soliton frequency shift combined with a prolonged interaction time with the control pulse opens a new way to super-continuum generation [22, 21]. All these results were derived by trial and error from numerical simulations of pulse propagation equations. Very recently (2015) the concept was realized experimentally [80].

This work proposes a theoretical framework for the description of interactions at the optical event horizons. The derived model equations combine methods from nonlinear optics and quantum mechanics. The proposed model helps to a better understanding of the interaction dynamic, it provides suitable parameter ranges for numerics and experiment, and yields quantitative predictions for, e.g., pulse compression rate and limits.

Structure of the thesis

In Chapter 2 the pulse interaction of interest is described phenomenologically, and a summary of already known numerical and experimental results is given. Based on previous studies empirical rules are formulated which favor an effective soliton manipulation.

The derivation of the model equations is provided in Chapter 3. A signal soliton of high intensity generates a refractive index barrier, at which a low-intensity dispersive wave is scattered. Using methods from quantum mechanics the scattering process of a low-intensity continuous dispersive wave at a dynamically changing solitonic barrier is analytically de-

scribed. The low-intensity dispersive wave is used as a control pulse. Under its influence all interesting soliton parameters change, for example the soliton frequency shifts and the soliton is adiabatically compressed. The soliton dynamics is described by a properly modified soliton perturbation theory.

In Chapter 4 the derived adiabatic model equations are carefully tested by comparison with numerical simulations of pulse propagation equations. They are then used to address the following problems. (1) Which signals can be manipulated? (2) What is the range of control pulses that effectively interact with a given signal? (3) How to explain and quantify the already known empirical rules? (4) Which control pulses provide the most effective change of signal parameters? In all such cases the adiabatic model is precise and much more fruitful than the direct numerical simulation of pulse propagation equations.

In Chapter 5 the implications of Raman effect on the soliton-dispersive wave interaction is discussed. The Raman effect is an ubiquitous higher order nonlinear effect which affects especially high-intensity and short pulses like the signal soliton. It is not dealt with in most previous works on dispersive wave scattering. The adiabatic model equations are applied to identify control pulses which cancel signal degradation due to the Raman effect.

Chapter 6 concludes this work and gives an outlook to the topic.

2 Interactions of solitons with dispersive waves

This chapter provides background information and a review of literature. Section 2.1 briefly summarizes how the propagation of optical pulses in nonlinear fibers is described. The generalized nonlinear Schrödinger equation is introduced as the appropriate equation for numerical simulation. Section 2.2 introduces the interaction between a soliton and a dispersive wave which is the main interest of this work. In Section 2.3 a number of conditions are collected that must be fulfilled for the interaction to take place. This list of conditions is derived entirely from observations in numerical simulations. Later on in this work these conditions are revisited and given a quantitative foundation.

2.1 Light propagation in optical fibers

Before introducing the specific light interaction which is the main subject of this thesis, the commonly used theoretical framework for pulse propagation in optical fibers will be resumed, and its specific assumptions will be made explicit.

In full generality, light, i. e. an electromagnetic field, inside a medium is described by Maxwell's equations combined with a set of relations describing the influence of the electric field on the material properties [45]. The focus is here on the propagation of light pulses in a single-mode fiber made from, e.g., silica glass. The typical material and geometry of the fiber strongly simplify the mathematical description of light propagation. In a series of approximations Maxwell's equations are reduced to a nonlinear Schrödinger equation for light waves in fibers [1, 56]. The assumptions underlying this reduction are briefly recalled.

Fibers are made of glass, a dielectric, so it is assumed that there are no free charges, no currents and no magnetization (Approximation 1). Thus the medium's response to the electric field is restricted to material polarization which is influenced by the applied field.

To formulate a relation between the material polarization $\vec{P}$ and the electric field $\vec{E}$, some quantum mechanical argumentation is needed in general. Yet, as long as the frequency range of the electric field is far from any material resonances, it is assumed that the material instantaneously responds to changes in the field strength (Approximation 2). Then, for a polarization preserving fiber, the polarization can be written

$$P = \varepsilon_0 \left[\chi^{(1)} E + \chi^{(2)} E^2 + \chi^{(3)} E^3 + \dots \right]. \tag{2.1}$$

ε_0 is the electric permittivity in vacuum. The optical susceptibilities $\chi^{(j)}$, $j \geq 1$, describe the optical properties of the medium. The susceptibilities reduce to mere scalars instead of tensors as already indicated in (2.1), because it is assumed that the fiber maintains the polarization state of the electric field, thus the polarization of the material is always parallel to the field strength (Approximation 3).

The leading order of (2.1) describes the linear response of the medium. In the frequency domain the first order susceptibility is related to the frequency dependent refractive index $n(\omega)$ and an absorption coefficient $\alpha(\omega)$ through the relative dielectric constant $[1 + \chi^{(1)}] = \varepsilon = [n + i\alpha c/[2\omega]]^2$, where c is the speed of light in vacuum. It is assumed that the fiber has very low losses, as extreme pure silica glass, thus absorption is neglected (Approximation 4). With $\alpha \approx 0$, the relative dielectric constant is real, $\varepsilon = n^2$. Higher orders in (2.1) describe nonlinear medium response. The higher order contributions become important for higher field intensities, and are treated as small perturbations to the linear contribution. The second order susceptibility $\chi^{(2)}$ vanishes in silica glass due to its inversion symmetry. The contribution of the next order containing $\chi^{(3)}$ is non vanishing. It is assumed that further higher order terms can safely be neglected, because they are only recognizable at extreme field intensities (Approximation 5). So the series (2.1) is truncated after the third order. The nonlinear contribution leads to a modification of the refractive index, $\tilde{n} = n(\omega) + n_2|E|^2$. The nonlinear refraction index $n_2 = 3\chi^{(3)}/[8n]$ is a small correction to n. It introduces a dependence on light intensity to the effective refractive index $\tilde{n}$. The intensity dependence of the refractive index is called Kerr effect or Kerr nonlinearity. n_2 is only very weakly dependent on frequency and is usually evaluated at reference frequency and taken as constant. The Kerr nonlinearity is responsible for the dominant nonlinear effects in fiber optics like self-phase modulation and cross-phase modulation.

The fiber's wave-guiding property simplifies the mathematical description of the electric field: In single-mode fibers light does not diffract, therefore transversal effects can be neglected. Remembering that the fiber was assumed to maintain polarization, the electric field reduces to a scalar function of time t and one spatial dimension z, which designates the direction of propagation along the fiber.

The slowly varying envelope formulation (Approximation 6) allows to separate the electric field $E(z,t) = \mathrm{Re}\left(\psi(z,t)e^{-i\omega_0 t + i\beta(\omega_0)z}\right)$ into an envelope function ψ and a fast carrier wave with (circular) frequency ω_0 and propagation constant $\beta(\omega_0)$. A light pulse considered here is assumed to be broad enough to contain several optical cycles, i.e. oscillations of the field, such that the envelope changes very little over one oscillation period.

The propagation constant β is written as a Taylor expansion around ω_0:

$$\beta(\omega) = \beta(\omega_0) + \beta'(\omega_0)\,[\omega - \omega_0] + \frac{\beta''(\omega_0)}{2}\,[\omega - \omega_0]^2 + \dots \tag{2.2}$$

The first derivative β' describes the inverse group velocity of light propagating along the fiber. The second derivative β'' describes group velocity dispersion (GVD). Given the assumptions of the slowly varying envelope formulation, it is okay to truncate the expansion after the second order. Both frequency profiles of β' and β'' for silica glass are shown in Figure 2.1. Silica exhibits one zero dispersion frequency (ZDF) at which the GVD vanishes. Waves show different behavior depending on which side of the ZDF their carrier frequencies lie. In the normal dispersion regime for frequencies above the ZDF, light with lower frequencies travels faster than that with higher frequencies. In the anomalous regime for frequencies below the ZDF the opposite is true.

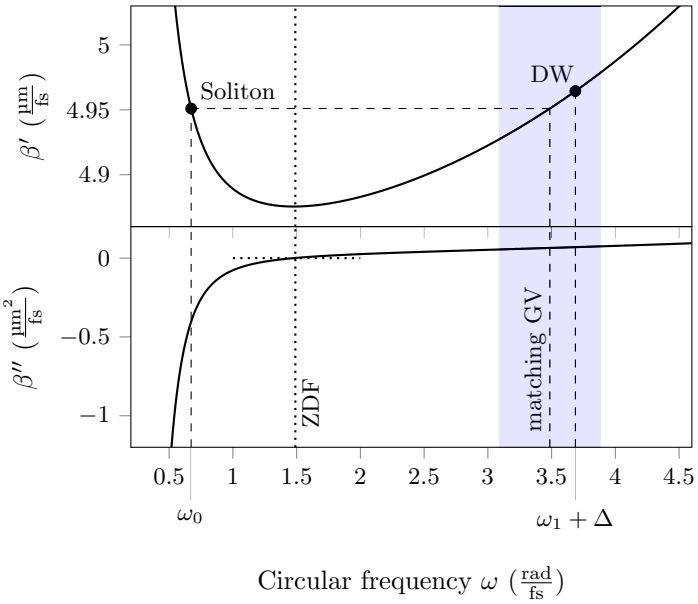

Figure 2.1: Inverse group velocity β' and group velocity dispersion (GVD) β'' for silica. The zero dispersion frequency (ZDF) of silica is indicated by a dotted line. Carrier frequencies of soliton and DW are indicated by black bullets. For a given initial soliton frequency ω_0 the frequency of matching group velocity is indicated by a dashed line. The DW frequency $\omega_1 + \Delta$ should lie in a rather small interval around this frequency to ensure an effective interaction. The precise calculation of this interval is one of the results of the present work.

The simplest form of the resulting propagation equation for the field envelope $\psi = \psi(z, \tau)$ is the nonlinear Schrödinger (NLS) equation

$$i\partial_z \psi - \frac{\beta''(\omega_0)}{2}\partial_\tau^2 \psi + \gamma_0 |\psi|^2 \psi = 0, \tag{2.3}$$

which includes GVD $\beta''(\omega_0)$ and the Kerr nonlinearity with nonlinear coefficient $\gamma_0 = \omega_0 n_2(\omega_0)/c$. The retarded time $\tau = t - z/\beta_0'$ defines a reference frame moving with group velocity $1/\beta'(\omega_0)$ at frequency ω_0.

Equation (2.3) allows to investigate the dominant nonlinear effects in optical fibers, including self-phase and cross-phase modulation. For anomalous dispersion ($\beta''(\omega_0) < 0$) it supports soliton solutions. Equation (2.3) is meaningful far beyond the realm of optics. It is valid for nearly all weakly nonlinear systems that support envelope solitons [88, 2, 46, 86].

Equation (2.3) properly describes propagation of pulses with durations in the picosecond range. It can be generalized to account for short pulses (in sub-picosecond range) which are relevant for the present purpose. Higher order dispersion terms must be included. A more thorough treatment of the nonlinear polarization reveals additional (non-instantaneous) nonlinear effects. It is still assumed that the material response is localized, non-resonant, dependent on intensity. Cubic nonlinear polarization is given by a delay integral

$$P_{nl} = \varepsilon \chi^{(3)} E(z,t) \int_{-\infty}^{\infty} R(t') \left|E(z, t-t')\right|^2 dt', \tag{2.4}$$

where R is a nonlinear response function. In this way, instantaneous as well as vibrational effects, in particular the Raman effect, can be described by a suitable response function.

Generalized nonlinear Schrödinger equation The result is a generalized nonlinear Schrödinger (GNLS) equation, which includes higher order dispersion and nonlinear terms and governs the propagation of optical pulses with pulse durations in the femtosecond range. The GNLS equation for the field envelope $\psi(z,\tau)$ reads

$$\begin{aligned}\partial_z\psi(z,\tau) &= i\hat{D}\left(i\partial_\tau\right)\psi(z,\tau)\\ &\quad + i\gamma_0\left[1+i\eta_0\partial_\tau\right]\left[\psi(z,\tau)\int_{-\infty}^{\infty}R(\tau')\left|\psi(z,\tau-\tau')\right|^2 d\tau'\right].\end{aligned} \tag{2.5}$$

τ still is the retarded time in a reference frame moving with group velocity $v_0 = 1/\beta'(\omega_0)$ at reference frequency. The nonlinear parameter $\gamma_0 = \omega_0 n_2(\omega_0)/c$ is defined as before. $\eta_0 = 1/\omega_0$ is the self-steepening parameter at reference frequency ω_0.

The convention of using brackets adopted here is: $(\cdot)$ to indicate arguments of functions and operators, and brackets $[\cdot]$, $\{\cdot\}$ for all other purposes.

In (2.5) the dispersion operator is defined as

$$\hat{D}(i\partial_\tau)\psi(z,\tau) = \mathcal{F}^{-1}(D(\omega)\hat{\psi}(z,\omega)) = \frac{1}{2\pi}\int_{-\infty}^{\infty}D(\omega)\hat{\psi}(z,\omega)e^{-i\omega\tau}\,d\omega, \tag{2.6}$$

where $\mathcal{F}$ denotes the Fourier transform, and the dispersion function D is defined for the frequency offset $\Delta\omega$ from reference frequency ω_0 as

$$D(\Delta\omega) = \beta\left(\omega_0+\Delta\omega\right) - \beta\left(\omega_0\right) - \beta'\left(\omega_0\right)\Delta\omega. \tag{2.7}$$

In this way the dispersion for any frequency not necessarily close to the reference frequency ω_0 is described properly. With this dispersion operator the GNLS equation properly describes waves in the anomalous and normal dispersion regime. Note that the dispersion operator can formally be written as an expansion

$$\hat{D}(i\partial_\tau) \equiv \sum_{m=2}^{\infty}\frac{\beta^{(m)}(\omega_0)}{m!}[i\partial_\tau]^m, \tag{2.8}$$

where $\beta^{(m)}(\omega_0)$ is the $m-$the order dispersion coefficient in unit $\mathrm{ps}^\mathrm{m}/\mathrm{km}$. It says "formally" because the above expansion is built by inverse Fourier transformation of the Taylor expansion of $D(\omega)$ around ω_0. In the notation of (2.8) it is clear how higher order dispersion terms are included into the GNLS equation.

Instantaneous electronic and delayed vibrational Raman contributions are included by

$$R(\tau) = \left[1-f_R\right]\delta(\tau) + f_R h(\tau)\Theta(\tau) \tag{2.9}$$

δ is the delta function, Θ the Heaviside step function. f_R is the fractional contribution of delayed Raman response to nonlinear polarization. The Raman response function is

$$h(\tau) = \frac{\nu_1^2+\nu_2^2}{\nu_1}e^{-\nu_2\tau}\sin\nu_1\tau \tag{2.10}$$

and $f_R = 0.18$, $1/\nu_1 = 12.2\,\mathrm{fs}$, and $1/\nu_2 = 32\,\mathrm{fs}$, where $12.2\,\mathrm{fs}$ and $32\,\mathrm{fs}$ are characteristic response times of fused silica fibers [11].

Validity for ultra–short pulses The GNLS equation is usually derived from Maxwell's equations by use of a slowly varying envelope approximation. For the approximation to be valid, a pulse must contain a sufficient number of optical cycles. This might seem controversial, as ultra–short pulses (in the femtosecond range) may only contain a few optical cycles, and a slowly varying envelope may not be well defined. Yet numerical simulations using the GNLS equation (2.5) demonstrate, that the propagation of such ultra–short pulses is still well described. In fact, the optical GNLS equation was shown to be independent of the slowly varying envelope approximation [12, 36, 47], the general dispersion operator emerging naturally in these authors' derivation.

Numerical solution Here, all numerical solutions are solutions of instances of (2.5). The method is a Runge-Kutta (4,5) algorithm applied to a resulting ordinary differential equation (ODE) in the frequency domain, following the approach in [31]. For more information see Appendix A.

In the following the co-propagation of two pulses, a soliton and dispersive wave (DW), is considered. In order to evaluate (2.5) numerically the following initial envelope is used

$$\psi(0,\tau) = \sqrt{P_0}\frac{1}{\cosh\left(\frac{\tau-\tau_0}{\sigma_0}\right)} + \sqrt{P_1}\frac{e^{-i[\omega_{\mathrm{DW}}-\omega_0]\tau}}{\cosh\left(\frac{\tau-\tau_1}{\sigma_1}\right)}. \tag{2.11}$$

The soliton has initial carrier frequency ω_0, initial peak power P_0, initial duration σ_0, and initial delay τ_0 generally equal to zero, $\tau_0 = 0$. The soliton's initial carrier frequency ω_0 is used as reference frequency in the pulse evolution equation (2.5). ω_1 is the frequency of matching group velocity to the initial soliton, $\beta'(\omega_0) = \beta'(\omega_1)$, cf. Figure 2.1. The initial DW frequency $\omega_{\mathrm{DW}} = \omega_1 + \Delta$ is chosen such that Δ is a small initial frequency offset from ω_1. This way soliton and DW have almost equal group velocities. The DW has an initial time delay τ_1, an initial duration σ_1 much wider than initial soliton duration, and initial peak power P_1 much below initial soliton peak power.

2.2 Soliton switching by dispersive waves

In this section the interaction between a soliton and a dispersive wave (DW) is introduced. Figures 2.2 and 2.3 show the typical interaction pictures of interest in time and frequency domain, and show relative pulse velocities. The main features to be observed are: The time domain shows a strong soliton and a low-intensity DW co-propagating along the length of the fiber with almost equal group velocities. The temporal evolution is shown in a co-moving frame moving with group velocity $v_0 = 1/\beta'(\omega_0)$ of the initial soliton. The DW approaches the soliton from one side. As it reaches the soliton, it is reflected at the soliton in the co-moving frame. During the reflection process the soliton is accelerated or decelerated (depending on the relative velocities of soliton and DW), which is recognized by the deflection of the soliton's temporal trajectory. Under favorable conditions the soliton is compressed or broadend. In

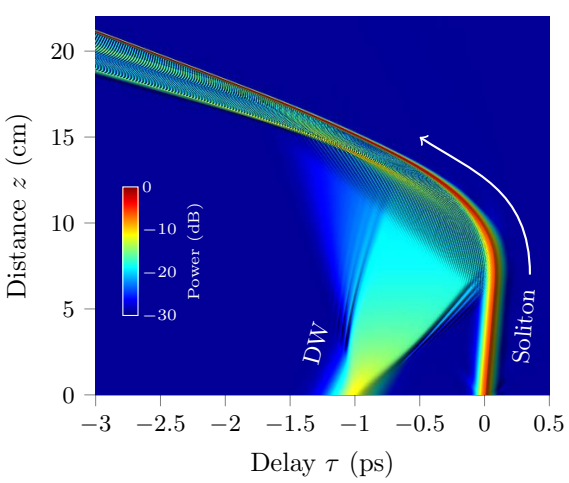

(a) Temporal evolution. Reflection of a DW (left pulse) at a soliton (right pulse). The soliton is accelerated.

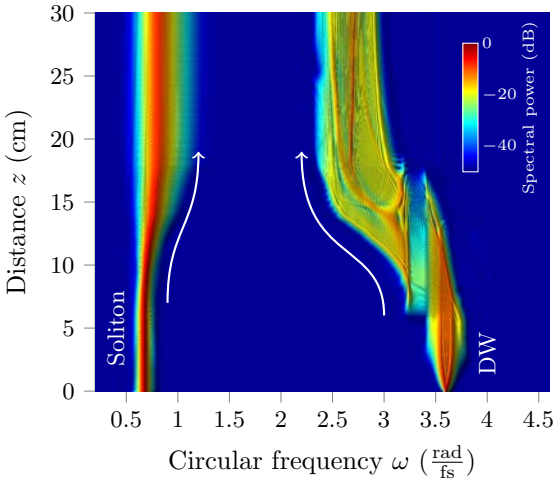

(b) Spectral evolution. Up-shift of the soliton carrier frequency and down-conversion of the DW frequency.

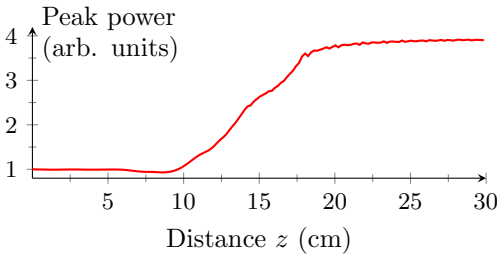

(c) Soliton peak power is amplified by almost a factor 4.

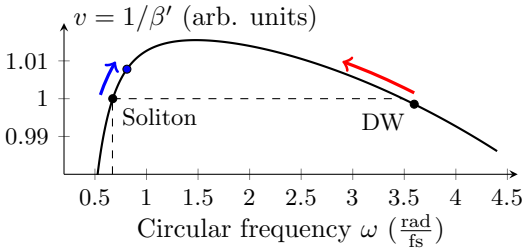

(d) Relative group velocities of both pulses. The incoming DW is slower than the soliton, the scattered DW is faster than the soliton.

Figure 2.2: Up-switching of a soliton by a dispersive control pulse. Numerical solution of GNLS equation (2.5). The used initial parameters for the soliton are $\omega_0 = 0.67\,\text{rad}\,\text{fs}^{-1}$, $\sigma_0 = 30\,\text{fs}$. The initial parameters for the DW are $\Delta = 0.11\,\text{rad}\,\text{fs}^{-1}$ ($\omega_{\text{DW}} = 3.6\,\text{rad}\,\text{fs}^{-1}$), $\sigma_1 = 100\,\text{fs}$, $P_1/P_0 = 0.25$, $\tau_1 = -1000\,\text{fs}$.

spectral domain the DW frequency is converted during the reflection process. The soliton's carrier frequency is permanently shifted.

The soliton-DW interaction can appear in two forms, which will be called up-switching and down-switching[1].

Up-switching (Figure 2.2) The incoming DW has a slightly lower group velocity than the soliton. As the DW is reflected at the approaching soliton, the DW frequency is converted to lower frequencies. The soliton frequency is up-shifted. Both pulses are accelerated (the soliton trajectory is bent to the left). The soliton is compressed and thereby

[1]The choice of name as "switching" is to be understood very generally. It was chosen with respect to the resulting amplification or weakening of the soliton's peak power. It is not to be confounded with "switching" in the sense of a directional change of a signal pulse traveling along a transmission line.

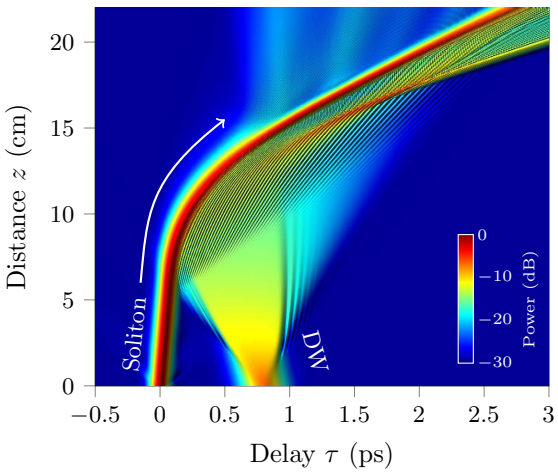

(a) Temporal evolution. Reflection of the DW (right pulse) at the soliton (left pulse). The soliton is decelerated.

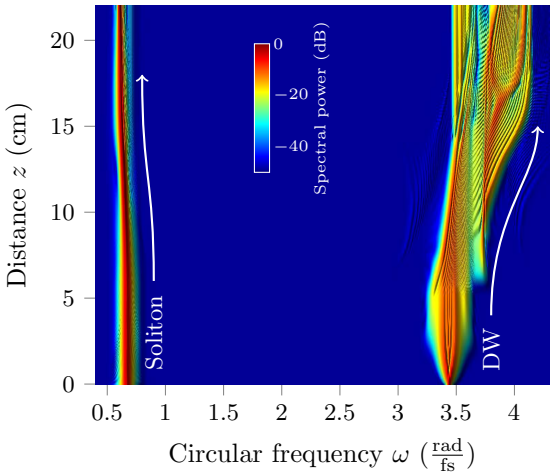

(b) Spectral evolution. Down-shift of the soliton carrier frequency and up-conversion of the DW frequency.

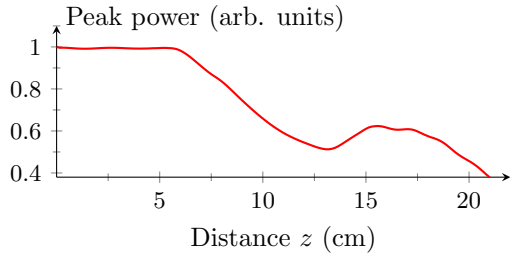

(c) The soliton loses peak power.

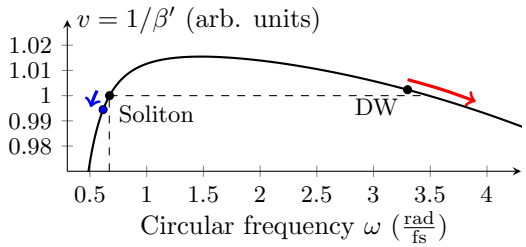

(d) Group velocities of both pulses. The incoming DW is faster than the soliton.

Figure 2.3: Down-switching of a soliton by a dispersive control pulse. Numerical solution of GNLS equation (2.5). The used initial parameters for the soliton are $\omega_0 = 0.67\,\text{rad}\,\text{fs}^{-1}$, $\sigma_0 = 30\,\text{fs}$. The initial parameters for the DW are $\Delta = -0.05\,\text{rad}\,\text{fs}^{-1}$ ($\omega_{\text{DW}} = 3.44\,\text{rad}\,\text{fs}^{-1}$), $\sigma_1 = 80\,\text{fs}$, $P_1/P_0 = 0.25$, $\tau_1 = 800\,\text{fs}$.

amplified, hence the term "up-switching".

Down-switching (Figure 2.3) The incoming DW has a slightly higher group velocity than the soliton. All properties of the up-switching are reversed: As the DW attempts to overtake the soliton, it is trapped behind it and reflected. The DW frequency is converted to higher frequencies while the soliton's frequency is shifted down. Both pulses are decelerated (the soliton trajectory is bent to the right). The soliton broadens and so loses peak power.

At first glance the picture of the temporal evolution might seem contra-intuitive due to the time delay variable. It helps the intuition to read the temporal picture from right to left. For example, in the up-switching case (Figure 2.2a) the initially faster soliton approaches the slower dispersive pulse on the left. As the soliton is accelerated, it bends to the left towards

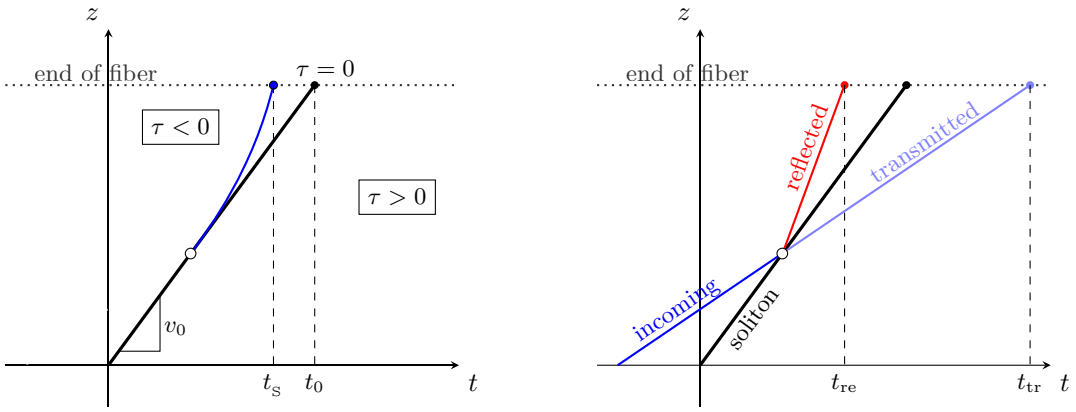

(a) Delay in a reference frame co-moving with the initial soliton. An accelerated soliton is deflected towards negative delays.

(b) In the up-switching scenario, the reflected wave is accelerated.

Figure 2.4: Schematic of the relation between the time delay variable τ and physical time t.

negative time delays. Figure 2.4 schematically shows the connection between time delay τ and physical time t. An unperturbed soliton propagates with constant group velocity v_0. In the $(t-z)-$plane the group velocity v_0 is the slope of the soliton trajectory (Figure 2.4a). The unperturbed soliton reaches the end of the fiber at time t_0. An accelerated soliton travels with increasing group velocity. The slope of the soliton trajectory in the $(t-z)-$plane increases, and it bends towards negative time delays. The accelerated soliton reaches the end of the fiber at an earlier time $t_\mathrm{S} < t_0$ compared to an unperturbed soliton. A DW with lower group velocity is launched into the fiber before the soliton (Figure 2.4b). Part of the DW is reflected forward at the approaching soliton and is accelerated, so that it reaches the end of the fiber before the soliton. Part of the DW may be transmitted through the soliton and travel on with unchanged group velocity, reaching the end of the fiber after the soliton.

On the whole, the interaction with a low-intensity dispersive pulse bears the possibility to effectively manipulate a soliton and produce possibly extreme changes in its parameters: shift of its carrier frequency up or down, compression or broadening of the soliton, thereby amplification or weakening of its peak power. The main focus of this work is the question if the manipulation of the soliton can be done in a controlled and predictable manner. To this end, a quantitative description of the soliton-DW interaction has been developed to be explained in the following chapters. But of course, the interaction can be viewed in a variety of perspectives, and accordingly there is a large number of studies, in which the interaction has been investigated numerically and experimentally, both in a variety of situations involving different optical fibers and initial conditions, and possible applications. Some of these studies shall briefly be mentioned in the rest of this section[2].

The possibility to manipulate a soliton with a DW is a quite recent observation [23].

[2]The interaction is found in the literature under several synonymous names, depending on the respective focus of investigation, e.g. "DW scattering", "DW trapping", "soliton feeding". Based on a specific interpretation or explanation it is often called "mixing" of solitons and DWs, and an "optical event horizon".

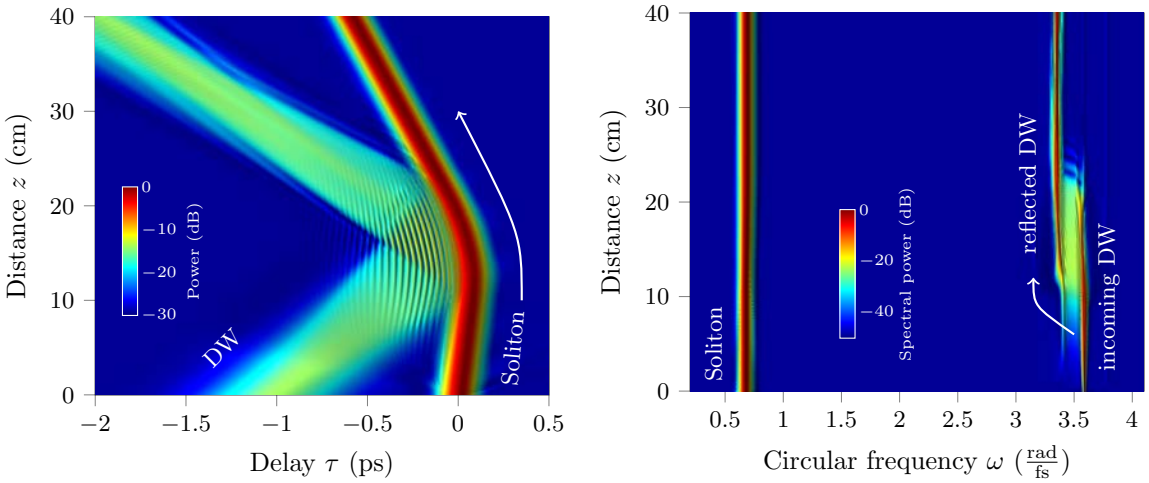

(a) Temporal evolution. The soliton is only slightly accelerated during the DW reflection. The soliton's peak power is amplified by only a factor 1.1 (not shown).

(b) Spectral evolution. The soliton's frequency shift is hardly visible. The DW frequency is converted down to one quite distinct frequency.

Figure 2.5: Weak up–switching of a soliton by dispersive pulse. The effect on the soliton is only minimal. Numerical solution of GNLS equation (2.5). The used initial parameters for the soliton are $\omega_0 = 0.67\,\text{rad}\,\text{fs}^{-1}$, $\sigma_0 = 40\,\text{fs}$. The initial parameters for the DW are $\Delta = 0.1\,\text{rad}\,\text{fs}^{-1}$ ($\omega_{\text{DW}} = 3.59\,\text{rad}\,\text{fs}^{-1}$), $\sigma_1 = 200\,\text{fs}$, $P_1/P_0 = 0.04$, $\tau_1 = -1000\,\text{fs}$.

Before, the focus was on the DW, on its reflection and its frequency conversion. The reflection of the DW is the underlying process of the interaction. Only under favorable conditions (which will be discussed in Section 2.3) the soliton parameters are visibly changed during the reflection process. Figure 2.5 shows an example of a reduced interaction picture where the DW is fully reflected, but the impact on the soliton is only minimal. The soliton frequency shift is hardly visible at all. In this example the soliton's peak power is amplified only by a factor 1.1. The soliton's deflection in space-time domain is usually the most pronounced of all changes. Here the soliton is only slightly accelerated. As a consequence the DW frequency is converted to one quite distinct frequency. In the examples of Figures 2.2 and 2.3 the frequency of the reflected DW is not distinct, because the DW is reflected at a continuously accelerated soliton. While in the given example (Figure 2.5) minimal changes in the soliton can still be seen, in many circumstances the soliton is practically unaffected by the DW.

Studies focussing on the DW reflection include a variety of settings. DW packets or dispersive radiation can be trapped by a single soliton [39, 84], it can be repeatedly reflected at a soliton which is continuously decelerated, e.g. due to Raman scattering, [38, 40], or it can bounce between two solitons [89, 26, 26]. The trapping and frequency conversion of low intensity waves at a soliton barrier were observed in various experiments [62, 64, 68, 70, 85, 15, 79].

The specific properties of the fiber dispersion profile are crucial for a soliton-DW interaction. Photonic crystal fibers are particularly interesting because their optical properties

(like dispersion, birefringence and nonlinearity) can be engineered by controlling the geometry of the fiber, i.e. the arrangement of hollow tubes pervading the length of the fiber [91]. The pulse behavior can be controlled by the design of the dispersion-engineered photonic crystal fibers [69]. The dispersion profile for the interaction of interest can be selected to produce or enhance a certain behavior. For example simply the group velocity matching of desired wavelengths can be favored [68], or the point of collision can be controlled [5]. For a variety of special fibers and arrangements the interaction has been demonstrated experimentally [82, 16, 17, 55]. The next section will display the minimal requirements for the fiber properties.

Several applications have been suggested. The role of DW frequency conversion at a soliton barrier for the generation of new frequencies has been investigated numerically, especially to explain the appearance of certain frequencies in super-continua [77, 78, 29]. A sequence of solitons can act as an optical Bragg resonator [81]. The DW trapping was experimentally tested as an optical switching mechanism [63] where weak dispersive pulses are used as the signal controlled by the stronger soliton. The present work corroborates, that it is actually possible to use a weak dispersive pulse to control the stronger soliton.

The reflection of a DW at an unchanged soliton has been interpreted as an optical event horizon, i.e. the optical analog to the event horizons at black and white holes [68, 85]. The concept stems from an similarity between the relevant optical equations and the equations of general relativity. Moreover, physical effects that should result in an optical analogue to Hawking radiation were observed in [74, 9]. Further uses of the analogy include, e.g. "black hole laser" - optical radiation that is trapped between two horizons (solitons) and enhanced by successive reflections [33, 35]. By the way, the term "optical event horizon" is often used loosely for the reflection of a DW at a soliton barrier, also in situations where the soliton is visibly affected, and parts of the DW are transmitted.

Even analog kinds of reflection and trapping of DWs by higher order solitons [65] and dark solitons [66] have been numerically investigated. It has also been investigated if up- and down-conversion of the DW frequency should be done by reflection at a bright soliton as discussed here for the up-conversion and by reflection at a dark soliton for the down-conversion of the frequency [27].

Studies focusing on the soliton's reaction to DW scattering started only during the last decade. If the soliton is visibly affected by the reflection process, the strongest change and the most likely to be observed, is the deflection of the soliton trajectory which accompanies the soliton frequency shift, cf. Figure 2.5. The small soliton frequency shift due to DW scattering was observed in numerical simulation [24]. If two solitons trap a DW in-between, this soliton cavity will collapse: the two solitons are deflected towards each other until they collide [28, 89], as experimentally demonstrated [83]. Though it is quite difficult to adjust suitable initial parameters for input pulses, the soliton compression was observed experimentally in an isolated setting of two interacting pulses [80].

In the frequency domain the DW frequency conversion is continuous as the soliton is accelerated. Instead of a single converted frequency, a broad band of new DW frequencies

is observed. Broad spectra can be generated, which is interesting in itself. Usually super-continua can be generated by soliton fission [30]. Soliton switching can serve as an additional way to produce super-continua, as numerically shown for fused silica fiber [22, 21].

The change in soliton peak power can be massive, if a suitable DW is chosen. Soliton switching was proposed as a robust mechanism leading to the formation of rogue waves independent of higher order effects specific to the optical context (like Raman scattering) [24, 19, 75]. Interestingly, the same mechanism was used to suppress the formation of rogue waves by launching an additional DW to destroy any potential rogue soliton in the super-continuum [13].

In conclusion, a soliton experiences frequency shifting, a deflection of peak position and undergoes compression or broadening, all due to the DW reflection. So it is natural to ask, whether the behavior can be controlled by a suitable choice of DW [23]. This question will be addressed in the present work by constructing a quantitative theory of such interactions. The following section recaptures and summarizes the state of the art and gives some empirical rules for an effective soliton manipulation derived from observations in numerical simulations.

2.3 Conditions for efficient soliton manipulation

The findings of previous numerical and experimental studies [23, 24, 22, 25, 21, 19] suggest that a soliton can be manipulated and controlled by the interaction with a suitably chosen DW. From these previous studies a number of useful conditions can be extracted to enable effective soliton control.

The first two conditions are necessary to ensure the reflection of the DW:

Rule of opposite dispersion regimes The carrier frequencies of soliton and DW lie on either side of the ZDF (Figure 2.1). The soliton belongs to the anomalous dispersion regime, so the GVD $\beta''(\omega_0)$ is negative. The DW belongs to the normal dispersion regime, where $\beta''(\omega_1 + \Delta)$ is positive [23]. DWs in the anomalous dispersion regime are less effective in changing soliton properties.

Velocity-matching condition Group velocities of soliton and DW should be reasonably close (Figure 2.1). If they are too different, the pulses pervade each other unchanged. If they are too close, the pulses may never meet [23, 52]. So the initial DW frequency offset Δ should lie in a rather small interval around ω_1.

These two conditions can always be satisfied if the fiber dispersion profile has at least one ZDF, as it happens for nearly all optical materials.

Even if a DW is reflected, this does not suffice for any effective change in the soliton. The impact of a DW on a soliton strongly on the fiber dispersion profile. So in many situations only the reflection and frequency conversion of the DW are observed while the soliton is unaffected by the interaction, i.e. its frequency, trajectory and peak power remain unchanged [78].

The underlying reflection process of the DW is mediated by cross-phase modulation (XPM) [23, 68], which is a manifestation of the optical Kerr effect. The soliton's high in-

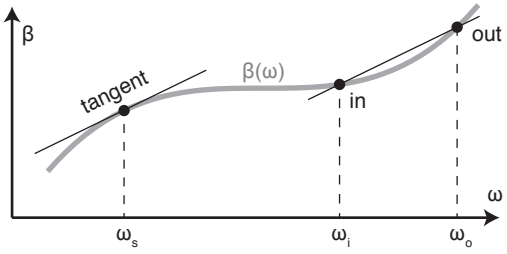

Figure 2.6: Input and output frequencies of a DW reflected at a moving soliton, according to (2.14). The input DW frequency and the soliton carrier frequency ω_{S} yield the output frequency of the scattered DW.

tensity changes the refractive index locally. Each other field sees the effective index and interacts with it. The strong soliton constitutes a barrier, an inhomogeneity moving with constant velocity in an otherwise transparent medium, at which an incoming DW is scattered. To get an idea of the frequency conversion of the reflected DW one can calculate the Doppler relation for incoming and outgoing frequencies ω_{in}, ω_{out}. Consider an incoming wave $\exp(i\beta(\omega_{\mathrm{in}})z - i\omega_{\mathrm{in}}t)$ and outgoing wave $\exp(i\beta(\omega_{\mathrm{out}})z - i\omega_{\mathrm{out}}t)$ propagating along the $z-$direction, with the dispersion relation given by a function $\beta(\omega)$. Requiring continuity at the inhomogeneity at position $z = vt$ along the fiber, the exponents of incoming and outgoing waves should coincide at any time [73, 72]:

$$\beta(\omega_{\mathrm{in}})v - \omega_{\mathrm{in}} = \beta(\omega_{\mathrm{out}})v \mp \omega_{\mathrm{out}} \tag{2.12}$$

The fiber dispersion is defined as $\beta(\omega) = n(\omega)\omega/c$ where c is speed of light in vacuum, then

$$\omega_{\mathrm{out}} = \omega_{\mathrm{in}}, \qquad \omega_{\mathrm{out}} = \frac{1 - n(\omega_{\mathrm{in}})\frac{v}{c}}{1 + n(\omega_{\mathrm{out}})\frac{v}{c}}\omega_{\mathrm{in}} \tag{2.13}$$

are the frequencies of the transmitted and backward reflected wave in a co-moving frame, respectively. The velocity v of the inhomogeneity can be approximated by the group velocity $v_0 = 1/\beta'(\omega_0)$ of a soliton with carrier frequency ω_0, and (2.13) yields

$$\beta'(\omega_0) = \frac{\beta(\omega_{\mathrm{out}}) - \beta(\omega_{\mathrm{in}})}{\omega_{\mathrm{out}} - \omega_{\mathrm{in}}}. \tag{2.14}$$

As illustrated in Figure 2.6 the possible values of ω_{out} are given by ω_{in} and ω_0 [P1]. In terms of the dispersion function (2.7) the relation (2.14) reads

$$D\left(\omega_{\mathrm{out}} - \omega_0\right) = D\left(\omega_{\mathrm{in}} - \omega_0\right). \tag{2.15}$$

A relation of this kind was also derived in a more general framework of four wave mixing, where the mixing of solitons with DWs yields radiation at new frequencies, if the corresponding phase-matching/resonance conditions are met [90, 77, 32]. This is why (2.15) is often called the resonance condition for DW frequency conversion.

The Doppler relation (2.13) gives a good approximation of the DW frequency conversion at a soliton of constant velocity as experimentally confirmed in [85]. It nicely predicts the

converted DW frequency also in simple cases like shown in Figure 2.5b, where the soliton is only slightly if at all affected, and the converted DW frequency is quite distinct. In a situation of a dynamically changing soliton it has to be taken into account that the frequency of the outgoing DW changes with the accelerated soliton. A more accurate description will be provided in Section 3.3.

More conditions are needed to ensure the desired impact of the soliton-DW interaction on the soliton. The first of these pertains to the fiber dispersion profile, the second one singles out a feature of the DW. In order to enable soliton amplification, require:

Steep anomalous GVD profile The GVD profile $\beta''(\omega)$ should be steep in the anomalous region for the soliton and only slightly sloping in the normal region for the DW (Figure 2.1) [23]. Otherwise the DW is still scattered but the soliton remains nearly unchanged [24].

The compression and amplification of the soliton is mainly a reshaping process. The soliton energy $\mathscr{E} = 2\sqrt{P_0|\beta''(\omega_0)|/\gamma_0}$ is given through initial soliton peak power P_0, GVD coefficient $\beta''(\omega_0)$, and fiber nonlinearity γ_0. During the reflection process due to XPM no exchange of energy between soliton and DW is expected, so the soliton energy should stay unchanged. γ_0 also does not vary appreciably. Then soliton peak power and the GVD coefficient fulfill the simple relation $P_0 \cdot |\beta''(\omega_0)| = \text{const}$. A decreasing β'' is compensated by an increase in soliton peak power (and vise versa) [24]. This mechanism is known as adiabatic soliton compression [14]. The fiber dispersion must vary sufficiently slowly, so the soliton can adiabatically adapt. Normally the change in the GVD coefficient is achieved by using a dispersion-decreasing fiber. Here however, the GVD coefficient changes due to the shifting soliton frequency induced by the DW scattering. Numerical simulation showed only a slight change in soliton energy accompanying the soliton frequency shift [24]. It slightly increases in the up-switching case, and decreases in the down-switching case, which in both cases just supports the above arguments.

The following are rules of thumb for a suitable choice of DW for an efficient soliton amplification:

Broad low-amplitude dispersive wave A broad low-amplitude DW packet has a stronger effect than a short DW packet of the same energy [22]. The initial delay between the DW pulse and the soliton should be large enough to ensure pulse spreading due to dispersion (Figures 2.2 and 2.3) before the point of collision. This is favorable especially if an initially short DW was chosen. The DW can be several orders of magnitude weaker than the soliton, and still produce multi-fold amplification in the soliton amplitude.

High reflection rate/Conversion efficiency In a favorable situation the DW is almost perfectly reflected at the soliton (Figures 2.2 and 2.3). That is, the intensity of the transmitted wave is very low as compared to the intensity of the reflected wave [23, 15]. The situation is often described as *a group velocity event horizon* by analogy with [68].

Numerical investigations suggest that other possible DW properties, like an initial frequency chirp, have less influence on soliton compression [6].

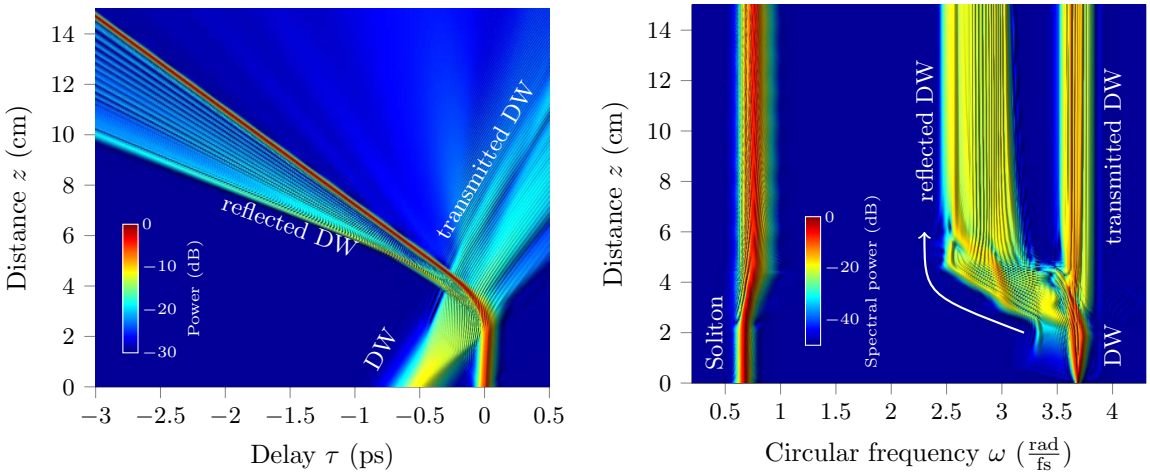

(a) Temporal evolution. An essential part of the dispersive wave is transmitted through the soliton. Soliton peak power is amplified by only a factor 2 (not shown).

(b) Spectral evolution. Soliton frequency is up-shifted. The transmitted parts of the DW keep their initial carrier frequency. The frequency of the reflected parts of the DW is converted down.

Figure 2.7: Imperfect reflection of a dispersive wave at a soliton. Numerical solution of GNLS equation (2.5). The used initial parameters for the soliton are $\omega_0 = 0.67\,\text{rad}\,\text{fs}^{-1}$, $\sigma_0 = 30\,\text{fs}$. The initial parameters for the DW are $\Delta = 0.2\,\text{rad}\,\text{fs}^{-1}$ ($\omega_{\text{DW}} = 3.69\,\text{rad}\,\text{fs}^{-1}$), $\sigma_1 = 100\,\text{fs}$, $P_1/P_0 = 0.0225$, $\tau_1 = -500\,\text{fs}$.

Figure 2.7 shows an example of an undesirable situation. The DW has not enough time to broaden before it reaches the soliton. The reflection is imperfect, as part of the incoming DW is transmitted through the soliton. Though there is still a clearly visible impact on the soliton, the effectiveness of the interaction is impaired. In comparison to the four fold amplification in the desirable example of Figure 2.2, here the soliton peak power is amplified by only a factor 2.

A natural choice for the control wave is a low-amplitude continuous wave, since a broad low-amplitude DW is most desirable. For a basic understanding, finite pulses (usually used in previous numerical studies) are less suitable, because many more parameters would have to be managed. To solve the simulation equation (2.5) numerically for the co-propagation of a soliton and a continuous DW the following initial envelope is used

$$\psi(0,\tau) = \sqrt{P_0}\frac{1}{\cosh\left(\frac{\tau-\tau_0}{\sigma_0}\right)} + \sqrt{P_1}e^{-i[\omega_{\text{DW}}-\omega_0]\tau}. \tag{2.16}$$

So the only control parameters are DW frequency and peak power. An example of the soliton up-switching by a continuous DW is shown in Figure 2.8. All desired features of the soliton manipulation are achieved by the mentioned simple choice of DW. The soliton frequency is up-shifted, the soliton is accelerated and compressed. In the temporal domain (Figure 2.8a) one additional feature is the point at which the soliton becomes transparent to the incoming continuous wave.

The present work will come up with a quantitative insight on suitable conditions for

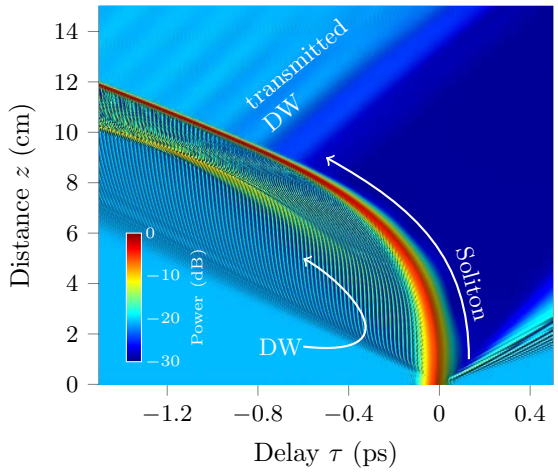

(a) Temporal evolution. The DW is reflected at the soliton, which is accelerated in the course of the interaction.

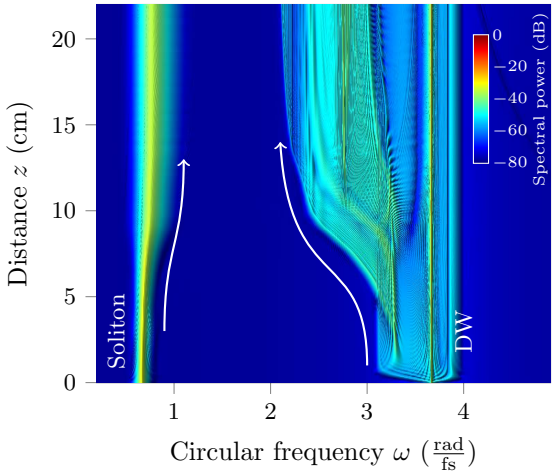

(c) Spectral evolution. Up-shift of soliton frequency. The DW frequency is converted down at the accelerated soliton barrier.

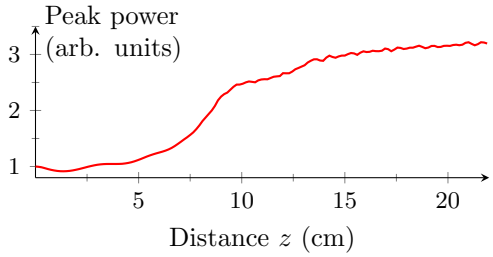

(b) Soliton peak power is amplified by almost a factor 4.

Figure 2.8: Up-switching of a soliton by a continuous DW. Numerical solution of GNLS equation (2.5). The used initial parameters for the soliton are $\omega_0 = 0.67\,\text{rad}\,\text{fs}^{-1}$, $\sigma_0 = 30\,\text{fs}$. The initial parameters for the DW are $\Delta = 0.18\,\text{rad}\,\text{fs}^{-1}$ ($\omega_{\text{DW}} = 3.67\,\text{rad}\,\text{fs}^{-1}$), $P_1/P_0 = 0.0225$. All desired features of the soliton manipulation are achieved by this simple choice of a control wave, cf. Figure 2.2.

soliton control by DW reflection: Model equations (4.5) will be established that quantify the DW reflection at a dynamically changing soliton, enabling a systematic choice of proper initial conditions for an effective soliton manipulation. Resulting predictions will be compared with results from numerical simulations.

3 Model equations

In this chapter model equations are derived for the interaction of a soliton with a weak continuous dispersive wave as control wave [P1]. The model is based on two coupled generalized nonlinear Schrödinger equations, one for the soliton and one for the control wave, which are introduced in Section 3.1. Both equations are solved by different methods tailored to the specific behavior of the soliton and dispersive wave, respectively. On one side, the soliton is reshaped under the influence of a small perturbation constituted by the weak dispersive wave. Situations of this kind are often described by soliton perturbation theory. For the present case, a suitably modified soliton perturbation theory is necessary, which is introduced in Section 3.2. The modified theory enables prediction of the soliton amplification, in contrast to standard perturbation theory. On the other side, the behavior of the dispersive wave is treated as a scattering problem analog to the quantum mechanical problem of a plane wave which is (partially) reflected or transmitted at a potential barrier. Here the soliton constitutes a continuously changing barrier. The adequate scattering problem is formulated and solved in Section 3.3. Together, the derived model equations provide a powerful analytical tool to assess the soliton switching process, which is discussed in Chapter 4.

3.1 Reduction to coupled generalized nonlinear Schrödinger equations

As a first step to problem specific model equations, the full GNLS equation (2.5) is reduced to a simpler form sufficient to capture the soliton-DW interaction. The spectra of both pulses stay neatly separated for the entire propagation distance, so firstly it is possible to split the simulation equation into two coupled GNLS equations, one each for the envelopes ψ_{S} of the soliton and ψ_{DW} of the DW [1].

A common frame of reference is introduced, which is co-moving with the initial soliton. Let ω_0 be the initial soliton carrier frequency chosen in the negative dispersion regime. Then let ω_1 be the frequency for which the corresponding group velocities are equal, $\beta'(\omega_0) = \beta'(\omega_1)$. The two frequencies will have negative and positive GVD respectively (Figure 2.1). With the common delay variable

$$\tau = t - z\beta'(\omega_0) = t - z\beta'(\omega_1), \tag{3.1}$$

a reference frame is introduced which is suitable for both the soliton and the DW.

The soliton envelope $\psi_{\mathrm{S}}(z,\tau)$ is described by a GNLS equation centered at ω_0,

$$i\partial_z\psi_{\mathrm{S}}(z,\tau)+\hat{D}\left(i\partial_\tau\right)\psi_{\mathrm{S}}(z,\tau)+2\gamma_0\left[1+i\eta_0\partial_\tau\right]\left[\left|\psi_{\mathrm{DW}}(z,\tau)\right|^2\psi_{\mathrm{S}}(z,\tau)\right] \tag{3.2}$$
$$+\gamma_0\left[1+i\eta_0\partial_\tau\right]\left[\psi_{\mathrm{S}}(z,\tau)\int_{-\infty}^{\infty}R(\tau')\left|\psi_{\mathrm{S}}(z,\tau-\tau')\right|^2d\tau'\right]=0.$$

The envelope $\psi_{\mathrm{DW}}(z,\tau)$ of the DW is governed by a GNLS equation centered at ω_1,

$$i\partial_z\psi_{\mathrm{DW}}+\sum_{m\geq2}\frac{\beta_1^{(m)}}{m!}[i\partial_\tau]^m\psi_{\mathrm{DW}}+2\gamma_1\left[1+i\eta_1\partial_\tau\right]\left[\left|\psi_{\mathrm{S}}\right|^2\psi_{\mathrm{DW}}\right] \tag{3.3}$$
$$+\gamma_1\left[1+i\eta_1\partial_\tau\right]\left[\psi_{\mathrm{DW}}(z,\tau)\int_{-\infty}^{\infty}R(\tau')\left|\psi_{\mathrm{DW}}(z,\tau-\tau')\right|^2d\tau'\right]=0.$$

The abbreviations $\beta_0^{(m)}=\partial_\omega^m\beta(\omega_0)$ and $\beta_1^{(m)}=\partial_\omega^m\beta(\omega_1)$ will denote derivatives of $\beta(\omega)$ at the respective reference frequencies. The nonlinearity coefficients of each equation are evaluated at the respective reference frequency,

$$\gamma_0=\frac{n_{2,0}}{c}\omega_0,\quad \gamma_1=\frac{n_{2,1}}{c}\omega_1, \tag{3.4}$$

with nonlinear refractive indices $n_{2,0}=\frac{3\chi^{(3)}}{8n(\omega_0)}$ and $n_{2,1}=\frac{3\chi^{(3)}}{8n(\omega_1)}$. The same holds for the self-steepening parameters

$$\eta_0=\frac{1}{\omega_0},\qquad \eta_1=\frac{1}{\omega_1}. \tag{3.5}$$

The reference frequencies ω_0 and ω_1 are chosen such that $\beta''(\omega_0)<0$ and $\beta''(\omega_1)>0$, so (3.2) and (3.3) are one focusing and one defocusing GNLS equation coupled by the XPM terms [1]. The actual carrier frequency of the incoming DW is slightly offset from the reference frequency ω_1 of the DW equation (3.3) by amount Δ. The frequency of the incoming DW is denoted by $\omega_{\mathrm{DW}}=\omega_1+\Delta$. The offset Δ is hidden in the envelope $\psi_{\mathrm{DW}}\sim\exp\left(-i\Delta\tau\right)$. Numerical simulations have shown that the carrier frequency of the reflected wave $\omega_r\approx\omega_1-\Delta$ will lie on the other side of the reference frequency ω_1. The dispersion profile around ω_1 is not steep, which makes ω_1 a good choice for centering the GNLS equation (3.3).

One immediate simplification of (3.3) is done. The higher order terms, i.e. higher order dispersion terms with $m\geq3$, self-steepening and Raman scattering, are important for a short powerful soliton, but do not have significant influence onto a low–intensity continuous DW. Thus higher order terms in (3.3) can be neglected. Moreover, the equation can be linearized as the soliton is much more intense compared to the DW. Calculations show that (3.2) combined with the following reduction of (3.3):

$$i\partial_z\psi_{\mathrm{DW}}-\frac{\beta''(\omega_1)}{2}\partial_\tau^2\psi_{\mathrm{DW}}+2\gamma_1\left|\psi_{\mathrm{S}}\right|^2\psi_{\mathrm{DW}}=0, \tag{3.6}$$

adequately describes the evolution of the soliton under the influence of the DW. Equation (3.6) is mathematically equivalent to the standard (linear) Schrödinger equation of quantum mechanics.

The leading intuition for solving the coupled equations (3.2) and (3.6) is the following: While the DW transfers its energy and momentum to the soliton through a scattering process at a potential barrier as known e.g. from quantum mechanics, the soliton is compressed. It retains its soliton character and changes its shape adiabatically slow under the influence of the small perturbation constituted by the DW. Thus, the following two steps suggest themselves.

First, derivation of an approximate solution for the soliton based on a variational formulation for (3.2). This variational approximation uses a trial function for ψ_{S} depending on a small set of parameters, like frequency and duration, for which a set of ODEs is derived, [43]. It will be found that the direct variational approximation for the given equation does not capture the soliton dynamics - it misses to predict any change in soliton peak power. To derive a more successful solution, (3.2) must be adapted to the problem at hand. This is the key idea of the present model derivation. The soliton solution depends on the yet unknown DW solution ψ_{DW}, which enters the soliton equation as a perturbation term.

Second, to find a solution to the DW equation (3.6), the general ansatz for a soliton solution $|\psi_{\mathrm{S}}|^2$ is inserted into (3.6), and the envelope ψ_{DW} of the DW is calculated using a small extension of the standard quantum mechanical scattering theory. Finally, the result for ψ_{DW} is used to obtain self-consistent adiabatic ODEs for the soliton parameters.

Section 3.2 goes through all steps to produce an approximate solution of the soliton equation (3.2). In Section 3.3 the scattering problem for the DW is solved.

3.2 Variational approximation of soliton solution

The soliton equation (3.2) is reformulated as a perturbation equation for the standard NLS equation, following a well known procedure described, e.g., in [43].

The standard NLS equation describes the propagation of a soliton along the fiber to leading order. It includes second order (group velocity) dispersion and Kerr nonlinear refractive index. Compared to these, higher order dispersion, Raman scattering, self-steepening, are considered to be small and are treated as perturbations. The XPM effect of the second pulse on the soliton in (3.2) is also treated as a perturbation. The impact of all perturbations on the single soliton solution of NLS is studied by soliton perturbation theory (SPT).

SPT is a widely used method to determine propagation behavior of localized solutions under the influence of small perturbations. Various approaches have been developed: direct perturbation theory [88], variation of conserved quantities [41], variation of the scattering data of inverse scattering transform [48], and Lagrange formulation of perturbation theory [43].

Here, the Lagrange formulation of the NLS-perturbation theory is used, [43]. Section 3.2.1 briefly recaptures the Lagrangian formalism to derive an approximate solution for a perturbed NLS equation. In order to predict the evolution of all soliton parameters correctly, including peak power, the standard NLS equation underlying the perturbation theory needs to be adjusted. This is done in Section 3.2.2.

3.2.1 Perturbation theory of nonlinear Schödinger equation

The variational approximation is a method to determine the propagation behavior of localized solutions to evolution equations. It was first introduced for optical solitons in [4] as an approximate analytical procedure for solving a standard NLS equation

$$i\partial_z\psi(z,\tau) - \frac{\beta_0''}{2}\partial_\tau^2\psi(z,\tau) + \gamma_0\left|\psi(z,\tau)\right|^2\psi(z,\tau) = 0. \tag{3.7}$$

Higher order terms can be naturally included as perturbations influencing the solitonic solutions. It is a well established approach [43]. Here is a quick survey of the procedure, followed by general ODEs for a perturbed soliton propagation.

An ansatz function for the desired solution $\psi = \psi_{\mathrm{S}}$ is chosen, assuming that the soliton has a specific temporal shape, e.g. a hyperbolic secant or Gaussian shape, which is characterized by a specific set of parameters. A hyperbolic secant shape, which is motivated by a well-known exact NLS solution, is defined by

$$\psi_{\mathrm{S}}(z,\tau) = \frac{1}{\sigma}\sqrt{\frac{|\beta_0''|}{\gamma_0}}\,\mathrm{sech}\left(\frac{\tau-\tau_{\mathrm{S}}}{\sigma}\right)\exp\left(-i\nu\left[\tau-\tau_{\mathrm{S}}\right]+i\theta\right) \tag{3.8}$$

where the parameters are pulse duration $\sigma = \sigma(z)$, frequency shift $\nu = \nu(z)$, temporal delay $\tau_{\mathrm{S}} = \tau_{\mathrm{S}}(z)$, and phase $\theta = \theta(z)$. Typical initial values are $\nu(0) = 0$, $\tau_{\mathrm{S}}(0) = 0$, $\sigma(0) = \sigma_0$. Soliton peak power $P_{\mathrm{S}} = \frac{1}{\sigma^2}\frac{|\beta_0''|}{\gamma_0}$ in (3.8) is defined as function of the soliton duration. All parameters are assumed to evolve along z following the soliton. Their evolution equations can be derived from a variational formulation of NLS equation.

The standard NLSE (3.7) can equivalently be expressed as the variational problem[1]

$$\delta\iint\mathcal{L}\,d\tau\,dz = 0, \tag{3.9}$$

i.e.

$$\frac{\delta\mathcal{L}}{\delta\psi^*} = 0 \tag{3.10}$$

where

$$\frac{\delta}{\delta\psi^*} = \frac{\partial}{\partial\psi^*} - \frac{\partial}{\partial z}\frac{\partial}{\partial\left[\frac{\partial\psi^*}{\partial z}\right]} - \frac{\partial}{\partial\tau}\frac{\partial}{\partial\left[\frac{\partial\psi^*}{\partial\tau}\right]}, \tag{3.11}$$

corresponding to the Lagrangian density

$$\mathcal{L}_{\mathrm{NLS}} = \frac{i}{2}\left[\psi^*\frac{\partial\psi}{\partial z} - \psi\frac{\partial\psi^*}{\partial z}\right] + \frac{\gamma_0}{2}\left|\psi\right|^4 - \frac{\beta_0''}{2}\left|\frac{\partial\psi}{\partial\tau}\right|^2. \tag{3.12}$$

The variational problem (3.9) reduces to a finite-dimensional problem

$$\delta\int dz\,L = 0 \tag{3.13}$$

[1] All integrals here range from $-\infty$ to ∞ unless otherwise stated.

with the Lagrangian $L(\psi,\psi^*) = \int d\tau\, \mathcal{L}(\psi,\psi^*)$, where ψ is now the ansatz function (3.8) which depends on four parameters. Using the ansatz function the Lagrangian is evaluated to

$$L\left(\psi_{\mathrm{S}},\psi_{\mathrm{S}}^*\right) = -\left[\nu\frac{d\tau_{\mathrm{S}}}{dz} + \frac{d\theta}{dz}\right]\frac{2\beta_0''}{\gamma_0\sigma} - \frac{[\beta_0'']^2\nu^2}{\gamma_0\sigma} + \frac{[\beta_0'']^2}{3\gamma_0\sigma^3}\,. \tag{3.14}$$

Equation (3.13) yields the Euler–Lagrange equations

$$\frac{\partial L}{\partial r_j} - \frac{d}{dz}\frac{\partial L}{\partial \dot{r}_j} = 0 \tag{3.15}$$

for each soliton parameter $r_j = \sigma, \nu, \tau_{\mathrm{S}}, \theta$. They result in the following relations for the soliton parameters:

$$\frac{\beta_0''}{\gamma_0\sigma} = \mathrm{const}\,, \quad \nu = \mathrm{const}\,, \quad \frac{d\tau_{\mathrm{S}}}{dz} = -\beta_0''\nu\,, \quad \frac{d\theta}{dz} = -\nu\frac{d\tau_{\mathrm{S}}}{dz} + \frac{\beta_0''}{2}\left[\frac{1}{\sigma^2} - \nu^2\right]. \tag{3.16}$$

This means that a free soliton keeps its frequency offset (ν) and duration (σ). A constant frequency offset changes the group velocity, therefore the soliton delay $\tau_{\mathrm{S}}(z) = -z\beta_0''\nu$ is changing.

The soliton equation (3.2) involves higher order terms which can be included into the above formalism as perturbations to the standard NLS equation [43]. The perturbed soliton equation (3.2) is equivalent to the variational problem

$$\frac{\delta}{\delta\psi^*}\mathcal{L}_{\mathrm{NLS}}(\psi,\psi^*) = iF(\psi,\psi^*) \tag{3.17}$$

with perturbation

$$\begin{aligned} F(\psi,\psi^*,\psi_{\mathrm{DW}},\psi_{\mathrm{DW}}^*) = {} & -\beta_0'\partial_\tau\psi_{\mathrm{S}} + i\sum_{m=3}^{M}\frac{\beta_0^{(m)}}{m!}\left[i\partial_\tau\right]^m\psi \\ & + i2\gamma_0\left[1+i\eta_0\partial_\tau\right]\left[|\psi_{\mathrm{DW}}|^2\,\psi\right] - \gamma_0\eta_0\,\partial_\tau\left[|\psi|^2\,\psi\right] \\ & + if_R\gamma_0\left[1+i\eta_0\partial_\tau\right]\left[\psi(z,\tau)\int_{-\infty}^{\infty}H(\tau')\left|\psi(z,\tau-\tau')\right|^2 d\tau'\right] \end{aligned} \tag{3.18}$$

where $H(\tau) = h(\tau) - \delta(\tau)$ describes the delayed Raman response. XPM with the DW is also included as a perturbation. It is treated as a yet unknown function. If the perturbation is not vanishing, we follow Hasegawa [43] and use the chain rule

$$\frac{\partial\mathcal{L}}{\partial r_j} = \int d\tau\left[\frac{\delta\mathcal{L}}{\delta\psi_{\mathrm{S}}^*}\frac{\partial\psi_{\mathrm{S}}^*}{\partial r_j} + \frac{\delta\mathcal{L}}{\delta\psi_{\mathrm{S}}}\frac{\partial\psi_{\mathrm{S}}}{\partial r_j}\right], \tag{3.19}$$

resulting in equations

$$\frac{\partial L}{\partial r_j} - \frac{d}{dz}\frac{\partial L}{\partial\dot{r}_j} = i\int d\tau\,\left[F\,\frac{\partial\psi_{\mathrm{S}}^*}{\partial r_j} - F^*\,\frac{\partial\psi_{\mathrm{S}}}{\partial r_j}\right] = -2\int d\tau\;\mathrm{Im}\left(F\,\frac{\partial\psi_{\mathrm{S},0}^*}{\partial r_j}\right) \tag{3.20}$$

for each soliton parameter $r_j = \sigma, \nu, \tau_{\mathrm{S}}, \theta$. This set of ODEs can be solved by any appropriate means, analytically or numerically.

It should be mentioned that it is just as well possible to derive a variational approximation by stating the appropriate Lagrange density for the full equation (3.2) and proceeding as usual. The formulation of the variational approximation as a perturbation theory is actually much more general. It is not necessary for the perturbation to be small, nor must the unperturbed equation be integrable (e.g. by means of inverse scattering theory). The only necessities are that the full equation (here (3.2)) must have a variational form, i.e. it must be defined by some Lagrangian density, and the ansatz function must be localized in τ. Of course, this is not a rigorous procedure. To choose an ansatz function is prone to physical intuition, and not every choice may produce adequate results. Still, if a solution is tested against some exemplary cases, it is very likely producing good predictions in most cases. For further discussion and examples see [43, 53].

The described SPT for the given NLS equation and soliton ansatz function is a standard procedure. Yet, it has the shortcoming that the soliton compression and soliton peak power evolution are not always predicted correctly. When applied to the XPM interaction of soliton and DW considered here, it falsely predicts no changes in soliton amplitude and duration. Further, the solitons loss in peak power due to the Raman effect is not predicted. This shortcoming of the standard NLS-perturbation theory could be explained as follows. The dispersion coefficients, in particular the one for GVD $\beta''(\omega_0)$, are evaluated at the soliton carrier frequency, and should change when the soliton frequency is shifted due to XPM by the DW or Raman scattering. The GVD profile in the anomalous region is steep, and thus the GVD coefficient changes considerably even for a small shift in frequency. Since the soliton amplitude depends on the GVD coefficient, it changes accordingly. Yet, all coefficients in (3.2) are constant. In the following an evolution equation with frequency dependent GVD and nonlinear coefficients is derived. The perturbation theory for this modified equation will turn out to overcome the shortcomings of the standard perturbation theory.

3.2.2 z-dependence of dispersion and nonlinear coefficients

In order to incorporate the soliton's shifting carrier frequency, Equation (3.2) needs some reformulation [P1]. The soliton carrier frequency is permanently shifted in the course of interaction with the DW (Figure 2.8c), let it be

$$\omega_{\mathrm{S}}(z) = \omega_0 + \nu(z), \tag{3.21}$$

where $\nu(z)$ is a yet unknown shift from initial soliton frequency ω_0, so initially $\nu(0) = 0$. In contrast, the DW frequency offset Δ is given given in advance as a constant initial condition.

Introducing a new envelope for the soliton

$$\psi_{\mathrm{S}}(z,\tau) = \psi_0(z,\tau)\exp\left(-i\nu(z)\tau + i\int_0^z D(\omega_0+\nu(z'))dz'\right) \tag{3.22}$$

and plugging it into (3.2) yields a new perturbation equation which recognizes a varying

carrier frequency

$$
\begin{aligned}
& i\partial_z\psi_0 + \tau\left[\frac{d\nu}{dz}\right]\psi_0 + \sum_{m=1}^{M}\frac{D^{(m)}(\nu)}{m!}\left[i\partial_\tau\right]^m\psi_0 \\
& \quad + 2\gamma_{\mathrm{S}}\left[1+i\eta_{\mathrm{S}}\partial_\tau\right]\left[\left|\psi_{\mathrm{DW}}\right|^2\psi_0\right] \\
& \quad + \gamma_{\mathrm{S}}\left[1+i\eta_{\mathrm{S}}\partial_\tau\right]\left[\psi_0(z,\tau)\int_{-\infty}^{\infty}R(\tau')\left|\psi_0(z,\tau-\tau')\right|^2 d\tau'\right] = 0.
\end{aligned}
\tag{3.23}
$$

with the new $z-$dependent self-steepening and nonlinear parameters

$$
\eta_{\mathrm{S}}(z) = \frac{1}{\omega_0+\nu(z)} \quad \text{and} \quad \gamma_{\mathrm{S}}(z) = \frac{n_{2,0}\left[\omega_0+\nu(z)\right]}{c}. \tag{3.24}
$$

In the derivation of (3.23) the following property of the dispersion operator was used:

$$
D\left(i\partial_\tau\right)\left[\psi_0 e^{-i\nu\tau}\right] = e^{-i\nu\tau}D\left(\nu+i\partial_\tau\right)\psi_0 \tag{3.25}
$$

The dispersion operator can be expanded around ν:

$$
D\left(\nu+i\partial_\tau\right) = \sum_{m\geq 0}\frac{D^{(m)}(\nu)}{m!}[i\partial_\tau]^m \tag{3.26}
$$

The coefficients of this expansion can be written again in terms of the propagation constant β as

$$
\sum_{m\geq 1}\frac{D^{(m)}(\nu)}{m!}[i\partial_\tau]^m = i\left[\beta'(\omega_0+\nu)-\beta'(\omega_0)\right]\partial_\tau + \sum_{m\geq 2}\frac{\beta^{(m)}(\omega_0+\nu(z))}{m!}[i\partial_\tau]^m. \tag{3.27}
$$

The coefficients in (3.23) are functions of the $z-$dependent soliton frequency, and therefore change with the soliton frequency shift. Especially, the GVD is now evaluated accurately at any soliton carrier frequency $\omega_0+\nu(z)$, so the higher order dispersion terms become less important in the new equation (3.23) compared to (3.2). In all following calculations the maximal dispersion order $M=4$ is chosen as sufficient (after testing dispersion orders up to $M=6$). The new term involving $d\nu/dz$ is particularly important. The introduction of the additional shift ν is mathematically equivalent to introducing an accelerated coordinate system in classical quantum mechanics [67].

A SPT for a NLS equation with $z-$dependent coefficients is known, e.g. for dispersion managed soliton propagation [43]. The modified equation (3.23) is split up to formulate the new perturbation equation

$$
\begin{aligned}
& i\partial_z\psi_0 + i\left[\beta'(\omega_0+\nu(z))-\beta'(\omega_0)\right]\partial_\tau\psi_0 \\
& \quad - \frac{\beta''(\omega_0+\nu(z))}{2}\partial_\tau^2\psi_0 + \gamma_{\mathrm{S}}(z)\left|\psi_0\right|^2\psi_0 + \tau\frac{d\nu}{ds}\psi_0 = iF\left(\psi_0,\psi_{\mathrm{DW}}\right)
\end{aligned}
\tag{3.28}
$$

with perturbation function

$$F\left(\psi_0,\psi_{\mathrm{DW}}\right)=i\sum_{m=3}^{M}\frac{\beta^{(m)}(\omega_0+\nu(z))}{m!}\left[i\partial_\tau\right]^m\psi_0 \tag{3.29}$$
$$+i2\gamma_{\mathrm{S}}\left[1+i\eta_{\mathrm{S}}\partial_\tau\right]\left[\left|\psi_{\mathrm{DW}}\right|^2\psi_0\right]-\gamma_{\mathrm{S}}\eta_{\mathrm{S}}\partial_\tau\left[\left|\psi_0\right|^2\psi_0\right]$$
$$+if_R\gamma_{\mathrm{S}}\left[1+i\eta_{\mathrm{S}}\partial_\tau\right]\left[\psi_0(z,\tau)\int_{-\infty}^{\infty}H(\tau')\left|\psi_0(z,\tau-\tau')\right|^2d\tau'\right].$$

A Lagrangian which reproduces the unperturbed equation (3.28) by means of (3.10) is

$$\mathcal{L}_{(3.28)}=\frac{i}{2}\left[\psi^*\frac{\partial\psi}{\partial z}-\psi\frac{\partial\psi^*}{\partial z}\right]+\frac{i}{2}\left[\beta'(\omega_0+\nu(z))-\beta'(\omega_0)\right]\left[\psi^*\frac{\partial\psi}{\partial\tau}-\psi\frac{\partial\psi^*}{\partial\tau}\right] \tag{3.30}$$
$$-\frac{\beta''(\omega_0+\nu(z))}{2}\left|\frac{\partial\psi}{\partial\tau}\right|^2+\frac{\gamma_{\mathrm{S}}(z)}{2}\left|\psi\right|^4+\tau\frac{d\nu}{dz}\left|\psi\right|^2.$$

Then the procedure explained above can be directly applied. The detailed calculations are carried out in Appendix B. For a ansatz function

$$\psi_0(z,\tau)=\frac{1}{\sigma}\sqrt{\frac{\left|\beta''(\omega_0+\nu)\right|}{\gamma_{\mathrm{S}}}}\frac{\exp\left(i\theta\right)}{\cosh\frac{\tau-\tau_{\mathrm{S}}}{\sigma}} \tag{3.31}$$

and an unspecified perturbation F the following set of ODEs is derived describing the evolution of soliton duration

$$\frac{d}{dz}\left[\frac{1}{\sigma}\frac{\beta''(\omega_0+\nu)}{\gamma_{\mathrm{S}}}\right]=\int_{-\infty}^{\infty}d\tau\ \mathrm{Re}\left(F\psi_0^*\right) \tag{3.32a}$$

and soliton frequency shift, delay and phase

$$\frac{d\nu}{dz}=-\frac{\gamma_{\mathrm{S}}}{\beta''(\omega_0+\nu)}\int_{-\infty}^{\infty}d\tau\ \tanh\left(\frac{\tau-\tau_{\mathrm{S}}}{\sigma}\right)\mathrm{Im}\left(F\psi_0^*\right), \tag{3.32b}$$

$$\frac{d\tau_{\mathrm{S}}}{dz}=\beta'(\omega_0+\nu)-\beta'(\omega_0) \tag{3.32c}$$
$$+\frac{\gamma_{\mathrm{S}}\sigma^2}{\beta''(\omega_0+\nu)}\int_{-\infty}^{\infty}d\tau\ \frac{\tau-\tau_{\mathrm{S}}}{\sigma}\,\mathrm{Re}\left(F\psi_0^*\right),$$

$$\frac{d\theta}{dz}=\frac{\beta''(\omega_0+\nu)}{2}\frac{1}{\sigma^2} \tag{3.32d}$$
$$+\frac{\gamma_{\mathrm{S}}\sigma}{\beta''(\omega_0+\nu)}\int_{-\infty}^{\infty}d\tau\ \left[1-\frac{\tau-\tau_{\mathrm{S}}}{\sigma}\cdot\tanh\left(\frac{\tau-\tau_{\mathrm{S}}}{\sigma}\right)\right]\mathrm{Im}\left(F\psi_0^*\right).$$

To evaluate the ODEs (3.32) for the perturbation function (3.29), an explicit expression for the DW ψ_{DW} is required. The evolution of ψ_{DW} is governed by the GNLS equation (3.6).

3.3 Wave scattering at a moving solitonic barrier

This section attends to the DW equation (3.6)

$$i\partial_z\psi_{\mathrm{DW}}-\frac{\beta_1''}{2}\partial_\tau^2\psi_{\mathrm{DW}}+2\gamma_1\left|\psi_{\mathrm{S}}\right|^2\psi_{\mathrm{DW}}=0.$$

The soliton ansatz (3.31) is used to approximate the XPM term in (3.6) by

$$|\psi_{\mathrm{S}}|^2 = |\psi_0|^2 = \frac{1}{\sigma^2}\frac{|\beta''(\omega_0+\nu)|}{\gamma_{\mathrm{S}}}\frac{1}{\cosh^2\frac{\tau-\tau_0}{\sigma}}.$$

The soliton parameters σ, ν, τ_{S} are described by the set of ODEs (3.32), but for the following derivation they are treated as yet unknown parameters. It is assumed that the soliton parameters evolve slowly and that the DW can adjust itself to a slowly changing barrier height, delay and barrier velocity $d\tau_{\mathrm{S}}/dz$.

Equation (3.6) is mathematically equivalent to the quantum mechanical problem of a plane wave which is reflected or transmitted at a potential barrier. The problem of wave scattering at a moving barrier can be solved by a suitable transformation of the solution for the static barrier problem. A solution to the scattering problem of a plane wave at a static barrier of hyperbolic secant shape is known from quantum mechanics. In particular, an analytic solution to equation (3.6) could be directly plugged into the set of ODEs (3.32). The scattering problem of a continuous (or plane) wave at a solitonic barrier is solved here in optical terms, closely following the analog quantum mechanical solution. The results gained from the plane wave ansatz are quite far reaching, in the sense that they allow to make assumptions on appropriate initial parameters also for localized control pulses.

For the sake of self-containedness the related quantum mechanical equations are solved in Appendix C. To translate the quantum mechanical scattering problem and its solution into the optical terms, Table C.1 (Appendix C) can be used. It assigns to each quantum mechanical variable the equivalent optical one.

In analogy to (C.1) equation (3.6)

$$i\,\partial_z\psi_{\mathrm{DW}} - \frac{\beta_1''}{2}\partial_\tau^2\psi_{\mathrm{DW}} + V(\tau-\tau_{\mathrm{S}}(z))\psi_{\mathrm{DW}} = 0 \tag{3.33}$$

describes the scattering of a wave ψ_{DW} at a solitonic barrier

$$V(\tau) = \frac{V_0}{\cosh^2\frac{\tau}{\sigma}} \tag{3.34}$$

of height

$$V_0 = 2\frac{|\beta''(\omega_0+\nu)|}{\sigma^2}\frac{\gamma_1}{\gamma_{\mathrm{S}}}. \tag{3.35}$$

Far from the soliton the DW is assumed to be a plane wave

$$\psi_{\mathrm{DW}} = \sqrt{P_1}\cdot e^{\pm i\Delta\tau + i\kappa(\Delta)z} \tag{3.36}$$

obeying the dispersion relation

$$\kappa\,(\Delta) = \frac{\beta_1''}{2}\Delta^2. \tag{3.37}$$

P_1 denotes DW power.

The desired solutions are parametrized by the DW frequency Δ, which will be indicated as additional argument of the DW envelope $\psi_{\text{DW}}(z,\tau;\Delta)$. Remember, Δ is the offset from the frequency ω_1 of matching group velocity to soliton velocity, $\beta'(\omega_1) = \beta'(\omega_0)$, which defines the velocity $v_0 = 1/\beta'(\omega_0)$ of the co-moving τ-frame. The solutions must have a specific asymptotic property, which differs in the up- and down-switching case. Because the down-switching case can be easily mapped to the up-switching case, for now only the up-switching case is considered. Then the desired solution has the asymptotic properties, cf. (C.3),

$$\psi^{\uparrow}_{\text{DW}}(z,\tau;\Delta) = \sqrt{P_1}\cdot\begin{cases} e^{-i\Delta\tau+i\kappa(\Delta)z} + \text{r}\cdot e^{i\Delta_r\tau+i\kappa(\Delta_r)z} & \text{for} \quad \tau\to-\infty \\ \text{t}\cdot e^{-i\Delta\tau+i\kappa(\Delta)z} & \text{for} \quad \tau\to\infty \end{cases} \tag{3.38}$$

where $\text{t} = \text{t}(\Delta)$ and $\text{r} = \text{r}(\Delta)$ quantify transmission and reflection, respectively. The frequency offset Δ_r evolves with the soliton:

$$\Delta_r = \Delta - \frac{2}{\beta_1''}\frac{d\tau_{\text{S}}}{dz} \tag{3.39}$$

where the soliton moves with velocity $d\tau_{\text{S}}/dz$. Δ_r describes the frequency offset of the reflected wave from ω_1, so the frequency of the reflected wave is given by

$$\omega_r = \omega_1 - \Delta_r = \omega_1 - \Delta + \frac{2}{\beta_1''}\frac{d\tau_{\text{S}}}{dz}. \tag{3.40}$$

A full solution to (3.33) is derived in two steps. Firstly, the scattering problem at a moving barrier is mapped to a problem at a static barrier by a parameter transformation in analogy to the Galilei transformation (C.5). Equation (3.33) is solved by

$$\psi_{\text{DW}}\left(z,\tau;\bar{\Delta}\right) = \Phi(z,\xi)\cdot\exp i\left\{-\tau\left[\frac{1}{\beta_1''}\frac{d\tau_{\text{S}}}{dz}\right] + z\cdot\kappa\left(\frac{1}{\beta_1''}\frac{d\tau_{\text{S}}}{dz}\right)\right\}, \tag{3.41}$$

with

$$\xi = \tau - \tau_{\text{S}}(z), \quad \text{and} \quad \bar{\Delta} = \Delta - \frac{1}{\beta_1''}\frac{d\tau_{\text{S}}}{dz}, \tag{3.42}$$

if $\Phi(z,\xi)$ solves the static problem

$$i\,\partial_z\Phi - \frac{\beta_1''}{2}\partial_\xi^2\Phi + V(\xi)\Phi = 0 \tag{3.43}$$

with the asymptotic property

$$\Phi(z,\xi) = \sqrt{P_1}\cdot\begin{cases} e^{-i\Delta\xi+i\kappa(\Delta)z} + B^*\, e^{i\Delta\xi+i\kappa(\Delta)z} & \text{for} \quad \xi\to-\infty \\ A^* e^{-i\Delta\xi+i\kappa(\Delta)z} & \text{for} \quad \xi\to\infty \end{cases}. \tag{3.44}$$

The frequency of the reflected wave just changes its sign, and

$$A^*(\Delta) = \text{t}\left(\Delta - \frac{1}{\beta_1''}\frac{d\tau_{\text{S}}}{dz}\right) \quad \text{and} \quad B^*(\Delta) = \text{r}\left(\Delta - \frac{1}{\beta_1''}\frac{d\tau_{\text{S}}}{dz}\right). \tag{3.45}$$

The stars denote complex conjugates. They result from the translation of the quantum mechanical to optical variables, cf. C.1.

Secondly, the scattering problem (3.43) for a static barrier of hyperbolic secant shape is solved in analogy to a known analytic solution to the scattering problem (C.6) in quantum mechanics [50, 51, 34]. The ansatz $\Phi(z,\xi) = \sqrt{P_1}\,\phi(\xi)e^{i\kappa z}$ yields, cf. (C.12),

$$\partial_\xi^2\phi(\xi) + \left[\Delta^2 - \frac{2}{\beta_1''}V(\xi)\right]\phi(\xi) = 0. \tag{3.46}$$

Equation (3.46) can be transformed to a hypergeometric differential equation, cf. (C.21), which is solved in terms of a hypergeometric function ${}_2F_1$:

$$\phi(\xi) = A^* \cdot {}_2F_1\left(\mathscr{a}, \mathscr{b}; \mathscr{c}; \frac{1-\tanh\frac{\xi}{\sigma}}{2}\right)\left[e^{i\Delta\xi} + e^{-i\Delta\xi}\right] \tag{3.47}$$

with

$$A^* = \frac{\Gamma\left(\frac{1}{2} - i\sigma\Delta - i\mathfrak{s}\right)\Gamma\left(\frac{1}{2} - i\sigma\Delta + i\mathfrak{s}\right)}{\Gamma\left(1 - i\sigma\Delta\right)\Gamma\left(-i\sigma\Delta\right)} \tag{3.48}$$

and parameters

$$\mathscr{a} = 1 - i\sigma\Delta + i\mathfrak{s}\,, \quad \mathscr{b} = 1 - i\sigma\Delta - i\mathfrak{s}\,, \quad \mathscr{c} = 1 - i\sigma\Delta, \tag{3.49}$$

and

$$\mathfrak{s} = \frac{1}{2}\sqrt{\frac{8}{\beta_1''}\sigma^2 V_0 - 1}\,. \tag{3.50}$$

Details of the solution are found in Appendix C.

In the quantum mechanical formulation the amplitude of the incoming wave is set to 1. Here the DW power is given by P_1 and expressed relative to the initial soliton peak power $P_{\mathrm{S}}(0) = P_0$. Thus the DW power is defined as

$$P_1 = \mu \cdot P_0 = \mu\frac{|\beta''(\omega_0+\nu)|}{\sigma_0^2}\frac{1}{\gamma_{\mathrm{S}}} = \frac{\mu}{\gamma_{\mathrm{S}}L_0} \tag{3.51}$$

The DW power divided by the initial soliton peak power is denoted by $\mu = P_1/P_0 \ll 1$, and it is assumed to be small. $L_0 = \sigma_0^2/|\beta_0''|$ is the dispersion length of the initial soliton.

The resulting solution to the DW scattering problem (3.33) in the up-switching case is

$$\left|\psi_{\mathrm{DW}}^{\uparrow}(z,\tau;\bar{\Delta})\right|^2 = \frac{\mu}{\gamma_{\mathrm{S}}L_0}\cdot\mathcal{T}(\bar{\Delta})\cdot\left|{}_2F_1\left(\mathscr{a}, \mathscr{b}; \mathscr{c}; \frac{1-\tanh\frac{\tau-\tau_{\mathrm{S}}}{\sigma}}{2}\right)\right|^2 \tag{3.52}$$

with transmission coefficient

$$\mathcal{T}(\bar{\Delta}) = \left|t(\bar{\Delta})\right|^2 = \frac{\sinh^2\left(\pi\sigma\bar{\Delta}\right)}{\cosh^2(\pi\mathfrak{s}) + \sinh^2\left(\pi\sigma\bar{\Delta}\right)}. \tag{3.53}$$

The DW solution (3.52) can be inserted into the ODEs (3.32) describing the soliton evolution.

Lastly, remember, that the scattering solution has different asymptotic behavior in the up- and down-switching cases. In the down-switching case the frequency offset $\Delta < 0$ is negative, and the solution has the asymptotic properties

$$\psi^{\downarrow}_{\mathrm{DW}}(z,\tau;\Delta) = \begin{cases} t(\Delta)e^{i\Delta\tau+i\kappa(\Delta)z} & \text{for} \quad \tau \to -\infty \\ e^{i\Delta\tau+i\kappa(\Delta)Z} + r(\Delta)\, e^{-i\Delta_r\tau+i\kappa(\Delta_r)z} & \text{for} \quad \tau \to \infty \end{cases} \tag{3.54}$$

which can be easily traced back to the up-switching case by reversing τ. The solution to the static scattering problem then reads

$$\phi(\xi) = A^* \cdot {}_2F_1\left(a, b; c; y\right)\left[e^{i\Delta\xi} + e^{-i\Delta\xi}\right] \tag{3.55}$$

with the only new variable

$$y = \frac{1 - \tanh\frac{-\xi}{\sigma}}{2} = \frac{1 + \tanh\frac{\xi}{\sigma}}{2}. \tag{3.56}$$

while all other parameters are the same as in the up-switching case. Thus after the transformation (3.41) the solution to the DW scattering problem (3.33) in the down-switching case is

$$\left|\psi^{\downarrow}_{\mathrm{DW}}(z,\tau;\bar{\Delta})\right|^2 = \frac{\mu}{\gamma_{\mathrm{S}} L_0} \cdot \mathcal{T}\left(\bar{\Delta}\right) \cdot \left|{}_2F_1\left(a, b; c; \frac{1 + \tanh\frac{\tau-\tau_{\mathrm{S}}}{\sigma}}{2}\right)\right|^2. \tag{3.57}$$

The DW solution (3.52) and (3.57) for the up- and down-switching case, respectively, can be used directly together with the derived set of ODEs (3.32) describing the soliton evolution. The resulting model equations are discussed in the following chapter.

4 Soliton switching

The sequel expands on the insights offered by the modified soliton perturbation theory (SPT) on the interaction of solitons and a low-intensity continuous wave. Predictions based on the adiabatic theory of Chapter 3 are compared to results from numerical simulations. The adiabatic model equations yield a better understanding of the interaction, and they provide a practical tool to select appropriate initial parameters for numerical simulation or experiment. The new SPT allows to identify the self-steepening effect as an important contributor to the soliton switching process.

To get a clearer view on the soliton-dispersive wave interaction as such, Raman scattering is ignored (i.e. $f_R = 0$) in this chapter. The reported results are directly applicable to, e.g., Raman–free fibers. The Raman effect will be discussed separately in Chapter 5. The simulation equation (2.5) simplifies to an GNLS equation with Kerr nonlinearity:

$$i\partial_z\psi(z,\tau) + \hat{D}\left(i\partial_\tau\right)\psi(z,\tau) + \gamma_0\left[1 + i\eta_0\partial_\tau\right]\left[|\psi(z,\tau)|^2\,\psi(z,\tau)\right] = 0. \tag{4.1}$$

It still takes into account full dispersion ($\hat{D}$) and the self-steepening term ($\eta_0 \neq 0$).

Section 4.1 states the relevant set of ODEs describing soliton evolution for the soliton switching process. In Sections 4.2 and 4.3 example calculations for the soliton up- and down-switching are discussed in detail, predictions of the adiabatic model equations are compared to direct numerical simulation of (4.1). Section 4.4 shows how the adiabatic model equations help in finding initial pulse parameters for an effective interaction. We can determine the DW frequency interval suitable for an effective interaction [P2], thereby fully quantifying the essential *Velocity-matching condition* (p.14), which was stated before only as an empirical rule. In Section 4.5 the new SPT is applied to investigate the role of the self-steepening effect in soliton switching. Many numerical simulations indicated that the self-steepening term ($\sim \eta_0$) strongly aids soliton amplification. According calculations with the new SPT confirm this relation to be true.

4.1 Adiabatic model equations for soliton switching

For self-contained model equations the soliton and DW solutions derived in the last chapter must be combined. This section gives a brief survey of the perturbation equation which is relevant for the switching process, and states the resulting set of ODEs describing the evolution of the soliton under the influence of higher order dispersion, self-steepening, and XPM by the DW. In the next two sections the DW solutions for up- and down-switching cases are plugged into these ODEs, respectively, to obtain self-contained adiabatic model equations for either case.

Consider the propagation of a fundamental soliton with varying carrier frequency $\omega_0+\nu(z)$, $\nu(0) = 0$, and a low-intensity continuous DW with carrier frequency $\omega_1 + \Delta$, such that $\beta'(\omega_0) = \beta'(\omega_1)$. The evolution of a fundamental soliton (3.31)

$$\psi_0(z,\tau) = \frac{1}{\sigma}\sqrt{\frac{\beta''(\omega_0+\nu)}{\gamma_\mathrm{S}}}\frac{\exp(i\theta)}{\cosh\frac{\tau-\tau_\mathrm{S}}{\sigma}}$$

with delay $\tau_\mathrm{S}(z)$, duration $\sigma(z)$, shift of carrier frequency $\nu(z)$ and phase $\theta(z)$ is described by the perturbation equation (3.28)

$$\begin{aligned} &i\partial_z\psi_0 + i\left[\beta'(\omega_0+\nu) - \beta'(\omega_0)\right]\partial_\tau\psi_0 \\ &\quad - \frac{\beta''(\omega_0+\nu)}{2}\partial_\tau^2\psi_0 + \gamma_\mathrm{S}\left|\psi_0\right|^2\psi_0 + \tau\frac{d\nu}{dz}\cdot\psi_0 = iF\left(\psi_0,\psi_\mathrm{DW}\right). \end{aligned}$$

The perturbation function

$$\begin{aligned} F\left(\psi_0,\psi_\mathrm{DW}\right) = i\sum_{m=3}^{4}\frac{\beta^{(m)}(\omega_0+\nu)}{m!}\left[i\partial_\tau\right]^m\psi_0 \\ - \gamma_\mathrm{S}\eta_\mathrm{S}\partial_\tau\left[\left|\psi_0\right|^2\psi_0\right] + i2\gamma_\mathrm{S}\left[1+i\eta_\mathrm{S}\partial_\tau\right]\left[\left|\psi_\mathrm{DW}\right|^2\psi_0\right] \end{aligned} \tag{4.2}$$

includes effects of third ($\sim\beta^{(3)}$) and fourth ($\sim\beta^{(4)}$) order dispersion, self steepening ($\sim\eta_\mathrm{S}$) and XPM by the DW ψ_DW. The set of ODEs (3.32) describing the evolution of the soliton parameters under the influence of the perturbation F given by (4.2) takes the form

$$\frac{d}{dz}\left[\frac{\beta''(\omega_0+\nu)}{\sigma\gamma_\mathrm{S}}\right] = -2\eta_\mathrm{S}\frac{\beta''(\omega_0+\nu)}{\sigma^3}\int d\tau\,\frac{\tanh\frac{\tau-\tau_\mathrm{S}}{\sigma}}{\cosh^2\frac{\tau-\tau_\mathrm{S}}{\sigma}}\left|\psi_\mathrm{DW}(z,\tau)\right|^2, \tag{4.3a}$$

$$\frac{d\nu}{dz} = -\frac{2\gamma_\mathrm{S}}{\sigma^2}\int d\tau\,\frac{\tanh\frac{\tau-\tau_\mathrm{S}}{\sigma}}{\cosh^2\frac{\tau-\tau_\mathrm{S}}{\sigma}}\left|\psi_\mathrm{DW}(z,\tau)\right|^2, \tag{4.3b}$$

$$\begin{aligned} \frac{d\tau_\mathrm{S}}{dz} &= \beta'(\omega_0+\nu) - \beta'(\omega_0) + \eta_\mathrm{S}\frac{\beta''(\omega_0+\nu)}{\sigma^2} + \frac{\beta^{(3)}(\omega_0+\nu)}{6\sigma^2} \\ &\quad + \frac{2\gamma_\mathrm{S}}{\sigma}\eta_\mathrm{S}\int d\tau\,\frac{1-\frac{\tau-\tau_\mathrm{S}}{\sigma}\cdot\tanh\frac{\tau-\tau_\mathrm{S}}{\sigma}}{\cosh^2\frac{\tau-\tau_\mathrm{S}}{\sigma}}\left|\psi_\mathrm{DW}(z,\tau)\right|^2, \end{aligned} \tag{4.3c}$$

$$\begin{aligned} \frac{d\theta}{dz} &= \frac{\beta''(\omega_0+\nu)}{2}\frac{1}{\sigma^2} + \beta^{(4)}(\omega_0+\nu)\frac{7}{72}\frac{1}{\sigma^4} \\ &\quad + \frac{2\gamma_\mathrm{S}}{\sigma}\int d\tau\,\frac{1-\frac{\tau-\tau_\mathrm{S}}{\sigma}\cdot\tanh\frac{\tau-\tau_\mathrm{S}}{\sigma}}{\cosh^2\frac{\tau-\tau_\mathrm{S}}{\sigma}}\left|\psi_\mathrm{DW}(z,\tau)\right|^2. \end{aligned} \tag{4.3d}$$

The contributions of the different effects included in the specific perturbation function (4.2) are calculated individually in Appendix B.

An explicit expression for soliton duration σ as function of frequency shift ν can be derived. For this (4.3a) and (4.3b) are combined to

$$\frac{d}{dz}\left[\frac{\beta''(\omega_0+\nu)}{\sigma\gamma_\mathrm{S}}\right] = \frac{\beta''(\omega_0+\nu)}{\sigma\gamma_\mathrm{S}}\eta_\mathrm{S}\frac{d\nu}{dz}.$$

Integration of this relation results in

$$\frac{\sigma(z)}{\sigma(0)} = \frac{\beta''(\omega_0+\nu(z))}{\beta''(\omega_0)}\frac{\gamma_{\mathrm{S}}(0)}{\gamma_{\mathrm{S}}(z)}\frac{\eta_{\mathrm{S}}(z)}{\eta_{\mathrm{S}}(0)} = \frac{\beta''(\omega_0+\nu(z))}{\beta''(\omega_0)}\frac{1}{\left[1+\frac{\nu(z)}{\omega_0}\right]^2}. \tag{4.4}$$

According to (4.4) the soliton duration changes due to the frequency dependent group velocity dispersion coefficient β'' and the frequency dependent self-steepening and nonlinearity coefficients η_{S} and γ_{S}. The approximate solution to the soliton equation (3.28), (4.2) is given by (3.31), the parameters of which are the solutions to ODEs (4.3b)-(4.3d) together with (4.4). The main interest here lies on the expected changes in soliton frequency, duration and delay. The phase shift is of less concern here and will be neglected in subsequent considerations. Judging from (4.3b) and (4.3c) it can already be stated that the expected soliton frequency shift is due solely to XPM by the dispersive wave, represented by the integral term in (4.3b). The soliton delay changes due to frequency dependent group velocity ($\sim \beta'$), self-steepening ($\sim \eta_{\mathrm{S}}$), third order dispersion ($\sim \beta^{(3)}$) and XPM represented by the integral term in (4.3c).

The integrals appearing in (4.3), which describe the effect of XPM, depend on the intensity $|\psi_{\mathrm{DW}}|^2$ of the DW. The scattering problem (3.6) for the weak continuous control wave at a moving barrier constituted by the fundamental soliton (3.31) was solved in Section 3.3 for both settings, up- and down switching.

4.2 Up-switching. Comparison to numerics

In this section the adiabatic model equations for soliton-up switching by a continuous DW are stated, and their predictions are compared to the results of a numerical solution of (4.1). For the up-switching case, the set of ODEs (4.3b) and (4.3c) are combined with the solution (3.52) to the DW scattering problem in the up-switching case. Evolution of the soliton frequency shift ν and delay τ_{S} are described by the two ODEs:

$$\frac{d\nu}{dz} = \frac{4\mu}{\sigma L_0}\left[1+\frac{\nu}{\omega_0}\right]\mathcal{I}_1, \tag{4.5a}$$

$$\frac{d\tau_{\mathrm{S}}}{dz} = \mathcal{B} + \frac{4\mu}{\omega_0 L_0}\mathcal{I}_2. \tag{4.5b}$$

The auxiliary parameter

$$\mathcal{B} = \left[\beta'(\omega_0+\nu)-\beta'(\omega_0)\right] - \eta_{\mathrm{S}}\frac{\beta''(\omega_0+\nu)}{\sigma^2} + \frac{\beta^{(3)}(\omega_0+\nu)}{6\sigma^2} \tag{4.6}$$

describes how the soliton delay is influenced by self-steepening ($\sim \eta_{\mathrm{S}}$) and higher order dispersion ($\sim \beta^{(3)}$). The integral terms involve the DW solution and are given by

$$\mathcal{I}_1 = \mathcal{T}\int_0^1 dy\ |{}_2F_1\,(a,b;c;y)|^2\cdot[2y-1]\,, \tag{4.7a}$$

$$\mathcal{I}_2 = \mathcal{T}\int_0^1 dy\ |{}_2F_1\,(a,b;c;y)|^2\cdot[1-[2y-1]\operatorname{arctanh}(2y-1)]\,, \tag{4.7b}$$

They result from the integral terms in (4.3) by introducing the new integration variable $y = \frac{1}{2}\left[1 - \tanh\frac{\tau-\tau_\mathrm{S}}{\sigma}\right]$. The hypergeometric function ${}_2F_1$ takes arguments

$$\mathscr{a} = \frac{1}{2} - i\sigma\bar{\Delta} - i\mathscr{s}, \quad \mathscr{b} = \frac{1}{2} - i\sigma\bar{\Delta} + i\mathscr{s}, \quad \mathscr{c} = 1 - i\sigma\bar{\Delta}, \tag{4.8}$$

with parameters

$$\mathscr{s} = \frac{1}{2}\sqrt{16\frac{|\beta''(\omega_0+\nu)|}{\beta_1''}\frac{\omega_1}{\omega_0+\nu} - 1}, \tag{4.9}$$

and

$$\bar{\Delta} = \Delta - \frac{1}{\beta_1''}\frac{d\tau_\mathrm{S}}{dz}. \tag{4.10}$$

The transmission coefficient is

$$\mathscr{T} = \frac{\sinh^2\left(\pi\sigma\bar{\Delta}\right)}{\sinh^2\left(\pi\sigma\bar{\Delta}\right) + \cosh^2\left(\pi\mathscr{s}\right)}. \tag{4.11}$$

Note that the ODE for the frequency shift ν does not depend on soliton delay τ_S.

The ODE system (4.5) is solved within seconds, if the integrals (4.7) are tabulated beforehand. For fixed DW parameters Δ and μ the integrals $\mathscr{I}_1(\nu)$, $\mathscr{I}_2(\nu)$ are calculated for values of ν in a generously chosen interval around $\nu = 0$. Both integrals involve the converted DW frequency $\bar{\Delta}$ which is depending on $d\tau_\mathrm{S}/dz$. The tabulation used the approximation $d\tau_\mathrm{S}/dz \approx \mathscr{B}$ by the auxiliary parameter (4.6) according to (4.5b). The ODE system (4.5) provides a quick and easy tool to inspect the (approximate) soliton behavior and to gather information aiding a better understanding of the interaction.

In Figure 4.1 the predictions of (4.5) are compared to a numerical solution of the GNLS equation (4.1). Results are shown for the interaction of a soliton with initial (circular) frequency $\omega_0 = 0.67\,\mathrm{rad\,fs^{-1}}$ and initial duration $\sigma_0 = 40\,\mathrm{fs}$ (2.8 µm wavelength, 70.5 fs full width at half maximum (FWHM)) with a continuous DW with initial frequency offset $\Delta = 0.1\,\mathrm{rad\,fs^{-1}}$ and 1 % initial soliton peak power ($\omega_1+\Delta = 3.586\,\mathrm{rad\,fs^{-1}}$ or 0.525 µm wavelength, $\mu = 0.01$).

The temporal evolution of both pulses is depicted in Figure 4.1a. The soliton trajectory is well reproduced by the adiabatic model equations as indicated by the dashed line. All visibly distinct patterns of the interaction picture are tagged with letters: (A) is the incoming DW. Initially the soliton and the incoming wave are superimposed. The correct combination of the reflected and the transmitted waves is then self-organized as the system evolves. (B) shows the interference of the incoming and the scattered DW. The line separating regions (A) and (B) stems from the adjusting of the initially superimposed pulses. This line also appears on the right hand side of the soliton – as the DW is fully reflected by the soliton, only the relaxing of the DW part initially overlapping with the soliton is seen. (C) indicates the point at which the compressed soliton becomes transparent to the DW, more and more parts of which are transmitted through the soliton. Pattern (D) represents a caustic structure created by the

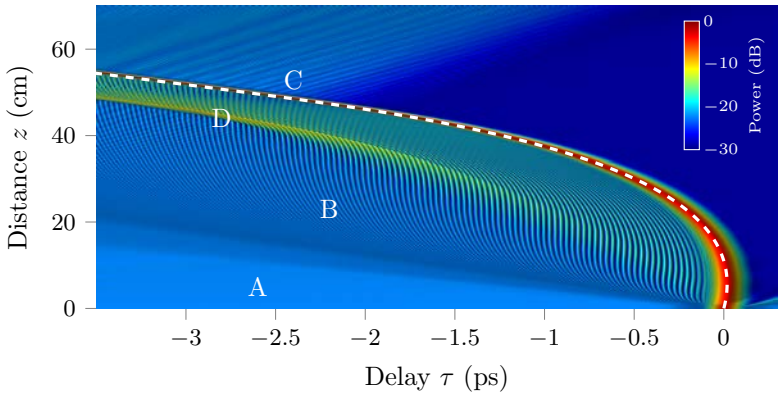

(a) Temporal evolution. White dashed lines indicate predictions from the adiabatic model equations.

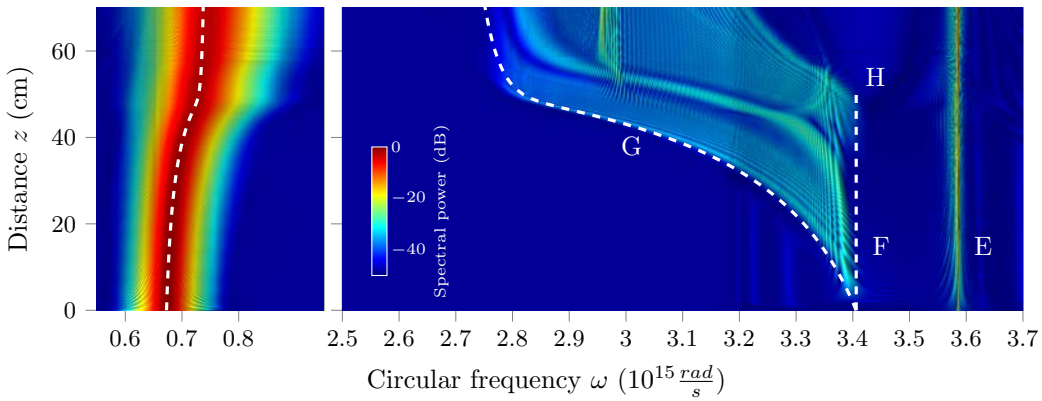

(b) Spectral evolution of soliton (left frame) and DW (right frame). White dashed lines indicate predictions from the adiabatic model equations.

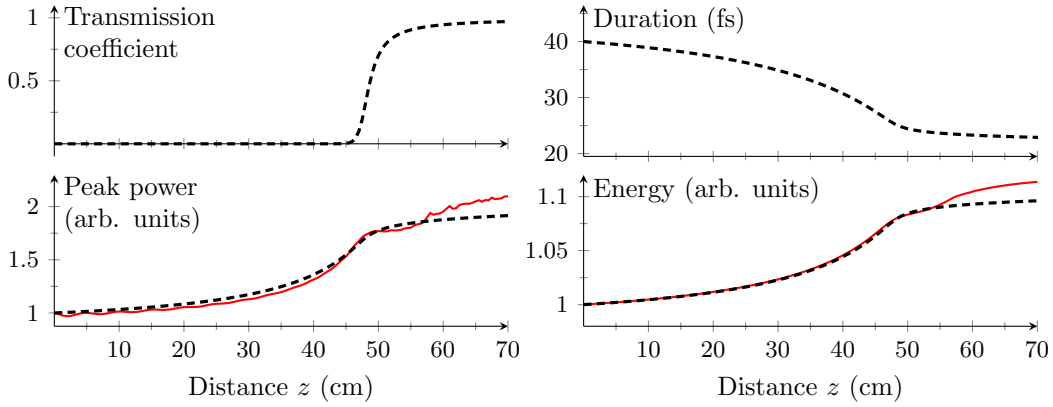

(c) Evolution of the soliton parameters along the fiber. Black dashed lines result from the adiabatic model equations; red solid lines are from the numerical solution of the full GNLSE.

Figure 4.1: Interaction of a soliton of initial (circular) frequency $\omega_0 = 0.67\,\mathrm{rad\,fs^{-1}}$ and initial duration $\sigma_0 = 40\,\mathrm{fs}$ (2.8 µm wavelength, 70.5 fs FWHM) with a continuous DW of initial frequency offset $\Delta = 0.1\,\mathrm{rad\,fs^{-1}}$ and 1 % initial soliton peak power ($\omega_1 + \Delta = 3.586\,\mathrm{rad\,fs^{-1}}$ or 0.525 µm wavelength, $\mu = 0.01$). Comparison of numerical and analytical results.

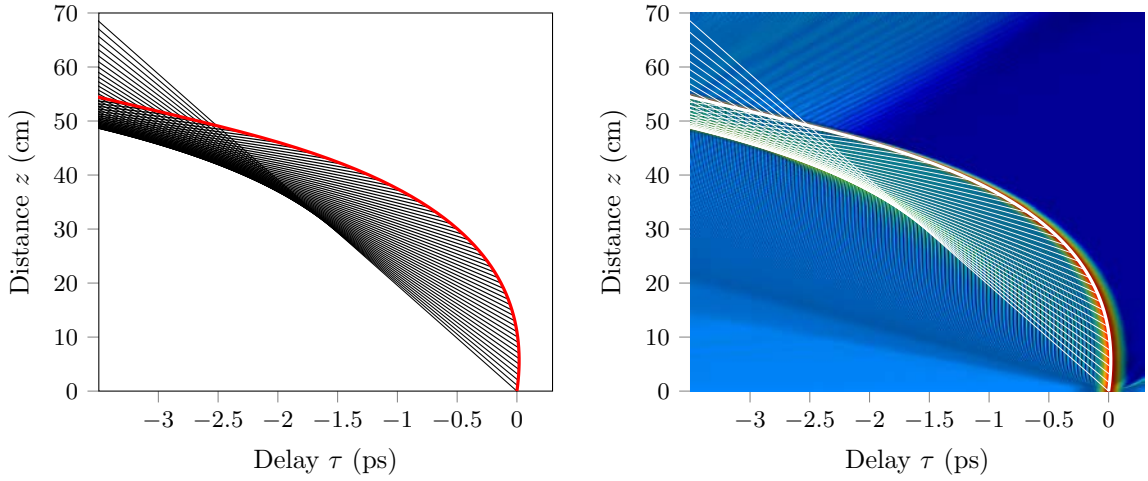

(a) The light rays of the DW reflected at the accelerated soliton (red line) form a caustic structure.

(b) Comparison of the caustic structure of frame (a) to numerical simulation.

Figure 4.2: Soliton trajectory (thick line) and geometric rays for the reflected parts of theDW (thin lines) are plotted for the calculation in Fig. 4.1. The caustic structure corresponds to that in Figure 4.1a. Note that some rays can intersect the soliton trajectory once again (starting from $z \approx 50\,\mathrm{cm}$); the reflected parts of the DW then experience their second scattering.

reflected DWs. In ray optics a caustic is the envelope of the light rays which are reflected from a curved mirror. Here the accelerated soliton acts as a curved mirror (Figure 4.2). In Figure 4.2a the rays for the reflected DW are plotted in the sense of geometrical optics using the frequency of the reflected wave (3.40)

$$\omega_r = \omega_1 - \Delta + \frac{2}{\beta_1''}\frac{d\tau_\mathrm{S}}{dz}$$

at each point of the soliton trajectory $\tau_\mathrm{S}(z)$. Figure 4.2b shows a direct comparison to the numerical calculation. The power density plot of the temporal domain is the same as in Figure 4.1a. Another observation made in Figure 4.2a is that the accelerated soliton catches up with the already reflected DWs, which are then scattered once again. This second reflection can again influence the soliton parameters.

The spectral window for the soliton is shown in Figure 4.1b (left frame). The evolution of the soliton carrier frequency is well reproduced by the adiabatic equations (indicated by the white dashed line). The soliton frequency shifts from initially $0.67\,\mathrm{rad\,fs^{-1}}$ (wavelength $2.8\,\mu\mathrm{m}$) to about $0.73\,\mathrm{rad\,fs^{-1}}$ (wavelength $2.58\,\mu\mathrm{m}$) at 50 cm propagation distance right before the reflected DW is reflected a second time at the soliton.

The spectral window for the DWs is shown in Figure 4.1b (right frame). (E) is the spectral envelope of the incident dispersive pump wave at carrier frequency $3.59\,\mathrm{rad\,s^{-1}}$ (wavelength $0.525\,\mu\mathrm{m}$). Line (F) indicates the converted frequency of the wave reflected by the soliton that is initially motionless in the reference frame. This frequency can be predicted by the Doppler relation (2.13). It was calculated in [90, 32, 77] and measured in [32, 85]. In the

introductory Section 2.3 the relation (2.14)

$$\beta'(\omega_0) = \frac{\beta(\omega_{\rm out}) - \beta(\omega_{\rm in})}{\omega_{\rm out} - \omega_{\rm in}}.$$

occurred for the frequencies $\omega_{\rm in}$, $\omega_{\rm out}$ of incoming and outgoing/reflected waves at a solitonic barrier moving with constant velocity $1/\beta'(\omega_{\rm S})$. In the terms of the present chapter the constant soliton frequency ω_0 is replaced by the $z-$dependent frequency $\omega_{\rm S}$,

$$\beta'(\omega_{\rm S}) = \frac{\beta(\omega_{\rm out}) - \beta(\omega_{\rm in})}{\omega_{\rm out} - \omega_{\rm in}},$$

and the frequency of the incoming wave is $\omega_{\rm in} = \omega_1 + \Delta$. Quadratic approximation of $\beta(\omega)$ near the reference frequency ω_1 reduces the implicit relation (2.14) between frequencies of the in- and outgoing waves to the following explicit form

$$\omega_{\rm out} = \omega_1 - \Delta + \frac{2}{\beta''(\omega_1)}\left[\beta'(\omega_0+\nu) - \beta'(\omega_0)\right]. \tag{4.12}$$

Yet, the soliton does not remain motionless nor is it moving with constant velocity, it is accelerated. The frequency of the reflected wave quickly changes as the soliton moves along the trajectory shown in Figure 4.1a. The frequency (3.40) of the reflected DW together with the ODE (4.5b) for the soliton delay:

$$\omega_r = \omega_1 - \Delta + \frac{2}{\beta_1''}\left[\left[\beta'(\omega_0+\nu) - \beta'(\omega_0)\right] - \eta_{\rm S}\frac{\beta''(\omega_0+\nu)}{\sigma^2} + \frac{\beta^{(3)}(\omega_0+\nu)}{6\sigma^2} + \frac{4\mu}{\omega_0 L_0}\mathcal{J}_2\right]$$

provides line (G), which accurately quantifies the range of DW frequencies that are observed in numerics. Once the soliton becomes transparent, the frequency conversion ceases. It is clear from direct comparison, that the relation (3.40) for the reflected wave's frequency derived from the adiabatic model equations generalizes (4.12), since it additionally describes the influence of self-steepening, higher order dispersion and the acceleration by XPM, cf. (4.5b). The depletion zone (H) in the spectral evolution of the reflected wave appears due to the second scattering of the reflected waves (Figure 4.2a), as their frequency is converted down once more.

With the solution of the ODEs (4.5) also the evolution of all other soliton parameters can be accessed. In Figure 4.1c are plotted against propagation distance z: the transmission coefficient (4.11), soliton peak power

$$\begin{aligned}\frac{P_{\rm S}(z)}{P_{\rm S}(0)} &= \left[\frac{\sigma(0)}{\sigma(z)}\right]^2 \frac{\gamma_{\rm S}(0)}{\gamma_{\rm S}(z)}\frac{\beta''(\omega_0+\nu)}{\beta''(\omega_0)} = \frac{\gamma_{\rm S}(z)}{\gamma_{\rm S}(0)}\left[\frac{\eta_{\rm S}(0)}{\eta_{\rm S}(z)}\right]^2 \frac{\beta''(\omega_0)}{\beta''(\omega_0+\nu(z))} \\ &= \left[1+\frac{\nu}{\omega_0}\right]^3 \frac{\beta''(\omega_0)}{\beta''(\omega_0+\nu(z))}\end{aligned} \tag{4.13}$$

and soliton energy

$$\frac{\mathscr{E}_{\rm S}(z)}{\mathscr{E}_{\rm S}(0)} = \frac{\sigma(0)}{\sigma(z)}\frac{\gamma_{\rm S}(0)}{\gamma_{\rm S}(z)}\frac{\beta''(\omega_0+\nu(z))}{\beta''(\omega_0)} = 1 + \frac{\nu(z)}{\omega_0}.$$

The energy $\mathscr{E}_\mathrm{S} = \int |\psi_0(z,\tau')|^2 d\tau' = \frac{2}{\sigma}\frac{|\beta''(\omega_0+\nu)|}{\gamma_\mathrm{S}}$ is calculated using the soliton ansatz function (3.31).

The transmission coefficient for a soliton that is motionless in the reference frame was estimated in [15] using two coupled NLS equations. Equation (4.11) provides a better insight on $\mathscr{T}|_{z=0}$ because it accounts for the self-steepening and higher order dispersion. Moreover, the adiabatic ODEs quantify the increase in the transmission coefficient with z as shown in Figure 4.1c (top left frame). For the given example, the DW is no longer entirely reflected starting at $z \approx 45\,\mathrm{cm}$ until the soliton becomes fully transparent at about 50 cm, which matches the observation in Figure 4.1a (C).

Figure 4.1c (bottom left frame) shows the increase in soliton peak power as derived from the adiabatic ODEs (red line) and from the numerical solution of the full GNLSE (black dashed line). The slight disagreement over the course of the peak power curve is to be expected since, e.g., oscillations of the soliton amplitude cannot be captured by the SPT [49]. Moreover, the soliton peak power undergoes a further slight amplification at $z \approx 50\,\mathrm{cm}$, when the reflected waves are reflected a second time. The second scattering is beyond the scope of this study, yet it explains the underestimation of the final soliton peak power by the adiabatic ODEs. Nevertheless, the adiabatic ODEs yield the correct trend and provide a reasonable estimate of the final peak power. The increase in peak power and the simultaneous decrease in soliton duration confirms the idea that the soliton is compressed, cf. Figure 4.1c (top right frame). The amplification of peak power by a factor 2 is accompanied by an increase in the soliton energy by only a factor 1.1 as shown in Fig. 4.1c (bottom right frame). This is a manifestation of the fact that soliton amplification occurs via a relatively small carrier frequency shift that is imposed on a very steep GVD profile.

4.3 Down-switching. Comparison to numerics

In the down switching scenario the soliton is slightly slower than the control wave. In the co-moving frame, the control wave approaches the soliton from the right. The model equations differ only slightly from the ones in the up-switching case. The adiabatic ODEs for the soliton (4.3b)-(4.3c) are combined with the solution (3.57) for a scattering problem with the asymptotic limits suitable for the down-switching case. The resulting ODEs for soliton frequency shift and peak position are

$$\frac{d\nu}{dz} = -\frac{4\mu}{\sigma L_0}\left[1+\frac{\nu}{\omega_0}\right]\mathcal{I}_1, \tag{4.14a}$$

$$\frac{d\tau_\mathrm{S}}{dz} = \mathscr{B} + \frac{4\mu}{\omega_0 L_0}\mathcal{I}_2. \tag{4.14b}$$

All parameters involved are defined as in the up-switching case. Also the integrals $\mathcal{I}_1$ and $\mathcal{I}_2$ are still defined by (4.7), with the only exception that the hypergeometric functions depend on the variable $y = \frac{1}{2}\left[1+\tanh\frac{\tau-\tau_\mathrm{S}}{\sigma}\right]$, in contrast to the up-switching case. The introduction of y as new integration variable ultimately results in a change of sign of the XPM contribution

in the frequency equation (4.14a). This is the only difference in the resulting adiabatic model equations compared to the equations of the up-switching case.

In Figure 4.3 the predictions of (4.14) are compared to a numerical solution of the GNLS equation (4.1). Considered is the interaction of a soliton with the same initial parameters as used in the up-switching example in Figure 4.1 of initial (circular) frequency $\omega_0 = 0.67\,\mathrm{rad\,fs^{-1}}$ and initial duration $\sigma_0 = 40\,\mathrm{fs}$ with a continuous DW of initial frequency offset $\Delta = -0.1\,\mathrm{rad\,fs^{-1}}$ and 1 % initial soliton peak power.

Analogous patterns as in the up-switching case can be identified. In the space-time domain (Figure 4.3a) the incoming DW (A) is reflected at the soliton. The superposition of incoming and reflected waves produce the interference picture (B). The soliton is decelerated, its trajectory is well reproduced by the adiabatic ODEs as indicated by the white dashed line. At $z \approx 25\,\mathrm{cm}$ the soliton becomes transparent, and parts of the DW are transmitted (C). This coincides well with the predicted soliton transmission coefficient as shown in Figure 4.3c (top left frame). The caustic (D) created by the reflected parts of the DW is reproduced in Figure 4.4 utilizing (3.40) and (4.14b).

The soliton broadened during the interaction. Its duration increases (Figure 4.3c, top right frame), and its peak power decreases (Figure 4.3c, bottom left frame). Here the oscillation of soliton amplitude is more pronounced than in the up-switching case. Again, those oscillations are not reproduced by the SPT [49]. The once reflected parts of the DW are not reflected a second time within the observed propagation distance, so there appears no further loss in peak power. The adiabatic ODEs give a good estimate of the final soliton peak power. Again the considerable loss in peak power by a factor 0.8 is accompanied by a decrease in soliton energy of only a factor 0.96.

The spectral window for the soliton is shown in Figure 4.3b (left frame). The down shift of soliton carrier frequency is well reproduced by the adiabatic equations (indicated by the white dashed line). The spectral window for the DW is shown in Figure 4.3b (right frame). Line (E) represents the carrier frequency of the incoming wave. Line (F) indicates the wave reflected by the soliton that is initially motionless in the reference frame. Line (G) traces the changing conversion frequencies of the waves reflected at the decelerating soliton, which is well captured by (3.40) and (4.14b).

The adiabatic model equations quantify the evolution of the soliton parameters and the DW frequency conversion, for both up- and down-switching. Moreover, the model equations allowed a better understanding of the interaction picture, i.e. in the identification of the caustic structure.

4.4 Parameter interval of interaction and choosing initial parameters

For given initial parameters the adiabatic model equations provide good predictions of pulse evolution as demonstrated in the last two sections. This section shows how the adiabatic

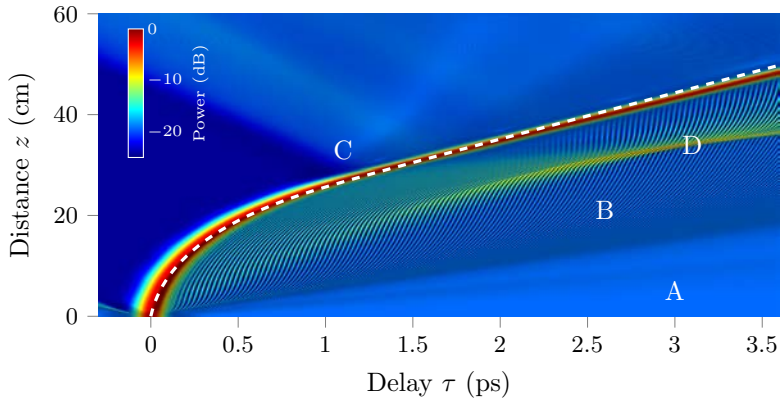

(a) Temporal evolution. White dashed lines indicate results from the adiabatic model equations.

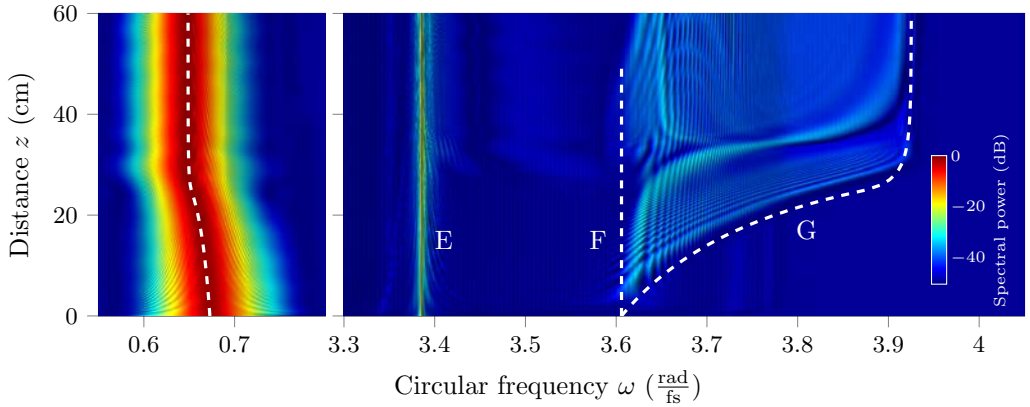

(b) Spectral evolution of soliton (left frame) and DW (right frame). White dashed lines indicate results from the adiabatic model equations.

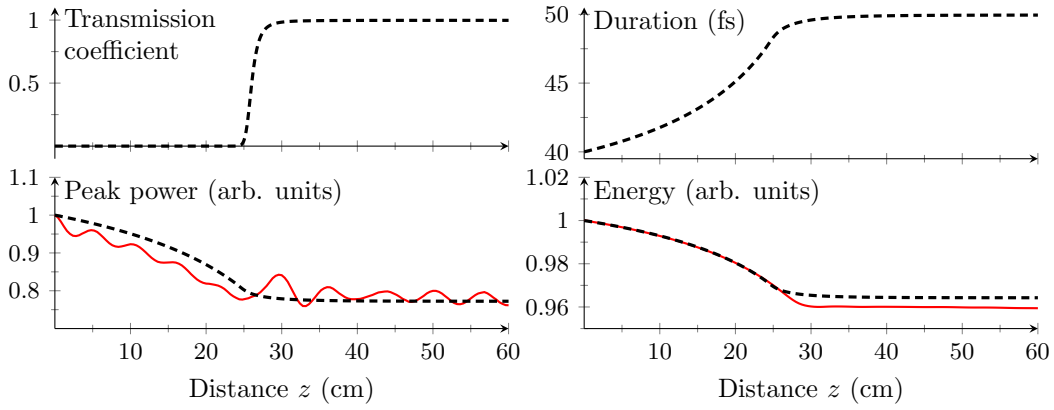

(c) Evolution of the soliton parameters. Black dashed lines result from the adiabatic model equations; red solid lines result from the numerical solution of (4.1).

Figure 4.3: Interaction of a soliton of initial (circular) frequency $\omega_0 = 0.67\,\text{rad}\,\text{fs}^{-1}$ and initial duration $\sigma_0 = 40\,\text{fs}$ (2.8 µm wavelength, 70.5 fs FWHM) with a continuous DW of initial frequency offset $\Delta = -0.1\,\text{rad}\,\text{fs}^{-1}$ and 1 % initial soliton peak power ($\omega_1 + \Delta = 3.386\,\text{rad}\,\text{fs}^{-1}$ or 0.556 µm wavelength, $\mu = 0.01$). Comparison of numerical and analytical results.

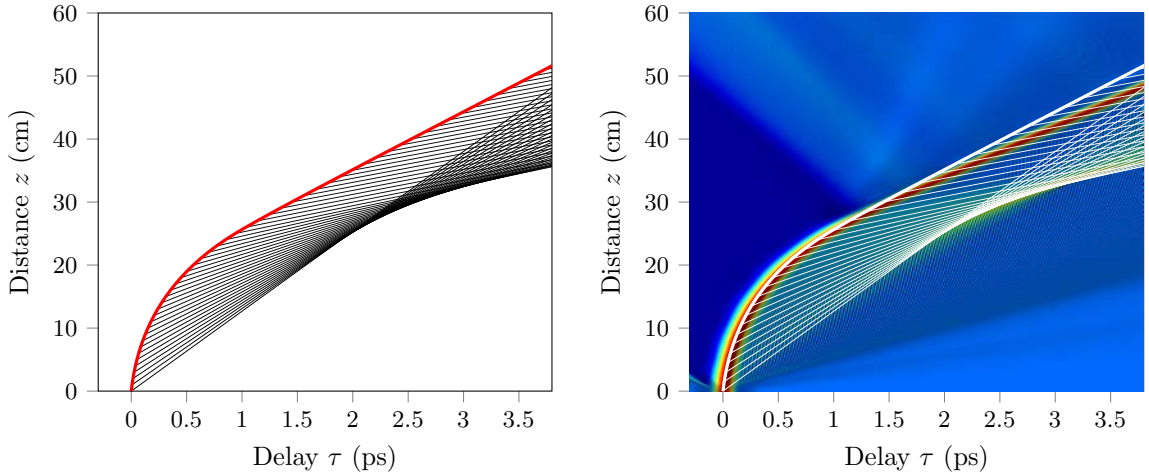

(a) The light rays of the DW reflected at the accelerated soliton (thick red line) form a caustic structure.

(b) Comparison of the caustic structure of frame (a) to numerical simulation.

Figure 4.4: Soliton trajectory (thick line) and geometric rays for the reflected DWs (thin lines) are plotted for the calculation in Fig. 4.3. The caustic structure corresponds to pattern D in Fig. 4.3a. Note that some rays can intersect the soliton trajectory once again; DWs then experience their second scattering.

model equations provide appropriate initial conditions for an effective interaction in the first place [P2]. Not every DW is reflected at a given soliton, and not every reflected DW is able to effectively change the soliton parameters. The two control parameters for the present choice of control pulse are the DW frequency and peak power. Both are covered by the adiabatic model equations. The solution to the scattering problem enables a quantification of the empirical rules for effective soliton manipulation presented in Section 2.3.

Interaction interval The easiest and least time consuming way to identify the $\Delta-$interval around the frequency ω_1 of matching group velocity, is to evaluate the initial reflection coefficient $\mathscr{R} = 1 - \mathscr{T}$ with $\mathscr{T}$ as in (4.11)

$$\mathscr{R} = 1 - \mathscr{T} = 1 - \frac{\sinh^2(\pi\sigma_0\Delta)}{\sinh^2(\pi\sigma_0\Delta) + \cosh^2(\pi\mathfrak{z})}, \quad \mathfrak{z} = \frac{1}{2}\sqrt{16\frac{|\beta_0''|}{\beta_1''}\frac{\omega_1}{\omega_0} - 1},$$

for any combination of two initial carrier frequencies ω_0 and $\omega_1 + \Delta$ and possible values of initial soliton duration σ_0. Figure 4.5 shows the contours of the initial reflection coefficient depending on pairs of initial DW frequency offsets and soliton duration for given initial soliton carrier frequency $\omega_0 = 0.67\,\mathrm{rad\,fs^{-1}}$ (2.8 µm wavelength). The transition from a parameter domain of high reflection rate ($\mathscr{R} > 0.9$) to a domain of low reflection rate ($\mathscr{R} < 0.1$) is quite sharp. This fits nicely to observation in many numerical simulations, that a noticeable soliton transformation by a DW can be expected only for higher reflection rates as formulated in the rule of *high reflection rates* (p.16). Shorter soliton durations imply a larger frequency interval

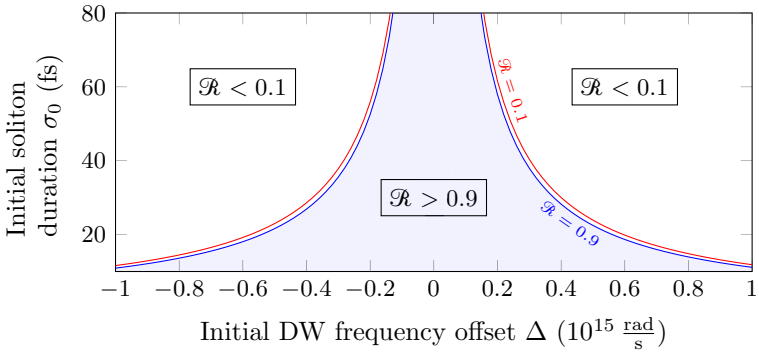

Figure 4.5: Contours of the initial reflection coefficient $\mathscr{R}$ depending on pairs of initial DW frequency offsets and soliton duration for given initial soliton carrier frequency $\omega_0 = 0.67\,\mathrm{rad\,fs^{-1}}$ (2.8 µm wavelength). There is a quite sharp transition from a parameter domain of high reflection rate ($\mathscr{R} > 0.9$) to a domain of low reflection rate ($\mathscr{R} < 0.1$).

of DWs which are almost entirely reflected. For fixed soliton carrier frequency a shorter soliton duration results in a higher barrier for a DW to pass. The quantum mechanical scattering is most effective when the kinetic energy corresponding to the incoming wave is lower than the height of the potential barrier.[1] In optical terms this means $\Delta^2\beta''(\omega_1)/2 \leq V_0$ with barrier height (3.35),

$$V_0 = 2\frac{|\beta''(\omega_0+\nu)|}{\sigma^2}\frac{\gamma_1}{\gamma_\mathrm{s}}.$$

Thus appropriate initial DW frequencies and soliton durations are subject to the inequality

$$\Delta \leq \frac{2}{\sigma}\sqrt{\frac{|\beta''(\omega_0)|}{\beta''(\omega_1)}\frac{\omega_1}{\omega_0}\frac{n_{2,1}}{n_{2,0}}}. \tag{4.15}$$

For a given initial soliton this is a good approximation of the DW frequency interval. In Section 2.3 it was stated as an empirical rule, that *steep anomalous GVD profile* (p.16) is aiding an effective soliton manipulation. The relation (4.15) gives a quantitative argument for this. $|\beta''(\omega_0)| > \beta''(\omega_1)$ will raise the barrier height.

When the appropriate DW frequency for a given soliton is chosen, the DW amplitude must be chosen below the initial soliton amplitude, it was given above relatively to the initial soliton amplitude as $\mu = P_1/P_0$. In the frequency ODEs (4.5a) or (4.14a) the propagation distance z can be rescaled to absorb μ. Therefore a weaker DW finally yields the same soliton frequency shift and the same peak power, but requires a longer propagation length.

Strongest initial impact on a soliton Figure 4.6 (top frame) shows the initial reflection coefficient versus initial DW frequencies for the initial soliton ($\omega_0 = 0.67\,\mathrm{rad\,fs^{-1}}$ and $\sigma_0 = 40\,\mathrm{fs}$) considered in the last two sections. Δ should lie in an interval from $-0.28\,\mathrm{rad\,fs^{-1}}$ to $0.3\,\mathrm{rad\,fs^{-1}}$ for the DW to be reflected. The approximate assessment of the interval boundary

[1] In the quantum mechanical notation of Appendix C this means $\frac{k^2}{2m} \leq V_0$.

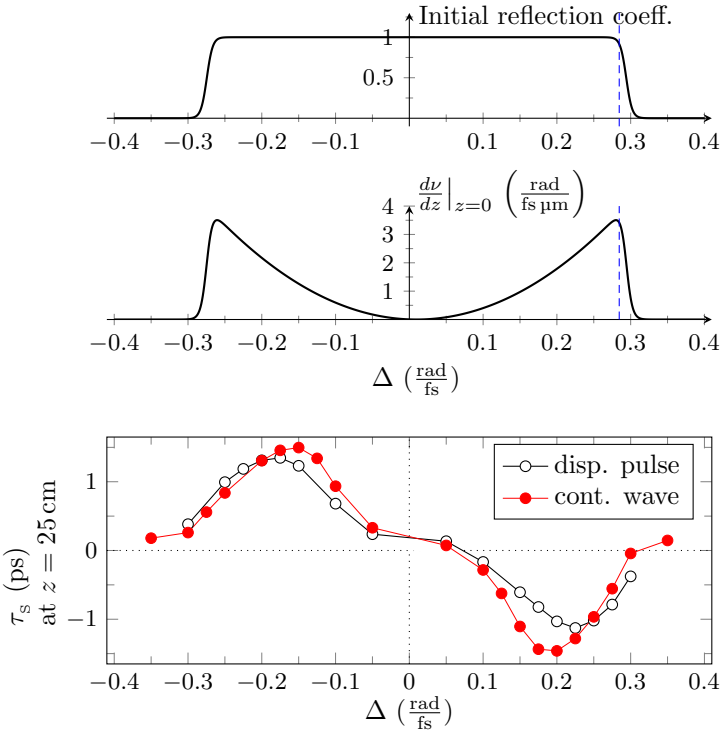

Figure 4.6: For a given soliton ($\omega_0 = 0.67\,\text{rad}\,\text{fs}^{-1}$ and $\sigma_0 = 40\,\text{fs}$) the initial reflection coefficient $\mathcal{R}(\Delta)$ indicates possible DW frequencies resulting in an interaction with the soliton (top frame). The initial effect of the DW on the soliton as predicted by the adiabatic model equations (middle frame). Soliton deflection at propagation distance of 25 cm after interaction with a continuous DW (red dots) and after interaction with a dispersive pulse of finite duration (black circles). Note that lines between dots are only plotted to aid readability.

by (4.15), $\Delta \leq 0.28\,\text{rad}\,\text{fs}^{-1}$, is indicated by the dashed blue line. So for a given soliton, the plotted reflection coefficient determines the DW frequency interval, which will result in an effective interaction, thereby fully quantifying the *velocity-matching condition* (p.14), which was stated before only as an empirical rule.

Another option is to evaluate the righthand side the frequency ODEs (4.5a) or (4.14a), $d\nu/dz|_{z=0}$, at the beginning of the fiber for varying Δ. The resulting curve is shown in Figure 4.6 (middle frame). The curve shows the DW frequency interval of interaction, which coincides with the frequency interval predicted by the reflection coefficient (top frame). The shape of the curve should indicate how strong the soliton is initially affected by a DW of a certain frequency. Towards the middle of the interaction interval, the effect on the soliton is reduced. At $\Delta = 0$ soliton and DW would propagate at exactly the same group velocity and no effect would be expected as indicated by the curve which drops to zero. At the peaks of the curve the strongest initial effect on the soliton should be found. A comparison with results from a series of numerical simulations with the full GNLS equation (4.1) confirms the validity of this expectation. The best indicator for a possible effect on the soliton is the soliton delay. Even for very small shifts in soliton frequency, the delay changes are clearly

visible. Figure 4.6 (bottom frame) shows the soliton delay τ_s at $z = 25\,\mathrm{cm}$ (red dots) read out from a series of numerical simulations with GNLS equation (4.1) for different values of Δ and fixed relative DW power $\mu = 0.1$. At $\Delta \approx 0.2\,\mathrm{rad\,fs^{-1}}$ the absolute soliton deflection becomes maximal. This is slightly below the predicted optimal value, though very close to it. This suggests that (for shorter solitons like the one considered here) it is advisable to choose a Δ closer to ω_1 than the optimal DW frequency predicted here, in favor of a longer interaction time between soliton and DW.

The adiabatic model still applies to the case of a localized dispersive pulse (of finite duration) interacting with a soliton. This is illustrated by the bottom frame of Figure 4.6 showing the soliton delay after a propagation distance of 25 cm read from a series of numerical simulations for the interaction with a pulse of varying carrier frequencies, fixed relative peak power $\mu = 0.2$, an initial duration of 200 fs and an initial time delay of 1000 fs away from the initial soliton. The resulting curve fits nicely to the prediction of $d\nu/dz|_{z=0}$ shown in the middle frame of Figure 4.6.

The predictions become more accurate (also for interactions with a continuous DW) if the chosen soliton is broader and contains more optical cycles. The soliton in the example of Figure 4.6 contains 7.5 optical cycles at half maximum. Figure 4.7 shows the interaction interval for a soliton at $\omega_0 = 1.22\,\mathrm{rad\,fs^{-1}}$ (1.55 µm wavelength) and duration of $\sigma_0 = 50\,\mathrm{fs}$ containing almost 19 cycles. Results here are only shown for the up-switching case. The soliton delay after a propagation distance of 100 cm is shown in the bottom frame. The maximal soliton delay is reached at about the predicted optimal DW frequency at $\Delta \approx 0.05\,\mathrm{rad\,fs^{-1}}$. Predictions and numerical results are in very good agreement.

Each dot of the numerical results in Figures 4.6 and 4.7 represent a full numerical solution to the pulse evolution equation 4.1. Each such numerical evaluation took 20 minutes to about 2 hours depending on the chosen discretization. The predictions for any Δ-interval by reflection coefficient $\mathscr{R}$ or even by $d\nu/dz|_{z=0}$ are done in a matter of seconds, and easily so for a wide range of initial soliton and DW combinations.

4.5 Influence of self-steepening on the switching process

So far, it has been established that the adiabatic model equations provide accurate predictions for single simulations with given initial conditions, and moreover yield suitable initial wave parameters to influence a soliton as strongly as possible. The present section deals with a more principle question and attends to the role of the self-steepening term: Excessive numerical simulations suggested, that an amplification of the soliton is much more difficult to achieve, if the self-steepening term is neglected. Predictions of the suitable adiabatic equations confirm this.

To demonstrate the effects of a missing self-steepening term, the up-switching example discussed in Section 4.2 is calculated numerically with the self-steepening term artificially

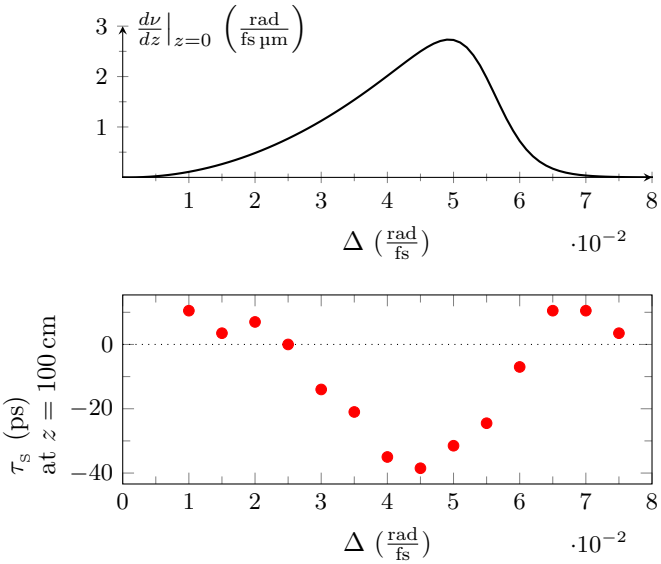

Figure 4.7: For a given soliton the initial reflection coefficient $\mathcal{R}(\Delta)$ indicates possible DW frequencies resulting in an effective interaction with the soliton (top frame). The initial effect of DWs with varying carrier frequency (relative peak power $\mu = 0.1$) on the soliton ($\omega_0 = 1.22\,\text{rad}\,\text{fs}^{-1}$, $\sigma_0 = 55\,\text{fs}$) as predicted by the adiabatic model equations (top frame). Soliton delay at propagation distance of 100 cm after the interaction read from a series of numerical simulations (bottom frame).

switched off. The simulation equations (4.1) with $\eta_0 \equiv 0$ reads:

$$i\partial_z\psi + \hat{D}\left(i\partial_\tau\right)\psi + \gamma_0\left|\psi\right|^2\psi = 0 \tag{4.16}$$

To obtain the appropriate adiabatic equations with self-steepening ignored one has to go back and reconsider how the new perturbation equation was derived. The soliton frequency shift ν entered the soliton equation (3.2) by introducing the new soliton envelope (3.22). During the derivation of the new perturbation equation the nonlinear parameter (3.24) became $z-$dependent due to the extra derivative by τ of the self-steepening term applied to the new envelope:

$$\begin{aligned}\gamma_0\left[1 + i\eta_0\partial_\tau\right]\left[\psi_0(z,\tau)e^{-i\nu(z)\tau}\right] &= \frac{n_{2,0}\omega_0}{c}\left[1 + \frac{i}{\omega_0}\partial_\tau\right]\left[\psi_0(z,\tau)e^{-i\nu(z)\tau}\right] \\ &= e^{-i\nu(z)\tau}\,\frac{n_{2,0}[\omega_0+\nu]}{c}\left[1 + \frac{i}{\omega_0+\nu}\partial_\tau\right]\psi_0(z,\tau)\end{aligned}$$

Thus the nonlinear parameter is not $z-$dependent, if the self-steepening term is not present ($\eta_0 \equiv 0$). Introducing the new envelope to a GNLS equation without self-steepening term results in the perturbation equation

$$\begin{aligned}&i\partial_z\psi_0 + \tau\left[\frac{d\nu}{dz}\right]\psi_0 + i\left[\beta'(\omega_0+\nu) - \beta'(\omega_0)\right]\partial_\tau\psi_0 \\ &\quad + \frac{\beta''(\omega_0+\nu(z))}{2}\left[i\partial_\tau\right]^2\psi_0 + \gamma_0\left|\psi_0\right|^2\psi_0 \\ &\quad = i\left\{i\sum_{m=3}^{4}\frac{\beta^{(m)}(\omega_0+\nu(z))}{m!}\left[i\partial_\tau\right]^m\psi_0 + i2\gamma_0\left|\psi_{\text{DW}}\right|^2\psi_0\right\}\end{aligned} \tag{4.17}$$

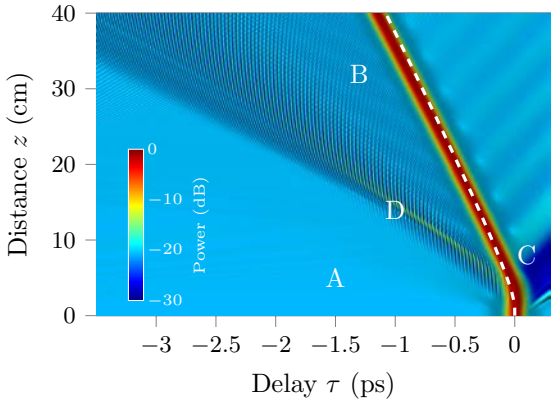

(a) Temporal evolution. White dashed lines indicate predictions by the adiabatic model equations.

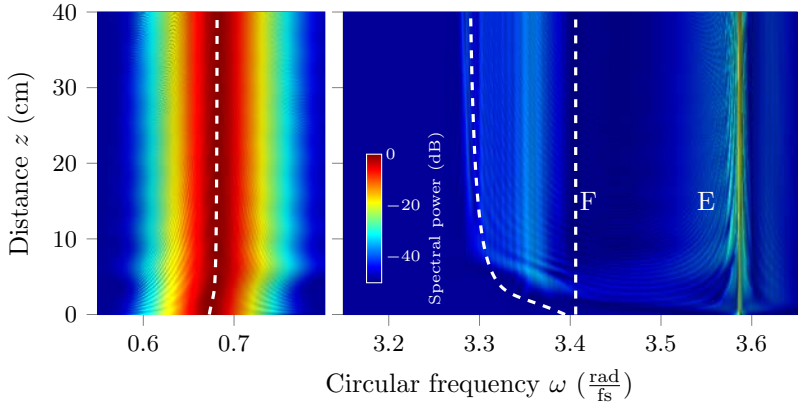

(b) Spectral evolution of soliton (left frame) and DW (right frame). White dashed lines indicate predictions by the adiabatic model equations.

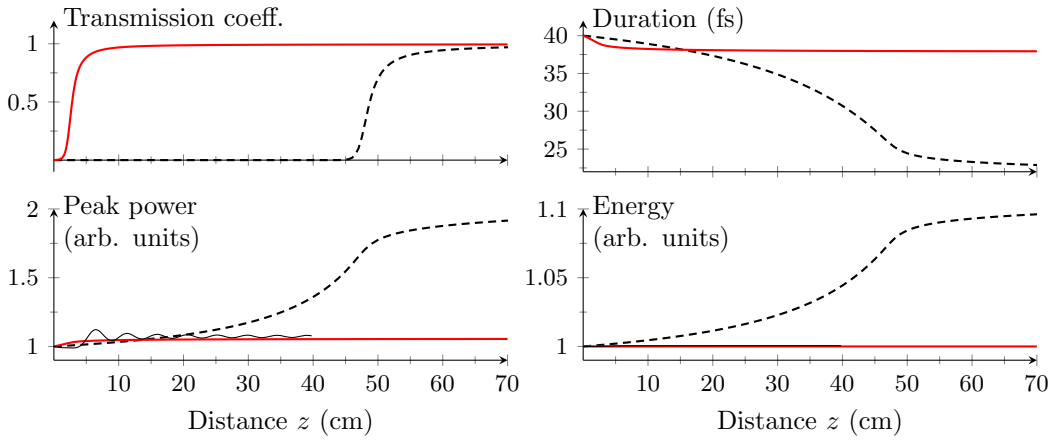

(c) Evolution of soliton parameters. Thick red lines result from the adiabatic model equation derived ignoring the self-steepening term; thin solid black lines are the result of the according numerical simulation of (4.16). Dashed black lines result from the adiabatic model equation stated in Section 4.2 including the self-steepening term.

Figure 4.8: Interaction of a soliton ($\omega_0 = 0.67\,\text{rad}\,\text{fs}^{-1}$, $\sigma_0 = 40\,\text{fs}$) with a continuous DW ($\Delta = 0.1\,\text{rad}\,\text{fs}^{-1}$, $\mu = 0.01$), if self-steepening is ignored. Comparison of numerical and analytical results.

with constant nonlinear parameter

$$\gamma_0 = \frac{n_{2,0}\omega_0}{c}. \tag{4.18}$$

The righthand side of (4.17) represents the perturbation by third and forth order dispersion, and by XPM with ψ_{DW}. The dispersion coefficients in (4.17) are still functions of the $z-$dependent soliton frequency, and therefore change with the soliton frequency shift. The soliton ansatz function (3.31) takes the constant nonlinear parameter,

$$\psi_0(z,\tau) = \frac{1}{\sigma}\sqrt{\frac{|\beta''(\omega_0+\nu)|}{\gamma_0}}\frac{\exp(i\theta)}{\cosh\frac{\tau-\tau_{\mathrm{S}}}{\sigma}}, \tag{4.19}$$

and the solution for the DW consequently reads

$$|\psi_{\mathrm{DW}}|^2 = \frac{\mu}{\gamma_0 L_0}\cdot\mathcal{T}\cdot\left|{}_2F_1\left(\mathcal{a},\mathcal{b};\mathcal{c};y\right)\right|^2.$$

The resulting set of ODEs describing soliton parameter evolution is:

$$\frac{d}{dz}\left[\frac{1}{\sigma}\frac{\beta''(\omega_0+\nu)}{\gamma_0}\right] = 0 \quad \Rightarrow \quad \frac{\sigma(z)}{\sigma(0)} = \frac{\beta''(\omega_0+\nu)}{\beta''(\omega_0)} \tag{4.20a}$$

$$\frac{dv}{dz} = \frac{4\mu}{\sigma L_0}\mathcal{I}_1 \tag{4.20b}$$

$$\frac{d\tau_{\mathrm{S}}}{dz} = \left[\beta'(\omega_0+\nu)-\beta'(\omega_0)\right] + \beta^{(3)}(\omega_0+\nu)\frac{1}{6}\frac{1}{\sigma^2} \tag{4.20c}$$

$$\frac{d\theta}{dz} = \frac{\beta''(\omega_0+\nu)}{2}\frac{1}{\sigma^2} + \beta^{(4)}(\omega_0+\nu)\frac{7}{72}\frac{1}{\sigma^4} + \frac{4\mu}{L_0}\mathcal{I}_2 \tag{4.20d}$$

The change in soliton duration is based only on the frequency dependent GVD coefficient. The same is true for soliton peak power

$$\frac{P_{\mathrm{S}}(z)}{P_{\mathrm{S}}(0)} = \frac{\beta''(\omega_0)}{\beta''(\omega_0+\nu(z))}. \tag{4.21}$$

The soliton energy is expected to be unchanged, because through XPM no energy should be exchanged between the soliton and DW. Accordingly the adiabatic model states for the soliton energy

$$\frac{\mathscr{E}_{\mathrm{S}}(z)}{\mathscr{E}_{\mathrm{S}}(0)} = \frac{\sigma(0)}{\sigma(z)}\frac{\beta''(\omega_0+\nu(z))}{\beta''(\omega_0)} = 1. \tag{4.22}$$

Figure 4.8 shows a comparison of predictions by (4.20) to the numerical solution of (4.16) for the same initial pulse parameters as used for the example in Figure 4.1. The reflection process still takes place, and the DW frequency is converted (Figure 4.8b). The conversion of the DW frequency is much less pronounced compared to the example with self-steepening included (Figure 4.1b). The soliton becomes transparent almost immediately (Figure 4.8c), a behavior quite different from what was seen in the example with self-steepening included, cf. Figure 4.1a. With this very short interaction time, the soliton frequency shift is not as significant, and the soliton peak power remains nearly unchanged.

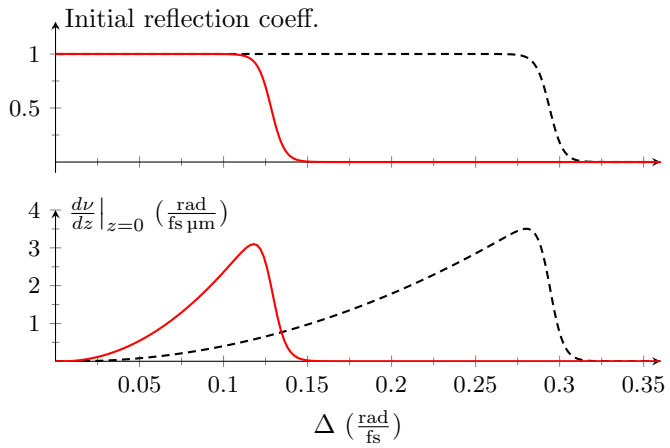

Figure 4.9: The possible range of DW frequencies which are initially reflected at a soliton ($\omega_0 = 0.67\,\text{rad}\,\text{fs}^{-1}$ and $\sigma_0 = 40\,\text{fs}$) is shown (top frame). The initial impact of a certain DW on the soliton is indicated (bottom frame). Red lines are for calculations ignoring self-steepening, black dashed lines result from calculations with self-steepening included. The disagreement is due to the artificially removed self-steepening term.

Looking at the reflection coefficient (Figure 4.9, top frame) to assess the interaction interval, as explained in Section 4.4, it is clear, that the range of possible DW frequencies for an effective interaction is much smaller if self-steepening is ignored. These findings suggest that the self-steepening term plays an essential role in a possibly strong soliton manipulation. Many previous studies neglected it, also due to the fact, that it is the weaker higher order nonlinear effect, e.g., compared to the Raman effect.

5 Raman effect and soliton self-frequency shift

In this chapter Raman scattering is incorporated into the new SPT and its impact on the soliton switching process is examined. While the control wave, a low-intensity continuous DW, will not notice the Raman effect, an ultrashort soliton (with duration in the femtosecond range) will be affected by Raman scattering. The soliton, as a very short pulse, exhibits a broad spectrum. Energy is transferred from the components with higher frequencies to those with lower frequencies, resulting in an continuous down-shift of the soliton's spectral envelope. This so-called soliton self-frequency shift (SSFS) was first experimentally observed by Mitschke and Mollenauer [57] and theoretically explained by Gordon [41]. Along with the SSFS the soliton is decelerated, i.e. its trajectory in space-time domain is strongly deflected, and it loses peak power.

Gordon's result for the SSFS can also be acquired by standard SPT, but this theory fails in producing an accurate prediction of the soliton's power loss. The first two sections of this chapter deal with a single soliton subject to Raman scattering, without any interaction with a second pulse. Section 5.1 demonstrates that the proposed modified perturbation theory generalizes Gordon's relation for the SSFS and furthermore correctly quantifies the decay in soliton peak power. Gordon's neat relation uses a rough approximation of the Raman effect. For calculations including the switching by a second wave a more accurate description is needed which uses the typical delay-integral formulation of the Raman effect and also includes the effects of self-steepening and higher order dispersion. In Section 5.2 the corresponding set of ODEs describing soliton evolution is provided.

The subsequent sections will discuss the influence of the Raman effect on soliton switching. Down-switching by a second wave and Raman scattering affect the soliton parameters in a similar way, so it is by far more interesting to look at the counteracting effects of up-switching and Raman scattering together. Section 5.3 inspects the predictions of the modified perturbation theory for the interaction of soliton and a DW under the influence of Raman scattering. A DW is singled out that succeeds in canceling the SSFS, and the stability of the cancellation is investigated. Finally, Section 5.4 shows, which DWs succeed in compressing a soliton despite the adverse influence of Raman scattering.

5.1 Approximate relation for the soliton self-frequency shift and for amplitude decay due to Raman effect

Consider a single soliton traveling along an optical fiber subject to Raman scattering. Expressions for the SSFS and also for the amplitude decay due to the Raman effect are to be calculated. To this end return to the modified perturbation equation (3.28) with floating car-

rier frequency, with the Raman scattering term as the only perturbation. To get a possibly simple expression, here the delayed integral description as in (3.29) of the Raman effect is replaced by its approximation valid for pulses of sufficient duration, [1],

$$F_{\text{Raman}}\left(\psi_0\right) = -i\gamma_0 T_R\, \psi_0\, \partial_\tau \left[\left|\psi_0\right|^2\right] \tag{5.1}$$

with $T_R = 3\,\text{fs}$ for silica fiber. The influence of the self-steepening effect on a single soliton is much weaker than the influence of Raman scattering. In the adiabatic equations the self-steepening term is ignored ($\eta_0 \equiv 0$). Thus the nonlinear parameter γ_0 is constant as explained in Section 4.5. The modified SPT results in the following set of ODEs describing the evolution of soliton parameters:

$$\frac{d}{dz}\left[\frac{1}{\sigma}\frac{\beta''(\omega_0+\nu)}{\gamma_0}\right] = 0, \tag{5.2a}$$

$$\frac{d\nu}{dz} = -T_R \frac{8}{15}\frac{\beta''(\omega_0+\nu)}{\sigma^4}, \tag{5.2b}$$

$$\frac{d\tau_{\text{S}}}{dz} = \left[\beta'(\omega_0+\nu) - \beta'(\omega_0)\right] + \frac{\beta^{(3)}(\omega_0+\nu)}{6\sigma^2}. \tag{5.2c}$$

Integrating (5.2a) leads to an explicit relation for soliton duration

$$\frac{\sigma(z)}{\sigma(0)} = \frac{\beta''(\omega_0+\nu(z))}{\beta''(\omega_0)}. \tag{5.3}$$

and with this an expression for the soliton peak power P_{S} is

$$\frac{P_{\text{S}}(z)}{P_{\text{S}}(0)} = \frac{\sigma(0)}{\sigma(z)} = \frac{\beta''(\omega_0)}{\beta''(\omega_0+\nu(z))}. \tag{5.4}$$

The relation (5.2b) is a slightly more general form of the important relation for the SSFS derived first by Gordon [41] by considering conservation laws for the GNLS equation[1]. Equation (5.2b) has the same form as the classical expression derived by Gordon, with the important difference of the $z-$dependent pulse duration (5.3) and the GVD coefficient β'' which recognizes the $z-$dependent soliton frequency. The changes in duration (5.3) and peak power (5.4) are traced simply to the frequency dependence of the GVD coefficient. The soliton amplification is stronger if the GVD $\beta''(\omega)$ is a possibly steep function in the anomalous dispersion domain.

The modified SPT extends the standard results for the SSFS and allows a prediction of the soliton's power loss by linking it to the frequency dependent GVD. The above treatment of the evolution of soliton parameters was done with the aim to extend Gordon's result, relying on the approximation (5.1) valid for broader solitons, but the main issue here is including the Raman effect in a manner that is realistic for the ultrashort soliton range in question.

[1] A more general approach based on the SPT [43] for the standard NLS equation provides the same self-frequency shift and stated that the soliton amplitude would not change.

5.2 Precise description of perturbation by Raman effect

In this section a more accurate description of the SSFS is derived, going back to the full description of the Raman effect by the delayed integral representation. Moreover, the influences of higher order dispersion and self-steepening are included. The perturbation function describing Raman scattering reads

$$F_{\mathrm{Raman}}\left(\psi_0\right) = i f_R \gamma_{\mathrm{S}} \left[1 + i\eta_{\mathrm{S}}\partial_\tau\right] \left[\psi_0(z,\tau) \int_{-\infty}^{\infty} H(\tau') \left|\psi_0(z,\tau-\tau')\right|^2 d\tau'\right]. \tag{5.5}$$

with $H(\tau) = h(\tau) - \delta(\tau)$. Detailed calculations following the derivation in Section 3.2 are found in Appendix B. The resulting ODE for the soliton frequency offset reads

$$\frac{d\nu}{dz} = -f_R \frac{\pi}{4} \sigma \beta''(\omega_0+\nu) \mathscr{R}_1, \tag{5.6a}$$

and for the soliton delay

$$\frac{d\tau_{\mathrm{S}}}{dz} = \mathscr{B} - f_R \frac{3\pi}{8} \frac{\sigma\beta''(\omega_0+\nu)}{\omega_0+\nu} \mathscr{R}_2. \tag{5.6b}$$

Soliton duration is described by (4.4),

$$\frac{\sigma(z)}{\sigma(0)} = \frac{\beta''(\omega_0+\nu)}{\beta''(\omega_0)} \frac{1}{\left[1+\frac{\nu(z)}{\omega_0}\right]^2}.$$

The auxiliary variable

$$\mathscr{B} = \left[\beta'(\omega_0+\nu) - \beta'(\omega_0)\right] - \eta_{\mathrm{S}} \frac{\beta''(\omega_0+\nu)}{\sigma^2} + \frac{\beta^{(3)}(\omega_0+\nu)}{6\sigma^2}$$

is the same as in (4.6) and includes effects of higher order dispersion and self-steepening. The integral terms $\mathscr{R}_1$, $\mathscr{R}_2$ read

$$\mathscr{R}_1 = i \int_{-\infty}^{\infty} d\omega\, \omega^3 \frac{\hat{h}(\omega) - \hat{h}(0)}{\sinh^2 \frac{\pi}{2}\sigma\omega}, \tag{5.7a}$$

$$\mathscr{R}_2 = \int_{-\infty}^{\infty} d\omega\, \omega^2 \frac{\hat{h}(\omega) - \hat{h}(0) + \frac{1}{3}\omega\hat{h}_\omega(\omega)}{\sinh^2 \frac{\pi}{2}\sigma\omega}. \tag{5.7b}$$

$\hat{h}(\omega)$ is the Fourier transform of Raman response function (2.10) with $h(\tau<0)\equiv 0$:

$$\hat{h}(\omega) = \frac{\nu_1^2+\nu_2^2}{\nu_1^2+\left[\nu_2 - i\omega\right]^2}, \qquad \hat{h}(0) = 1. \tag{5.8}$$

$\mathscr{R}_1$, $\mathscr{R}_2$ are depending on $\sigma(\nu)$ and are thereby functions of ν. For the calculation of the ODE system (5.6) it is convenient to tabulate integrals (5.7) for a (generously chosen) interval of values ν. Note that both integrals $\mathscr{R}_1$, $\mathscr{R}_2$ take real values. As in the Raman free case the ODE (5.6a) for soliton frequency shift only depends on ν and is decoupled from equation (5.6b) for time delay. So when considering the SSFS it suffices to consider (5.6a).

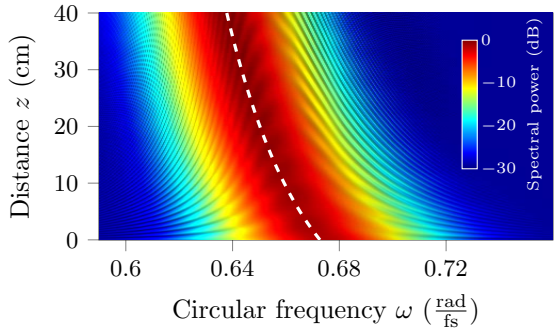

(a) Spectral domain. White dashed lines indicate predictions by the adiabatic model equations.

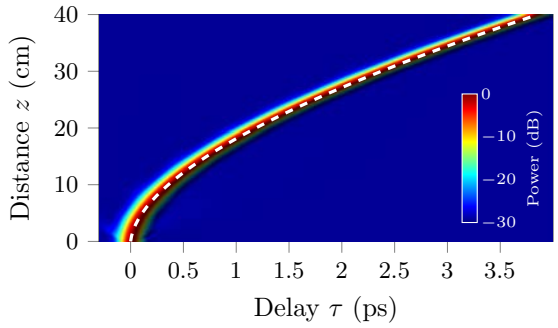

(b) Temporal domain. White dashed lines indicate predictions by the adiabatic model equations.

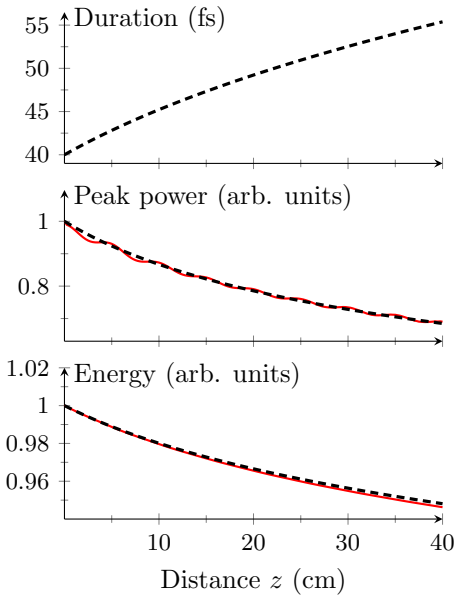

(c) Evolution of soliton parameters. Black dashed lines result from the adiabatic model equations; red solid lines result from the numerical solution of (2.5).

Figure 5.1: Single soliton ($\omega_0 = 0.67\,\text{rad}\,\text{fs}^{-1}$, $\sigma_0 = 40\,\text{fs}$) propagating subject to Raman scattering. Comparison of results from numerical simulation with predictions of adiabatic model equations.(a) Density plot in spectral domain, showing a continuous down-shift of carrier frequency, i.e. the SSFS. White dashed line indicates prediction of the model equations. (b) Density plot in temporal domain shows the deceleration of the soliton. (c) Evolution of soliton parameters. Soliton peak power decreases steadily as the soliton propagates.

Figure 5.1 compares the numerical solution of full GNLS equation (2.5) to the predictions of the adiabatic model equations (5.6) and (4.4) for a soliton with initial carrier frequency $\omega_0 = 0.67\,\text{rad}\,\text{fs}^{-1}$ and initial duration $\sigma_0 = 40\,\text{fs}$. The agreement is excellent for all soliton parameters.

The numerical simulation clearly shows that the soliton peak power decreases (Fig. 5.1 (b)). This is due to a change of GVD with shifting soliton carrier frequency. However, first order SPT for the standard NLS equation ignores the frequency dependence of GVD and consequently predicts that Raman scattering will not at all affect the soliton peak power [43]. It was explicitly stated in [88], that an adequate prediction was still to be found. The perturbation theory for the adjusted NLS equation (3.28) with floating soliton carrier frequency captures the evolution of all soliton parameters, accurately including peak power, [P3].

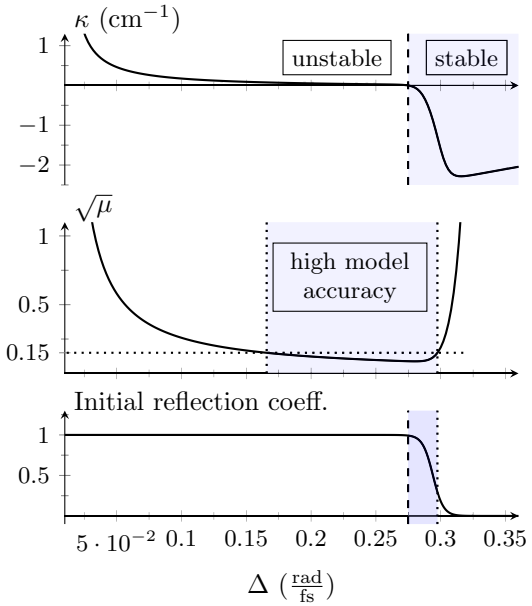

Figure 5.2: (Bottom frame) The initial reflection coefficient indicates for which frequencies a DW is effectively reflected at the soliton ($\omega_0 = 0.67\,\mathrm{rad\,fs^{-1}}$, $\sigma_0 = 40\,\mathrm{fs}$). (Middle frame) Pairs of Δ and relative DW amplitude $\sqrt{\mu}$ for which the soliton frequency does not change. Amplitude is plotted instead of power to facilitate readability. The DW should have much lower amplitude than the soliton to ensure an accurate description by the model equations. (Top frame) Stability analysis. The region of stable SSFS compensation is shaded blue.

5.3 Cancellation of soliton self-frequency shift by dispersive wave reflection

In order to see how Raman scattering affects the soliton-DW interaction, the term describing XPM by a DW in the up-switching case is included into the model equations. The resulting ODE for the soliton frequency shift reads [P3]

$$\frac{d\nu}{dz} = \frac{4\mu}{\sigma L_0}\left[1 + \frac{\nu}{\omega_0}\right]\mathcal{J}_1 - f_R\frac{\pi}{4}\sigma\beta''(\omega_0+\nu)\mathcal{R}_1, \tag{5.9a}$$

and for the soliton delay it is

$$\frac{d\tau_\mathrm{S}}{dz} = \mathcal{B} + \frac{4\mu}{\omega_0 L_0}\mathcal{J}_2 - f_R\frac{3\pi}{8}\frac{\sigma\beta''(\omega_0+\nu)}{\omega_0+\nu}\mathcal{R}_2. \tag{5.9b}$$

The auxiliary expression $\mathcal{B}$ is defined as in (4.6) and includes the influence of self-steepening and higher order dispersion onto the soliton delay. Integrals $\mathcal{J}_1$, $\mathcal{J}_2$ are given by (4.7).

The DW reflection which drives the frequency up, and the Raman effect which drives the frequency down, are represented by the first and the second term in (5.9a), respectively. To begin with, the consideration of Section 4.4 is taken up, and the reflection coefficient $\mathcal{R}$ for possible DW frequencies is inspected. The curve shown in Figure 5.2 (bottom frame) indicates the initial DW frequency interval for an effective interaction given a soliton of initial carrier

frequency $\omega_0 = 0.67\,\mathrm{rad\,fs^{-1}}$ and initial duration $\sigma_0 = 40\,\mathrm{fs}$. For an effective interaction Δ should lie in an interval from $0\,\mathrm{rad\,fs^{-1}}$ to $0.32\,\mathrm{rad\,fs^{-1}}$.

Can a dispersive wave be found which will counteract the Raman effect and cancel the SSFS exactly? In other words: The fixed points of (5.9a) must be identified; for a fixed soliton pairs of DW frequency offset Δ and relative peak power $\mu = P_1/P_0$ have to be singled out, such that the soliton frequency stays unchanged, i.e. $\nu(z) = 0$ for all z:

$$\left.\frac{d\nu}{dz}\right|_{\nu=0} = 0. \tag{5.10}$$

Figure 5.2 (middle frame) shows resulting pairs of DW frequency offsets and relative amplitudes. To either side of the interaction interval the relative DW amplitude quickly increases. The DW amplitude is required to be much lower compared to the soliton, in order to gain a valid approximate solution. If a threshold is chosen generously and the DW amplitude required to be at most 15 % the initial soliton amplitude (maximally 2.3 % of initial soliton peak power), cancellation of the SSFS for DW frequency offsets in an interval from about $0.16\,\mathrm{rad\,fs^{-1}}$ to $0.29\,\mathrm{rad\,fs^{-1}}$ is expected.

To test the stability of the fixed points, (5.9a) is linearized at $\nu = 0$,

$$\frac{d\nu}{dz} = \kappa\nu, \qquad \kappa = \left[\partial_\nu \frac{d\nu}{dz}\right]_{\nu=0} \tag{5.11}$$

The relevant quantity κ is shown in Figure 5.2 (top frame).

For $\kappa > 0$ the SSFS reappears if fiber length exceeds $\approx 1/\kappa$. Figure 5.3 shows the simulation for a soliton ($\omega_0 = 0.67\,\mathrm{rad\,fs^{-1}}$, $\sigma_0 = 40\,\mathrm{fs}$) and DW ($\Delta = 0.18\,\mathrm{rad\,fs^{-1}}$, $\mu = 0.0148$). The cancellation breaks down after a propagation distance of 60 cm.

For $\kappa < 0$ the cancellation is asymptotically stable. The region of feasible parameters is relatively small, its lower bound being determined by the condition $\kappa < 0$ for stability, and its upper bound by the condition of $\sqrt{\mu} < 0.15$ for sufficiently small DW amplitudes, as mentioned above. The according parameter region is shaded blue in 5.2 (bottom frame). Figure 5.4 shows the results of a simulation with parameters taken from that region ($\Delta = 0.286\,\mathrm{rad\,fs^{-1}}$, $\mu = 0.0081$). The transient phase in which the initial conditions adjust is very short. The soliton stabilizes at about $0.666\,\mathrm{rad\,fs^{-1}}$ (2.828 µm wavelength), very close to the initial $\omega_0 = 0.6727\,\mathrm{rad\,fs^{-1}}$ (2.8 µm wavelength). Figure 5.4b depicts the soliton power evolution. The soliton lost only 4 % of its peak power after propagating a distance of 40 cm. Traveling alone, the soliton lost about 30 % of its peak power due to the effects of Raman scattering, cf. Figure 5.1c.

The cancellation of the SSFS [P3] by controlled dispersive wave scattering as it is presented here was first suggested in [6]. The idea of suppressing the soliton self-frequency shift by utilizing interaction with low intensity radiation appeared in [76], [10]. SSFS cancellation by XPM occurs in [37]. Though the idea of SSFS cancelation by XPM is not new, a full analytic description of the soliton evolution and the prediction of parameter ranges for a stable compensation is.

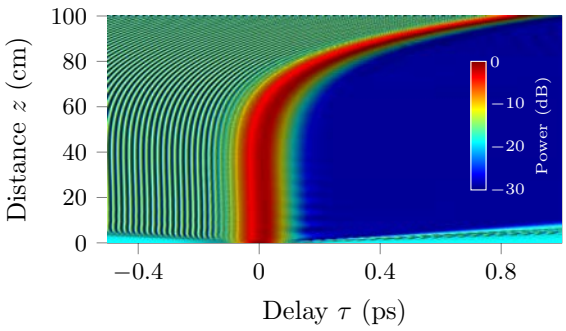

(a) Temporal evolution.

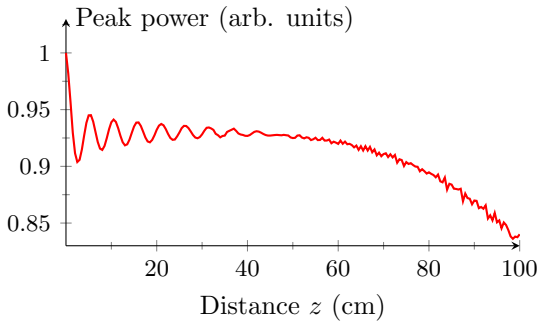

(b) Soliton peak power.

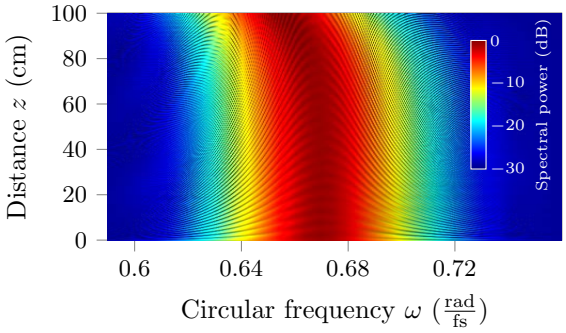

(c) Spectral window of the soliton.

Figure 5.3: Unstable compensation of SSFS by collision of a soliton ($\omega_0 = 0.67\,\mathrm{rad\,fs^{-1}}$, $\sigma_0 = 40\,\mathrm{fs}$) with a DW ($\Delta = 0.18\,\mathrm{rad\,fs^{-1}}$, $\mu = 0.0148$). After about 60 cm the compensation breaks down and the SSFS reappears. Note that the co-moving reference frame is chosen relative to the initial soliton after the relaxation of the artificial initial condition relaxed, therefore soliton delay and frequency are practically unchanged until the compensation breaks down. This reference frame was chosen to aid readability.

5.4 Soliton amplification under Raman scattering

Finally, a scenario is considered in which the DW scattering overpowers the Raman effect [P4]. Figure 5.5 depicts the collision of a soliton and a DW of $\Delta = 0.18\,\mathrm{rad\,fs^{-1}}$ and a peak power of 2.25 % of initial soliton peak power. Apart from initial relative peak power of the DW, those are the same initial conditions as seen in Figure 5.3 showing an unstable cancellation. During the course of the DW-reflection, the soliton is compressed. Its peak power amplifies by about a factor 1.3 (Figure 5.5c). The soliton frequency is up-shifted until it stabilizes at $0.7\,\mathrm{rad\,fs^{-1}}$ (2.69 µm wavelength). Accordingly, the soliton delay evolves with constant velocity (i.e. in a straight line) after the initial acceleration. Interestingly, the soliton never becomes fully transparent. The interaction stabilizes at a soliton transparency of about 40 %.

The analysis of the previous section provides a simple tool to identify those DWs which are capable of overpowering the Raman effect. Going back to Fig. 5.2 (middle frame), for a DW frequency offset Δ in the accepted interval now a DW normalized amplitude $\sqrt{\mu}$ is chosen higher than the one indicated for exact SSFS cancellation. Numerical simulations

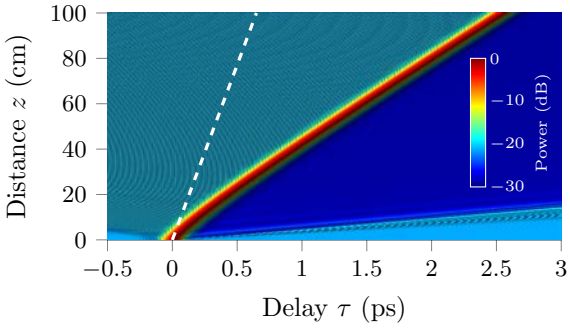

(a) Temporal evolution. White dashed line indicates predictions by the adiabatic model equations.

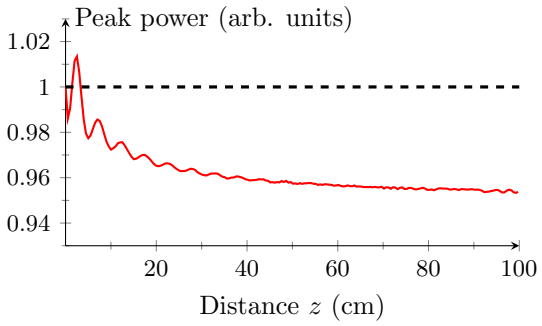

(b) Soliton peak power. Black dashed lines result from the adiabatic model equations; red solid lines result from the numerical solution of (2.5).

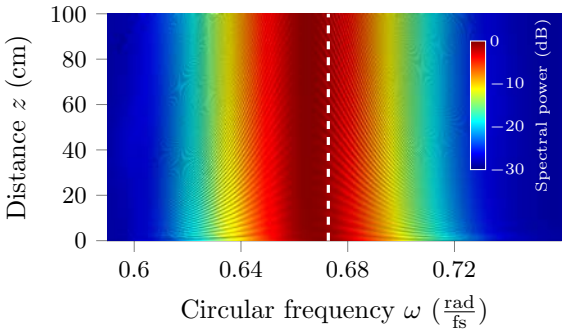

(c) Spectral window of the soliton. White dashed line indicates predictions by the adiabatic model equations.

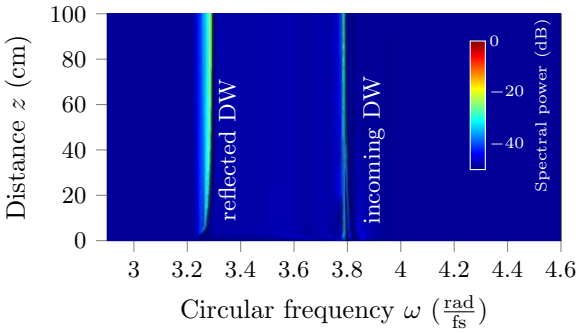

(d) Spectral window of the DW.

Figure 5.4: Compensation of SSFS of a soliton ($\omega_0 = 0.67\,\text{rad}\,\text{fs}^{-1}$, $\sigma_0 = 40\,\text{fs}$) by collision with a suitably prepared DW ($\Delta = 0.286\,\text{rad}\,\text{fs}^{-1}$, $\mu = 0.0081$). (a) Evolution of soliton together with a DW in time domain as results from GNLSE. (b) Soliton amplitude is almost unchanged. (c) Soliton frequency is locked. (d) the scattered DW frequency is now well defined.

indicate that a DW of this kind will compress the soliton, which then stabilizes at a fixed carrier frequency and propagates unchanged. In the example of Figure (5.5) the DW has a peak power of 2.25 % of initial soliton peak power, which is only 1.5 times the DW peak power predicted for exact (yet unstable) SSFS cancellation.

Thus the DW parameter region belonging to unstable cancellation of the SSFS is interesting in itself: If the DW amplitude is chosen higher than it is suggested by (5.10) for exact SSFS, the soliton is first compressed and then propagates without further changes. The adiabatic model equations provide a reasonable estimation of the final soliton parameters.

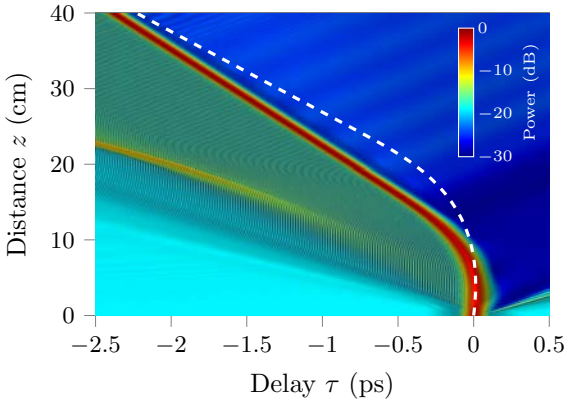

(a) Temporal evolution. White dashed lines indicate predictions by the adiabatic model equations.

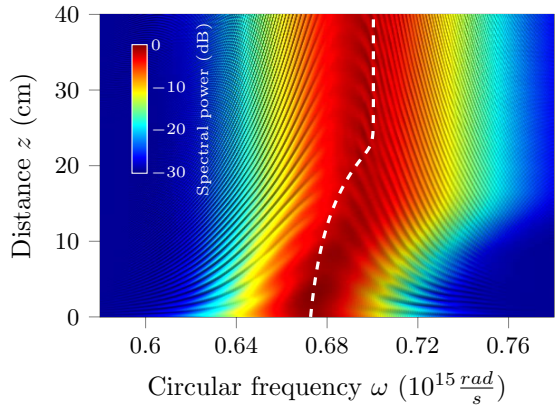

(b) Spectral evolution of the soliton. White dashed lines indicate predictions by the adiabatic model equations.

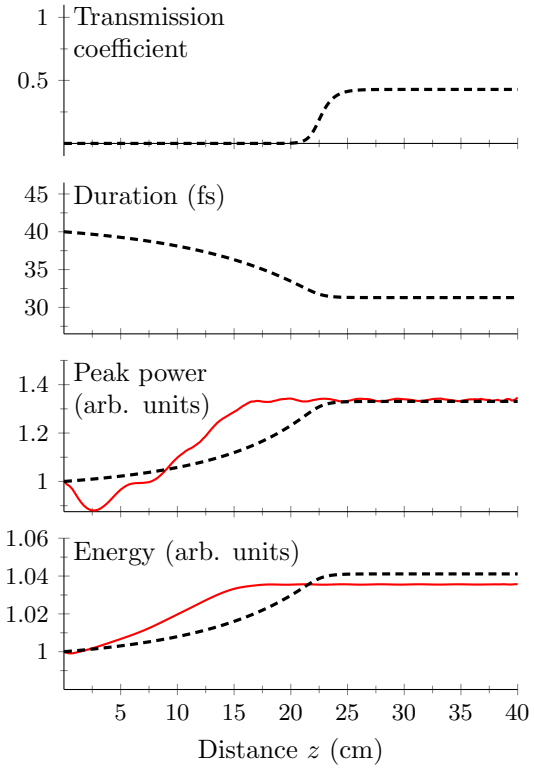

(c) Evolution of soliton parameters. Black dashed lines result from the adiabatic model equations; red solid lines result from the numerical solution of (2.5).

Figure 5.5: Soliton ($\omega_0 = 0.67\,\mathrm{rad\,fs^{-1}}$, $\sigma_0 = 40\,\mathrm{fs}$) amplified by a DW ($\Delta = 0.18\,\mathrm{rad\,fs^{-1}}$, $\mu = 0.0225$) despite the influence of Raman effect. (a) Density plot in temporal domain. The effect of the DW scattering overpowers the Raman effect and the soliton is accelerated. (b) Density plot in spectral domain. The soliton stabilizes at a carrier frequency of about $0.7\,\mathrm{rad\,fs^{-1}}$. (c) Evolution of soliton parameters. Soliton peak power is amplified by a factor of 1.3. The soliton stabilizes at a transparency of about 40 % which respect to the incoming DW.

6 Conclusion and Outlook

The present work is a contribution to the problem of efficient all-optical control of a fiber soliton. By applying properly chosen low-intensity dispersive light beams, the soliton's frequency, duration and intensity can be manipulated.

The proposed scheme is flexible, non destructive and can be used for a wide range of fiber dispersion profiles, and frequencies and intensities of the signal pulse. It has practically useful properties. The strong signal, i.e. the soliton, is manipulated by a much weaker control pulse, the dispersive wave, whereas most previous schemes of all-optical pulse control rely on strong control pulses and a weak signal [63]. Signal and control pulses can easily be separated because their spectra are disjoint. Control pulses can be applied to a soliton in a row [19], so the interaction can be cascaded. The only essential and rather weak pre-requirement is the existence of at least one zero-dispersion wavelength in the fiber transparency window.

The interaction between a soliton and a velocity matched low-intensity continuous pump wave is due to the cross-phase modulation (XPM) in a recently found peculiar regime that is referred to as an "optical event horizon" [68]. The main result of the present thesis is an analytic theory of XPM interactions of signals and control pulses at optical event horizons. It is based on scattering theory from quantum mechanics, and a modified soliton perturbation theory. The approach can be understood as follows. (1) A soliton of high intensity creates an inhomogeneity of the fiber material's refractive index, which constitutes a barrier at which a dispersive wave is scattered. This scattering of the dispersive wave at a dynamically changing solitonic barrier is analytically described in analogy to the scattering process as known from quantum mechanics. This implies that in the given situation the optical event horizons are fundamentally imperfect and can be described by transmission and scattering coefficients, just like potential barriers in quantum mechanics. Use of the quantum-mechanical language immediately distinguishes between "good" and "bad" signals and quantifies which control pulses are required to manipulate a good signal. Already this result greatly simplifies both experimental setups and numerical calculations. (2) Under its influence the soliton frequency shifts and the soliton is adiabatically compressed. The theoretical description of the soliton dynamic adopts multi-scale variational methods of nonlinear dynamics. One unexpected finding is that the standard approach, which has been used for decades in the framework of soliton perturbation theory, is not appropriate, as it fails to correctly predict the soliton compression observed in numerical simulation. The soliton perturbation theory was extended and adapted to the problem at hand. This modified perturbation theory provides a set of ODEs for pulse parameters, the results of which are carefully tested by comparison with the numerical simulations of the NLS equation.

The proposed adiabatic model equations lead to the following results, which could not be

obtained by previous approaches, and not at all by mere numerical simulation:

(1) The derived adiabatic model equations greatly simplify numerical calculations, because pulse propagation PDEs are replaced by much simpler ODEs. This allows quick and precise predictions of pulse behavior. The evolution of all soliton parameters is correctly predicted. In particular, the possible amplitude enhancement of solitons is successfully quantified. The proposed methods provide a basis for further investigation of experimentally relevant situations, e.g., when signal and control pulse are chirped.

(2) Furthermore, one can easily address an inverse problem: which control pulse provides a desired change of a signal. Cumbersome searches of the optimal signal/control pulse parameters are considerably simplified. General ranges for control parameters are quantitatively determined, which ensure an effective interaction.

(3) The derived theory allows a better understanding of the pulse manipulation at optical event horizons. For instance, one can directly trace how the pulse transmission coefficient changes with time till the signal becomes transparent for the control pulse and the interaction is switched off. Moreover, one can recognize different structures that appear in the course of pulse–pulse interaction, such as an interference pattern of the incoming/scattered control pulses and caustics, which are caused by scattering at a permanently changing signal pulse. The caustic structure was predicted using the analytical theory and only thereafter recognized as such in numerical solutions.

(4) The modified soliton perturbation theory is of interest for many applications beyond XPM interactions of optical pulses. The Raman effect is incorporated into the theory. The classical estimation of the Raman self-frequency shift is refined and expanded by a new relation for the amplitude loss arising with the Raman self-frequency shift. Furthermore, control pulses are identified which cancel soliton degradation due to Raman effect. In contrast to previously reported attempts with the interaction scheme under consideration, even parameters ranges are found which lead to a stable cancellation of the Raman effect.

(5) New qualitative insights into the underlying process emerged. The prominent role of the self-steepening effect could be isolated. Though the pulse interaction is mediated by XPM, the self-steepening effect does an essential enhancement leading to much stronger changes in soliton parameters. In many previous studies the self-steepening term was dismissed as not essential to the interaction scheme. The present findings urge to reinvestigate the role of self-steepening in different scenarios, e.g., in schemes of optical switching.

Hopefully, the results of the present thesis will become useful for experimental studies of pulse interactions at optical event horizons and their immediate applications, such as stable compensation of the soliton self-frequency shift and pulse compression. The proposed modification of the soliton perturbation theory is of interest for many nonlinear wave systems beyond fiber optics, as it is based on the widely applicable NLS equation.

Bibliography

[1] Govind P. Agrawal. *Nonlinear Fiber Optics*. Academic Press, 3rd edition, 2001.

[2] N. Akhmediev and A. Ankiewicz. *Solitons: Nonlinear Pulses and Beams*. Chapman and Hall, 1997.

[3] Sh. Amiranashvili, U. Bandelow, and A. Mielke. Padé approximant for refractive index and nonlocal envelope equations. *Optics Communications*, 283(3):480–485, 2010.

[4] D. Anderson. Variational approach to nonlinear pulse propagation in optical fibers. *Physical Review A*, 27(6):3135–3145, 1983.

[5] C. Mas Arabí, F. Bessin, A. Kudlinski, A. Mussot, D. Skryabin, and M. Conforti. Efficiency of four-wave mixing between orthogonally polarized linear waves and solitons in a birefringent fiber. *Physical Review A*, 94(6), 2016.

[6] Ihar Babushkin, Shalva Amiranashvili, Carsten Brée, Uwe Morgner, Gunter Steinmeyer, and Ayhan Demircan. The effect of chirp on pulse compression at a group velocity horizon. *IEEE Photonics Journal*, 8(3):1–13, 2016.

[7] A. A. Balakin, A. G. Litvak, V. A. Mironov, and S. A. Skobelev. Collapse of the wave field in a one-dimensional system of weakly coupled light guides. *Physical Review A*, 94:063806, 2016.

[8] T. Balciunas, C. Fourcade-Dutin, G. Fan, T. Witting, A. A. Voronin, A. M. Zheltikov, F. Gerome, G. G. Paulus, A. Baltuska, and F. Benabid. A strong-field driver in the single-cycle regime based on self-compression in a kagome fibre. *Nature Comm.*, 6(6117):6117, 2015.

[9] F. Belgiorno, S. L. Cacciatori, M. Clerici, V. Gorini, G. Ortenzi, L. Rizzi, E. Rubino, V. G. Sala, and D. Faccio. Hawking radiation from ultrashort laser pulse filaments. *Physical Review Letters*, 105(20):203901, 2010.

[10] F. Biancalana, D. V. Skryabin, and A. V. Yulin. Theory of the soliton self-frequency shift compensation by the resonant radiation in photonic crystal fibers. *Physical Review E*, 70(1), 2004.

[11] K.J. Blow and D. Wood. Theoretical description of transient stimulated raman scattering in optical fibers. *IEEE Journal of Quantum Electronics*, 25(12):2665–2673, 1989.

[12] Thomas Brabec and Ferenc Krausz. Nonlinear optical pulse propagation in the single-cycle regime. *Physical Review Letters*, 78(17):3282–3285, 1997.

[13] Carsten Brée, Günter Steinmeyer, Ihar Babushkin, Uwe Morgner, and Ayhan Demircan. Controlling formation and suppression of fiber-optical rogue waves. *Optics Letters*, 41(15):3515, 2016.

[14] S. V. Chernikov, D. J. Richardson, D. N. Payne, and E. M. Dianov. Soliton pulse compression in dispersion-decreasing fiber. *Optics Letters*, 18(7):476–478, 1993.

[15] Amol Choudhary and Friedrich König. Efficient frequency shifting of dispersive waves at solitons. *Optics Express*, 20(5):5538–5546, 2012.

[16] Charles Ciret and Simon-Pierre Gorza. Scattering of a cross-polarized linear wave by a soliton at an optical event horizon in a birefringent nanophotonic waveguide. *Optics Letters*, 41(12):2887, 2016.

[17] Charles Ciret, François Leo, Bart Kuyken, Gunther Roelkens, and Simon-Pierre Gorza. Observation of an optical event horizon in a silicon-on-insulator photonic wire waveguide. *Optics Express*, 24(1):114, 2016.

[18] A. M. C. Dawes, L. Illing, S. M. Clark, and D. J. Gauthier. All-optical switching in rubidium vapor. *Science*, 308(5722):672–674, 2005.

[19] A. Demircan, Sh. Amiranashvili, C. Brée, C. Mahnke, F. Mitschke, and G. Steinmeyer. Rogue wave formation by accelerated solitons at an optical event horizon. *Applied Physics B*, 115(3):343–354, 2014.

[20] A. Demircan, Sh. Amiranashvili, C. Brée, F. Mitschke, and G. Steinmeyer. From optical rogue waves to optical transistors. *Nonlinear Phenomena in Complex Systems*, 16(1):24–32, 2013.

[21] A. Demircan, Sh. Amiranashvili, C. Brée, U. Morgner, and G. Steinmeyer. Supercontinuum generation by multiple scatterings at a group velocity horizon. *Optics Express*, 22(4):3866–3879, 2014.

[22] A. Demircan, Sh. Amiranashvili, C. Brée, and G. Steinmeyer. Compressible octave spanning supercontinuum generation by two-pulse collisions. *Physical Review Letters*, 110(23):233901, 2013.

[23] A. Demircan, Sh. Amiranashvili, and G. Steinmeyer. Controlling light by light with an optical event horizon. *Physical Review Letters*, 106:163901, 2011.

[24] Ayhan Demircan, Shalva Amiranashvili, Carsten Brée, Christoph Mahnke, Fedor Mitschke, and Günter Steinmeyer. Rogue events in the group velocity horizon. *Scientific Reports*, 2(850), 2012.

[25] Ayhan Demircan, Shalva Amiranashvili, Carsten Brée, Uwe Morgner, and Günter Steinmeyer. Adjustable pulse compression scheme for generation of few-cycle pulses in the midinfrared. *Optics Letters*, 39(9):2735–2738, 2014.

[26] Zhixiang Deng, Xiquan Fu, Jun Liu, Chujun Zhao, and Shuangchun Wen. Trapping and controlling the dispersive wave within a solitonic well. *Optics Express*, 24(10):10302, 2016.

[27] Zhixiang Deng, Xiaohui Shi, Chao Tan, and Xiquan Fu. Reversible conversion between optical frequencies of probe and idler waves in regime of optical event horizon. *Journal of the Optical Society of America B*, 33(5):857, 2016.

[28] R. Driben, A. V. Yulin, A. Efimov, and B. A. Malomed. Trapping of light in solitonic cavities and its role in the supercontinuum generation. *Optics Express*, 21(16):19091–19096, 2013.

[29] Rodislav Driben, Fedor Mitschke, and Nickolai Zhavoronkov. Cascaded interactions between raman induced solitons and dispersive waves in photonic crystal fibers at the advanced stage of supercontinuum generation. *Optics Express*, 18(25):25993, 2010.

[30] J. M. Dudley, G. Genty, and S. Coen. Supercontinuum generation in photonic crystal fiber. *Reviews of Modern Physics*, 78(4):1135–1184, 2006.

[31] John M Dudley and James Roy Taylor. *Supercontinuum Generation in Optical Fibers*. Cambridge University Press, 2010.

[32] A. Efimov, A. V. Yulin, D. V. Skryabin, J. C. Knight, N. Joly, F. G. Omenetto, A. J. Taylor, and P. Russell. Interaction of an optical soliton with a dispersive wave. *Physical Review Letters*, 95(21), 2005.

[33] Daniele Faccio, Tal Arane, Marco Lamperti, and Ulf Leonhardt. Optical black hole lasers. *Classical and Quantum Gravity*, 29(22):224009, 2012.

[34] Siegfried Flügge. *Rechenmethoden der Quantentheorie*. Springer, 6 edition, 1999.

[35] José L. Gaona-Reyes and David Bermudez. The theory of optical black hole lasers. *Annals of Physics*, 380(Supplement C):41 – 58, 2017.

[36] G. Genty, P. Kinsler, B. Kibler, and J. M. Dudley. Nonlinear envelope equation modeling of sub-cycle dynamics and harmonic generation in nonlinear waveguides. *Optics Express*, 15(9):5382, 2007.

[37] T.P. Goldsmith, S. Coen, J.D. Harvey, and F. Vanholsbeeck. Cancellation of raman soliton self-frequency shift by cross-phase modulation. In *CLEO/Europe. 2005 Conference on Lasers and Electro-Optics Europe, 2005.* IEEE, 2005.

[38] A. V. Gorbach and D. V. Skryabin. Bouncing of a dispersive pulse on an accelerating soliton and stepwise frequency conversion in optical fibers. *Optics Express*, 15(22):14560, 2007.

[39] A. V. Gorbach and D. V. Skryabin. Light trapping in gravity-like potentials and expansion of supercontinuum spectra in photonic-crystal fibres. *Nature Photonics*, 1(11):653–657, 2007.

[40] Andrey V. Gorbach and Dmitry V. Skryabin. Theory of radiation trapping by the accelerating solitons in optical fibers. *Physical Review A*, 76(5), 2007.

[41] J. P. Gordon. Theory of the soliton self-frequency shift. *Optics Letters*, 11(10):662–664, 1986.

[42] Akira Hasegawa. Amplification and reshaping of optical solitons in a glass fiber-iv: Use of the stimulated raman process. *Optics Letters*, 8(12):650–652, 1983.

[43] Akira Hasegawa and Masayuki Matsumoto. *Optical Solitons in Fibers*. Springer, 3rd, rev. and enl. ed. edition, 2003.

[44] Hermann A. Haus and William S. Wong. Solitons in optical communications. *Reviews of Modern Physics*, 68(2):423–444, 1996.

[45] J. Jackson. *Classical electrodynamics*. Wiley, 3 edition, 1999.

[46] V. I. Karpman. *Non-linear waves in dispersive media*. Pergamon, 1975.

[47] P. Kinsler and G. H. C. New. Few-cycle soliton propagation. *Physical Review A*, 69(1):013805, 2004.

[48] Y. S. Kivshar and B. A. Malomed. Dynamics of solitons in nearly integrable systems. *Reviews of Modern Physics*, 61(4):763–915, 1989.

[49] E.A. Kuznetsov, A.V. Mikhailov, and I.A. Shimokhin. Nonlinear interaction of solitons and radiation. *Physica D: Nonlinear Phenomena*, 87(1-4):201–215, 1995.

[50] L. D. Landau and E. M. Lifshitz. *Quantum Mechanics*. Pergamon, 2 edition, 1965.

[51] L. D. Landau and E. M. Lifshitz. *The Classical Theory of Fields*. Pergamon, 4 edition, 1975.

[52] Valery E. Lobanov and Anatoly P. Sukhorukov. Total reflection, frequency, and velocity tuning in optical pulse collision in nonlinear dispersive media. *Physical Review A*, 82(3):033809, 2010.

[53] Boris A. Malomed. Variational methods in nonlinear fiber optics and related fields. In E. Wolf, editor, *Progress in Optics*, volume 43 of *Progress in Optics*, pages 71–193. Elsevier, 2002.

[54] D. A. B. Miller. Are optical transistors the logical next step? *Nature Photonics*, 4(1):3–5, 2010.

[55] V. Mishra, S. P. Singh, R. Haldar, P. Mondal, and S. K. Varshney. Intermodal nonlinear effects mediated optical event horizon in short-length multimode fiber. *Physical Review A*, 96:013807, 2017.

[56] F. Mitschke. *Fiber Optics*. Springer, 2010.

[57] F. M. Mitschke and L. F. Mollenauer. Discovery of the soliton self-frequency shift. *Optics Letters*, 11(10):569–661, 1986.

[58] L. F. Mollenauer and K. Smith. Demonstration of soliton transmission over more than 4000 km in fiber with loss periodically compensated by raman gain. *Optics Letters*, 13:675–677, 1988.

[59] L. F. Mollenauer and R. H. Stolen. The soliton laser. *Optics Letters*, 9(1):13–15, 1984.

[60] L. F. Mollenauer, R. H. Stolen, and J. P. Gordon. Experimental observation of picosecond pulse narrowing and solitons in optical fibers. *Physical Review Letters*, 45(13):1095–1098, 1980.

[61] M. Edward Motamedi. Micro-opto-electro-mechanical devices and on-chip optical processing. *Optical Engineering*, 36(5):1282, 1997.

[62] N. Nishizawa and T. Goto. Pulse trapping by ultrashort soliton pulses in optical fibers across zero-dispersion wavelength. *Optics Letters*, 27(3):152–154, 2002.

[63] N. Nishizawa and T. Goto. Ultrafast all optical switching by use of pulse trapping across zero-dispersion wavelength. *Optics Express*, 11(4):359–365, 2003.

[64] Norihiko Nishizawa and Toshio Goto. Characteristics of pulse trapping by use of ultrashort soliton pulses in optical fibers across the zero-dispersion wavelength. *Optics Express*, 10(21):1151–1159, 2002.

[65] I. Oreshnikov, R. Driben, and A. V. Yulin. Interaction of high-order solitons with external dispersive waves. *Optics Letters*, 40(23):5554, 2015.

[66] I. Oreshnikov, R. Driben, and A. V. Yulin. Weak and strong interactions between dark solitons and dispersive waves. *Optics Letters*, 40(21):4871, 2015.

[67] Asher Peres. *Quantum Theory: Concepts and Methods*, volume 72 of *Fundamental Theories of Physics*. Kluwer, 2002.

[68] T. G. Philbin, C. Kuklewicz, S. Robertson, S. Hill, F. König, and U. Leonhardt. Fiber-optical analog of the event horizon. *Science*, 319(5868):1367–1370, 2008.

[69] W. H. Reeves, D. V. Skryabin, F. Biancalana, J. C. Knight, P. St. J. Russell, F. G. Omenetto, A. Efimov, and A. J. Taylor. Transformation and control of ultra-short pulses in dispersion-engineered photonic crystal fibres. *Nature*, 424(6948):511–515, 2003.

[70] S. Robertson and U. Leonhardt. Frequency shifting at fiber-optical event horizons: The effect of Raman deceleration. *Physical Review A*, 81(6):063835, 2010.

[71] M. Romagnoli, S. Trillo, and S. Wabnitz. Soliton switching in nonlinear couplers. *Opt. Quantum Electron.*, 24(11):S1237–S1267, 1992.

[72] N. N. Rosanov. Transformation of electromagnetic radiation at moving inhomogeneities of a medium. *JETP Letters*, 88(8):501–504, 2009.

[73] N. N. Rosanov, N. V. Vysotina, and A. N. Shatsev. Forward light reflection from a moving inhomogeneity. *JETP Letters*, 93(6):308–312, 2011.

[74] E. Rubino, J. McLenaghan, S. C. Kehr, F. Belgiorno, D. Townsend, S. Rohr, C. E. Kuklewicz, U. Leonhardt, F. König, and D. Faccio. Negative-frequency resonant radiation. *Physical Review Letters*, 108(25), 2012.

[75] Mohammed F. Saleh, Claudio Conti, and Fabio Biancalana. Anderson localisation and optical-event horizons in rogue-soliton generation. *Optics Express*, 25(5):5457–5465, 2017.

[76] D. V. Skryabin. Soliton self-frequency shift cancellation in photonic crystal fibers. *Science*, 301(5640):1705–1708, 2003.

[77] D. V. Skryabin and A. V. Yulin. Theory of generation of new frequencies by mixing of solitons and dispersive waves in optical fibers. *Physical Review E*, 72(1), 2005.

[78] Dmitry V. Skryabin and Andrey V. Gorbach. Colloquium: Looking at a soliton through the prism of optical supercontinuum. *Reviews of Modern Physics*, 82(2):1287–1299, 2010.

[79] Luca Tartara. Frequency shifting of femtosecond pulses by reflection at solitons. *IEEE Journal of Quantum Electronics*, 48(11):1439–1442, 2012.

[80] Luca Tartara. Soliton control by a weak dispersive pulse. *Journal of the Optical Society of America B*, 32(3):395–399, 2015.

[81] T. Voytova, I. Oreshnikov, A. V. Yulin, and R. Driben. Emulation of fabry-perot and bragg resonators with temporal optical solitons. *Optics Letters*, 41(11):2442, 2016.

[82] S. F. Wang, A. Mussot, M. Conforti, A. Bendahmane, X. L. Zeng, and A. Kudlinski. Optical event horizons from the collision of a soliton and its own dispersive wave. *Physical Review A*, 92(2), 2015.

[83] S. F. Wang, A. Mussot, M. Conforti, X. L. Zeng, and A. Kudlinski. Bouncing of a dispersive wave in a solitonic cage. *Optics Letters*, 40(14):3320, 2015.

[84] Weibin Wang, Hua Yang, Pinghua Tang, Chujun Zhao, and Jing Gao. Soliton trapping of dispersive waves in photonic crystal fiber with two zero dispersive wavelengths. *Optics Express*, 21(9):11215, 2013.

[85] Karen E. Webb, Miro Erkintalo, Yiqing Xu, Neil G. R. Broderick, John M. Dudley, Goëry Genty, and Stuart G. Murdoch. Nonlinear optics of fibre event horizons. *Nature Communications*, 5:4969 EP –, 2014.

[86] G. B. Whitham. *Linear and nonlinear waves*. John Wiley & Sons, 1974.

[87] Alan E. Willner, Salman Khaleghi, Mohammad Reza Chitgarha, and Omer Faruk Yilmaz. All-optical signal processing. *Journal of Lightwave Technology*, 32(4):660–680, 2014.

[88] Jianke Yang. *Nonlinear Waves in Integrable and Nonintegrable Systems*. Society for Industrial & Applied Mathematics (SIAM), 2010.

[89] A. V. Yulin, R. Driben, B. A. Malomed, and D. V. Skryabin. Soliton interaction mediated by cascaded four wave mixing with dispersive waves. *Optics Express*, 21(12):14481, 2013.

[90] A. V. Yulin, D. V. Skryabin, and P. St. J. Russell. Four-wave mixing of linear waves and solitons in fibers with higher-order dispersion. *Optics Letters*, 29(20):2411–2413, 2004.

[91] A. M. Zheltikov. Microstructure optical fibers for a new generation of fiber-optic sources and converters of light pulses. *Usp. Fiz. Nauk*, 177(7):737–762, 2007.

List of publications

[P1] Sabrina Pickartz, Uwe Bandelow, and Shalva Amiranashvili. Adiabatic theory of solitons fed by dispersive waves. *Physical Review A*, 94(3):033811/1–12, 2016.

[P2] Sabrina Pickartz, Uwe Bandelow, and Shalva Amiranashvili. Efficient all-optical control of solitons. *Optical and Quantum Electronics*, 48(11):503/1–7, 2016.

[P3] Sabrina Pickartz, Uwe Bandelow, and Shalva Amiranashvili. Asymptotically stable compensation of the soliton self-frequency shift. *Optics Letters*, 42(7):1416–1419, 2017.

[P4] Sabrina Pickartz, Carsten Brée, Uwe Bandelow, and Shalva Amiranashvili. Cancellation of Raman self-frequency shift for compression of optical pulses. In *2017 International Conference on Numerical Simulation of Optoelectronic Devices (NUSOD)*. IEEE, 2017.

A Numerical method

The pulse propagation equation (2.5)

$$\partial_z \psi(z,\tau) - iD(i\partial_\tau)\psi(z,\tau) = i\gamma_0 \left[1 + \frac{i}{\omega_0}\partial_\tau\right] \left[\psi(z,\tau) \int_{-\infty}^{\infty} R(\tau') \left|\psi(z,\tau-\tau')\right|^2 \, d\tau'\right]$$

is numerically solved using an algorithm proposed in [31, Ch.3] which relies on a discretization scheme in the frequency domain.

For numerical evaluation the field envelope ψ is normalized by initial soliton peak power using

$$P_0 = \frac{1}{\gamma_0 L_0}, \quad \gamma_0 = \frac{\omega_0 n_{2,0}}{c}, \quad L_0 = \frac{\sigma_0^2}{|\beta_0''|}, \quad n_{2,0}P_0 = \frac{c}{L_0\omega_0} = \frac{c|\beta_0^{(2)}|}{\sigma_0^2\omega_0}. \tag{A.1}$$

The normalized envelope is defined as

$$A(z,\tau) = \frac{\psi(z,\tau)}{\sqrt{P_0}} \tag{A.2}$$

and the normalized equation (2.5) reads

$$\partial_z A - iD\left(i\partial_\tau\right) A = \frac{i}{L_0}\left[1 + \frac{i}{\omega_0}\partial_\tau\right] \left[A(z,\tau) \int_{-\infty}^{\infty} R(\tau') \left|A(z,\tau-\tau')\right|^2 \, d\tau'\right] \tag{A.3}$$

By this normalization, it is avoided the give an exact value for $n_{2,0} = n_2(\omega_0)$. The lefthand side or (A.3) describes the linear effect of fiber dispersion. It can be evaluated directly in the frequency domain by multiplication of the spectral envelope $\hat{A}(z,\omega)$ with the dispersion function $D(\omega)$. A transformation of (A.3) to frequency domain by Fourier transform and a change of variable to

$$\hat{A}'(z,\omega) = \hat{A}(z,\omega)\exp\left(-iD(\omega)z\right) \tag{A.4}$$

yields

$$\partial_z \hat{A}'(z,\omega) = \frac{i}{L_0}\left[1 + \frac{\omega}{\omega_0}\right] \exp(-iD(\omega)z)\, \mathcal{F}\left(A(z,\tau) \int_{-\infty}^{\infty} R(\tau') \left|A(z,\tau-\tau')\right|^2 \, d\tau'\right). \tag{A.5}$$

So the field $A(z,\tau)$ is integrated in the frequency domain. Equation (A.5) can be solved by standard methods for ordinary differential equations. Here a simple Runge-Kutta $(4,5)$ scheme was used. The evaluation of the righthand side of (A.5) needs back- and forth transformation between temporal and spectral domain by means of Fourier transformation. The following definition of the Fourier transform is used:

$$\mathcal{F}(f(t))(\omega) = \hat{f}(\omega) = \int_{-\infty}^{\infty} f(t) e^{i\omega t}\, dt \tag{A.6}$$

$$\mathcal{F}^{-1}(\hat{f}(\omega))(t) = f(t) = \frac{1}{2\pi}\int_{-\infty}^{\infty} \hat{f}(\omega) e^{-i\omega t}\, d\omega \tag{A.7}$$

The Raman integral term on the righthand side of (A.5)

$$\int_{-\infty}^{\infty} R(\tau')|A(z,\tau-\tau')|^2 d\tau' = (1-f_R)|A(z,\tau)|^2 + f_R \int_{-\infty}^{\infty} h(\tau')|A(z,\tau-\tau')|^2 d\tau'$$

is calculated using the convolution theorem, [31],

$$\int_{-\infty}^{\infty} h(\tau') \left|A(z,\tau-\tau')\right|^2 d\tau' = \left[h * |A|^2\right](\tau) = \mathcal{F}^{-1}\left(\mathcal{F}\left(h(\tau)\right) \cdot \mathcal{F}\left(|A(z,\tau)|^2\right)\right).$$

The refractive index used in the dispersion function is calculated according to [3].

The co-propagation of a soliton and a second pulse, a DW, in considered. The given data are initial carrier frequency ω_0 and initial duration σ_0 for the soliton, initial carrier frequency ω_{DW}, initial duration σ_1, initial time delay τ_1, and relative peak power $\mu = P_1/P_0$ for the DW. (A.3) is evaluated for the initial condition

$$A(0,\tau) = \frac{1}{\cosh\frac{\tau}{\sigma_0}} + \sqrt{\mu}\,\frac{e^{-i[\omega_{\text{DW}}-\omega_0]\tau}}{\cosh\frac{\tau-\tau_1}{\sigma_1}}. \tag{A.8}$$

If the co-propagation of a soliton with a continuous DW is considered, the initial condition is given by

$$A(0,\tau) = \frac{1}{\cosh\frac{\tau}{\sigma_0}} + \sqrt{\mu}\,e^{-i[\omega_{\text{DW}}-\omega_0]\tau}. \tag{A.9}$$

B Soliton perturbation theory with floating soliton carrier frequency

In this section the influence of higher order perturbation terms on a soliton is discussed, based on the perturbation theory for the modified evolution equation (3.28). The short-comings of perturbation theory for the standard NLS in predicting changes in soliton peak power, are overcome by the new theory. Also predictions of the standard theory are reproduced in cases where perturbations do not affect soliton frequency.

The coefficients of the soliton equation (3.28) are z-dependent through the included shift in soliton frequency $\nu(z)$. Using the following short notations

$$d_1(z) = \beta'(\omega_0 + \nu(z)) - \beta'(\omega_0), \tag{B.1}$$

$$d_2(z) = \beta''(\omega_0 + \nu(z)), \tag{B.2}$$

$$d_m(z) = \beta^{(m)}(\omega_0 + \nu(z)), \tag{B.3}$$

$$a^2(z) = \gamma_{\mathrm{S}}(z) = \frac{n_{2,0}}{c}\left[\omega_0 + \nu(z)\right], \tag{B.4}$$

$$s(z) = \eta_{\mathrm{S}}(z) = \frac{1}{\omega_0 + \nu(z)}, \tag{B.5}$$

the new perturbation equation reads

$$i\partial_z\psi + id_1\partial_\tau\psi - \frac{d_2}{2}\partial_\tau^2\psi + a^2\left|\psi\right|^2\psi + \tau\frac{d\nu}{dz}\,\psi = iF\left(\psi, \psi_{\mathrm{DW}}\right) \tag{B.6}$$

with a perturbation function

$$\begin{aligned} F\left(\psi, \psi_{\mathrm{DW}}\right) = i\sum_{m=3}^{M}\frac{d_m}{m!}\left[i\partial_\tau\right]^m\psi \\ - a^2 s\partial_\tau\left[\left|\psi\right|^2\psi\right] + i2a^2\left[1 + is\,\partial_\tau\right]\left[\left|\psi_{\mathrm{DW}}\right|^2\psi\right] \\ + if_R a^2\left[1 + is\partial_\tau\right]\left[\psi(z,\tau)\int_{-\infty}^{\infty}H(\tau')\left|\psi(z,\tau-\tau')\right|^2 d\tau'\right] \end{aligned} \tag{B.7}$$

including (in order of appearance) effects of higher order dispersion (d_m), self-steepening, cross-phase modulation by a DW ψ_{DW}, and Raman scattering described by the delay integral involving the response function $H(\tau) = h(\tau) - \delta(\tau)$.

The standard NLS equation is produced by the Lagrangian density (3.12). In (B.6) there are two additional terms (proportional to d_1 and $d\nu/dz$) which need representation. The

unperturbed floating NLS equation (B.6) is reproduced from the Lagrangian density:[1]

$$\begin{aligned}\mathcal{L} = \frac{i}{2}\left[\psi^*\psi_z - \psi\psi_z^*\right] + \frac{i}{2}d_1\left[\psi^*\psi_\tau - \psi\psi_\tau^*\right] \\ - \frac{d_2}{2}\left|\psi_\tau\right|^2 + \frac{a^2}{2}\left|\psi\right|^4 + \tau\nu_z\left|\psi\right|^2\end{aligned} \tag{B.8}$$

Alternatively and just as well, both additional terms could be included into the calculations as perturbation terms. Yet, as they have to be included in addition to any other perturbation under consideration, here it was preferred not having to explicitly mention them at all those times.

B.1 Soliton perturbation theory of nonlinear Schrödinger equation with $z-$dependent coefficients

The following ansatz function for the soliton is considered:

$$\psi_0(z,\tau) = \frac{1}{\sigma}\frac{\sqrt{d_2}}{a}\frac{\exp i\left(-w\left[\tau-\xi\right]+\theta\right)}{\cosh\frac{\tau-\xi}{\sigma}} \tag{B.9}$$

with initial delay $\xi = \xi(z)$, duration $\sigma = \sigma(z)$, phase $\theta = \theta(z)$, and an additional frequency shift/velocity $w = w(z)$ which must be kept for technical reasons and will be set to zero later on. Indeed, the equation is designed to already properly account for the solution frequency shift, remember the definition of the solutions envelope

$$\psi_{\mathrm{s}}(z,\tau) = \left[\psi_0(z,\tau)\right]_{w\equiv 0}\exp\left(i\int_0^z D(\nu(z'))dz' - i\nu\tau\right).$$

So finally it can be assumed that there is no additional shift from $\nu(z)$, i.e. $w(z)\equiv 0$.

The Lagrangian $L = \int d\tau\,\mathcal{L}(\psi_0,\psi_0^*)$ for the given soliton ansatz and Lagrangian density (B.8) is

$$L = \frac{2d_2}{a^2}\left[\frac{d_2}{6\sigma^3} - \frac{\theta_z}{\sigma} + \frac{\xi\nu_z}{\sigma} - \frac{w\xi_z}{\sigma} - \frac{d_2w^2}{2\sigma} + \frac{d_1w}{\sigma}\right]. \tag{B.10}$$

The Euler-Lagrange equations

$$\frac{\partial L}{\partial r_j} - \frac{d}{dz}\frac{\partial L}{\partial \dot{r}_j} = -2\int d\tau\ \mathrm{Im}\left(F\frac{\partial\psi_0^*}{\partial r_j}\right)$$

for the soliton parameters $r_j = \sigma, w, \xi, \theta$ given a perturbation F are calculated. Specifically they result in the following equation for soliton duration σ:

$$\frac{\partial L}{\partial \theta} - \frac{d}{dz}\frac{\partial L}{\partial \theta_z} = -2\int d\tau\ \mathrm{Im}\left(F\frac{\partial\psi_0^*}{\partial\theta}\right) \qquad \Rightarrow \qquad \frac{d}{dz}\left[\frac{d_2}{a^2\sigma}\right] = \int d\tau\ \mathrm{Re}\left(F\psi_0^*\right)$$

[1] Derivatives by τ or z are frequently indicated as indices, e.g., $d\nu/dz = \nu_z$.

for the soliton delay ξ:

$$\frac{\partial L}{\partial w} - \frac{d}{dz}\frac{\partial L}{\partial w_z} = -2\int d\tau\ \mathrm{Im}\left(F\,\frac{\partial \psi_0^*}{\partial w}\right)$$
$$\Rightarrow \qquad [\xi_z - d_1]\,\frac{d_2}{a^2\sigma} + \frac{d_2^2 w}{a^2\sigma} = \int d\tau\ (\tau-\xi)\,\mathrm{Re}\,(F\psi_0^*)$$

for the soliton frequency shift ν:

$$\frac{\partial L}{\partial \xi} - \frac{d}{dz}\frac{\partial L}{\partial \xi_z} = -2\int d\tau\ \mathrm{Im}\left(F\,\frac{\partial \psi_0^*}{\partial \xi}\right)$$
$$\Rightarrow \qquad \frac{d_2\nu_z}{a^2\sigma} + \frac{d}{dz}\frac{d_2 w}{a^2\sigma} = w\int d\tau\ \mathrm{Re}\,(F\psi_0^*) - \frac{1}{\sigma}\int d\tau\ \tanh\left(\frac{\tau-\xi}{\sigma}\right)\mathrm{Im}\,(F\psi_0^*)$$

and for the soliton phase θ:

$$\frac{\partial L}{\partial \sigma} - \frac{d}{dz}\frac{\partial L}{\partial \sigma_z} = -2\int d\tau\ \mathrm{Im}\left(F\,\frac{\partial \psi_0^*}{\partial \sigma}\right)$$
$$\Rightarrow \qquad \left[\theta_z - \xi\nu_z - \frac{d_2}{2\sigma^2}\right]\frac{d_2}{a^2\sigma^2} - \frac{d_2 d_1 w}{a^2\sigma^2} + \frac{d_2^2 w^2}{2a^2\sigma^2} + \frac{d_2 w\xi_z}{a^2\sigma^2}$$
$$= \frac{1}{\sigma}\int d\tau\ \mathrm{Im}\,(F\psi_0^*) - \frac{1}{\sigma^2}\int d\tau\ [\tau-\xi]\tanh\left(\frac{\tau-\xi}{\sigma}\right)\mathrm{Im}\,(F\psi_0^*)$$

The resulting ODEs ($w(z)\equiv 0$) describe the evolution of the soliton parameters under the influence of a perturbation F:

$$\left[\frac{d_2}{\sigma a^2}\right]_z = \int_{-\infty}^{\infty} d\tau\ \mathrm{Re}\,(F\psi_0^*) \tag{B.11a}$$
$$\nu_z = -\frac{a^2}{d_2}\int_{-\infty}^{\infty} d\tau\ \tanh\left(\frac{\tau-\xi}{\sigma}\right)\mathrm{Im}\,(F\psi_0^*) \tag{B.11b}$$
$$\xi_z = d_1 + \frac{a^2\sigma^2}{d_2}\int_{-\infty}^{\infty} d\tau\ \frac{\tau-\xi}{\sigma}\,\mathrm{Re}\,(F\psi_0^*) \tag{B.11c}$$
$$\theta_z = \frac{d_2}{2}\frac{1}{\sigma^2} + \frac{a^2\sigma}{d_2}\int_{-\infty}^{\infty} d\tau\ \left[1 - \frac{\tau-\xi}{\sigma}\cdot\tanh\left(\frac{\tau-\xi}{\sigma}\right)\right]\mathrm{Im}\,(F\psi_0^*) \tag{B.11d}$$

Unperturbed soliton In the trivial case, the soliton propagates unperturbed ($F\equiv 0$). The ODEs (B.11) yield the following relations for the evolution of the unperturbed soliton parameters:

$$\frac{d_2}{\sigma a^2} = \mathrm{const}, \quad \xi_z = d_1, \quad v = \mathrm{const}, \quad \theta_z = \frac{d_2}{2}\frac{1}{\sigma^2}.$$

With initial condition $v(0)=0$, $\xi(0)=0$, $\sigma(0)=1$, they read

$$v = \xi = 0 = \mathrm{const}, \quad \sigma = 1 = \mathrm{const}, \quad \theta = \frac{\beta_0''}{2}z + \theta_0.$$

This coincides with the predictions from the standard NLS equation, with constant coefficients, cf. (3.16).

In the following section possible perturbation terms are individually discussed.

B.2 Higher order effects on a soliton

B.2.1 Higher order dispersion

The perturbation function

$$F(\psi) = i \sum_{m=3}^{M} \frac{d_m(z)}{m!} [i\partial_\tau]^m \psi \tag{B.13}$$

described the influence of higher order dispersion up order M. The set of ODEs (B.11) for this specific perturbation function reduces to

$$\left[\frac{d}{\sigma a^2}\right]_z = 0 \tag{B.14a}$$

$$\nu_z = 0 \tag{B.14b}$$

$$\xi_z = d_1 + \frac{1}{6}\frac{d_3}{\sigma^2} + \frac{7}{360}\frac{d_5}{\sigma^4} + \dots \tag{B.14c}$$

$$\theta_z = \frac{d_2}{2\sigma^2} + \frac{7}{72}\frac{d_4}{\sigma^4} + \frac{31}{2160}\frac{d_6}{\sigma^6} + \dots \tag{B.14d}$$

The used frequency dependent coefficients $d_m(z) = D^{(m)}(\nu)$, $m \geq 2$, produce the exact values describing GVD and higher order dispersion at each point ν of evaluation. Thus the higher order coefficients become less important. By testing against results of numerical simulations, it was found that including terms up to fourth order ($M = 4$) is sufficient for the present purposes. The soliton delay is then influenced by third order dispersion. Fourth order dispersion only appears in the soliton phase, which is of less interest here.

B.2.2 Self-steepening effect

The perturbation by self-steepening is described by

$$F(\psi) = -a^2 s\, \partial_\tau \left[|\psi|^2 \psi\right] \tag{B.15}$$

In this case (B.11) results in $\sigma = \nu = \theta = \text{const}$ and

$$\xi_z = d_1 + s\frac{d_2}{\sigma^2}. \tag{B.16}$$

The self-steepening results in a constant shift in soliton delay $\xi(z) = \frac{\beta_0''}{\sigma_0^2} z$. The shift increases linear in z and is more pronounced for shorter solitons.

B.2.3 Cross–phase modulation

Perturbation function for cross-phase modulation reads

$$F(\psi, \psi_{\text{DW}}) = ia^2 \left[1 + is\partial_\tau\right] V(z,\tau)\psi(z,\tau), \qquad V(z,\tau) = 2\left|\psi_{\text{DW}}\right|^2. \tag{B.17}$$

Then

$$\mathrm{Re}\,(F\psi_0^*) = s\frac{d_2}{\sigma^3}\left(V\frac{\tanh\frac{\tau-\xi}{\sigma}}{\cosh^2\frac{\tau-\xi}{\sigma}} - \sigma V_\tau \frac{1}{\cosh^2\frac{\tau-\xi}{\sigma}}\right),$$
$$\mathrm{Im}\,(F\psi_0^*) = \frac{d_2}{\sigma^2}\frac{V}{\cosh^2\frac{\tau-\xi}{\sigma}}.$$

The evolution equations for soliton parameters are

$$\left[\frac{d_2}{\sigma a^2}\right]_z = s\frac{d_2}{\sigma^3}\int d\tau\, V(z,\tau)\frac{\tanh\frac{\tau-\xi}{\sigma}}{\cosh^2\frac{\tau-\xi}{\sigma}} - s\frac{d_2}{\sigma^2}\int d\tau\, V_\tau(z,\tau)\frac{1}{\cosh^2\frac{\tau-\xi}{\sigma}}, \tag{B.18a}$$
$$\nu_z = -\frac{a^2}{\sigma^2}\int d\tau\, V(z,\tau)\frac{\tanh\frac{\tau-\xi}{\sigma}}{\cosh^2\frac{\tau-\xi}{\sigma}}, \tag{B.18b}$$
$$\xi_z = d_1 + s\frac{a^2}{\sigma}\int d\tau\left(V(z,\tau)\frac{\frac{\tau-\xi}{\sigma}\cdot\tanh\frac{\tau-\xi}{\sigma}}{\cosh^2\frac{\tau-\xi}{\sigma}} - \sigma V_\tau(z,\tau)\frac{\frac{\tau-\xi}{\sigma}}{\cosh^2\frac{\tau-\xi}{\sigma}}\right), \tag{B.18c}$$
$$\theta_z = \frac{d_2}{2}\frac{1}{\sigma^2} + \frac{a^2}{\sigma}\int d\tau\, V(z,\tau)\frac{1-\frac{\tau-\xi}{\sigma}\cdot\tanh\frac{\tau-\xi}{\sigma}}{\cosh^2\frac{\tau-\xi}{\sigma}}. \tag{B.18d}$$

The terms involving derivatives of the potential V_τ are transformed using appropriate partial integrations:

$$\left[\frac{d_2}{\sigma a^2}\right]_z = -s\frac{d_2}{\sigma^3}\int d\tau\, V(z,\tau)\frac{\tanh\frac{\tau-\xi}{\sigma}}{\cosh^2\frac{\tau-\xi}{\sigma}} \tag{B.19a}$$
$$\nu_z = -\frac{a^2}{\sigma^2}\int d\tau\, V(z,\tau)\frac{\tanh\frac{\tau-\xi}{\sigma}}{\cosh^2\frac{\tau-\xi}{\sigma}} \tag{B.19b}$$
$$\xi_z = d_1 + \frac{a^2}{\sigma}s\int d\tau\, V(z,\tau)\frac{1-\frac{\tau-\xi}{\sigma}\cdot\tanh\frac{\tau-\xi}{\sigma}}{\cosh^2\frac{\tau-\xi}{\sigma}} \tag{B.19c}$$
$$\theta_z = \frac{d_2}{2}\frac{1}{\sigma^2} + \frac{a^2}{\sigma}\int d\tau\, V(z,\tau)\frac{1-\frac{\tau-\xi}{\sigma}\cdot\tanh\frac{\tau-\xi}{\sigma}}{\cosh^2\frac{\tau-\xi}{\sigma}} \tag{B.19d}$$

The first and second equation can be combined to

$$\left[\frac{d_2}{\sigma a^2}\right]_z = \frac{d_2}{a^2\sigma}s\nu_z, \qquad s = \frac{1}{\omega_0+v}.$$

Integration results in an explicit expression for the soliton duration:

$$\frac{\sigma(z)}{\sigma(0)} = \frac{d_2(z)}{d_2(0)}\frac{a^2(0)}{a^2(z)}\frac{s(z)}{s(0)} = \frac{d_2(z)}{d_2(0)}\left[\frac{\omega_0}{\omega_0+\nu(z)}\right]^2$$
$$= \frac{\beta''(\omega_0+\nu(z))}{\beta''(\omega_0)}\frac{1}{\left[1+\frac{\nu}{\omega_0}\right]^2}$$

To be a self-contained description of soliton evolution, the remaining ODEs need an explicit expression for the potential V, which is given through the second pulse, $V(z,\tau) = 2\,|\psi_{\mathrm{DW}}|^2$. The evolution of the second pulse ψ_{DW} is governed by the second NLS equation.

Scaling the integral according to DW solution The potential V depends on the second wave $V(z,\tau) = 2\left|\psi_{\mathrm{DW}}\right|^2$, where ψ_{DW} is a solution to a scattering problem as derived in Appendix C. According to this solution the potential can be written as

$$V(z,\tau) = \tilde{V}\left(z, \frac{1}{2}\left[1 - \tanh\frac{\tau-\xi}{\sigma}\right]\right)$$

depending on soliton delay ξ and duration σ. The two different integrals appearing in (B.19) can be simplified by two successive parameter transformations which make use of the special dependence. Firstly, let $x = \frac{\tau-\xi}{\sigma}$, $\frac{d\tau}{dx} = \sigma$. Secondly, let $y = \frac{1-\tanh x}{2}$, $\frac{dy}{dx} = -\frac{1}{2}\frac{1}{\cosh^2 x}$. For $x \in (-\infty, \infty)$ the integration interval changes to $y \in (1, 0)$:

$$\int d\tau\, V(z,\tau) \frac{\tanh\frac{\tau-\xi}{\sigma}}{\cosh^2\frac{\tau-\xi}{\sigma}} = -2\sigma \int_0^1 dy\ [2y-1]\,\tilde{V}(z,y)$$

$$\int d\tau\, V(z,\tau) \frac{1 - \frac{\tau-\xi}{\sigma}\cdot\tanh\frac{\tau-\xi}{\sigma}}{\cosh^2\frac{\tau-\xi}{\sigma}} = 2\sigma \int_0^1 dy\ [1 - [2y-1]\operatorname{arctanh}(2y-1)]\,\tilde{V}(z,y)$$

With this the set of ODEs (B.19) describing soliton parameter evolution reads

$$\left[\frac{d_2}{\sigma a^2}\right]_z = 2s\frac{d_2}{\sigma^2}\int_0^1 dy\ [2y-1]\,\tilde{V}(z,y), \tag{B.20a}$$

$$\nu_z = 2\frac{a^2}{\sigma}\int_0^1 dy\ [2y-1]\,\tilde{V}(z,y), \tag{B.20b}$$

$$\xi_z = d_1 + 2sa^2\int_0^1 dy\ [1 - (2y-1)\operatorname{arctanh}(2y-1)]\,\tilde{V}(z,y), \tag{B.20c}$$

$$\theta_z = \frac{d_2}{2}\frac{1}{\sigma^2} + 2a^2\int_0^1 dy\ [1 - (2y-1)\operatorname{arctanh}(2y-1)]\,\tilde{V}(z,y). \tag{B.20d}$$

B.2.4 Raman effect

The influence of the Raman effect is described by the perturbation function

$$F(\psi) = if_R a^2\left[1 + is\partial_\tau\right]\psi(z,\tau)\left[\int_{-\infty}^{\infty} h(\tau)\left|\psi(z,\tau-\tau')\right|^2 d\tau' - \left|\psi(z,\tau)\right|^2\right] \tag{B.21}$$

It is convenient to introduce $H(\tau) = h(\tau) - \delta(\tau)$. Before considering this general description of the Raman effect, first an approximate description is discussed.

Approximate Raman term For pulses, wide enough to contain many optical cycles, and with a slowly evolving envelope to Raman effect can be described by the approximate perturbation function, [1],

$$F = -a^2 s\partial_\tau\left|\psi\right|^2\psi - ia^2 T_R\psi\partial_\tau\left(\left|\psi\right|^2\right) + a^2 sT_R\partial_\tau\psi\partial_\tau\left(\left|\psi\right|^2\right) \tag{B.22}$$

The first term ($\sim s$) describes self-steepening, the second ($\sim T_R$) describes Raman effect, and the the third term ($\sim sT_R$) is a correction to second term which is normally neglected

due to its smallness. Equations (B.11) result in the following evolution equations for soliton parameters:

$$\left[\frac{d_2}{\sigma a^2}\right]_z = -sT_R\frac{8}{15}\frac{d_2^2}{a^2\sigma^5} \tag{B.23a}$$

$$\nu_z = -T_R\frac{8}{15}\frac{d_2}{\sigma^4} \tag{B.23b}$$

$$\xi_z = d_1 + s\frac{d_2}{\sigma^2} \tag{B.23c}$$

$$\theta_z = \frac{d_2}{2\sigma^2} \tag{B.23d}$$

If the shock term is neglected ($s = 0$) the evolution equations reduce again to the results from standard NLS equations, despite the dependence of dispersion operator on the frequency shift:

$$\left[\frac{d_2}{\sigma a^2}\right]_z = 0 \quad \Rightarrow \quad \frac{\sigma(z)}{\sigma(0)} = \frac{d_2(z)}{d_2(0)} \tag{B.24a}$$

$$\nu_z = -T_R\frac{8}{15}\frac{d_2}{\sigma^4} \tag{B.24b}$$

$$\xi_z = d_1 \tag{B.24c}$$

$$\theta_z = \frac{d_2}{2}\frac{1}{\sigma^2} \tag{B.24d}$$

Raman integral term Using the full Raman integral expression the perturbation terms can be written in the form

$$F(\psi) = ia^2\left(1 + is\partial_\tau\right)V(z,\tau)\psi(z,\tau), \tag{B.25}$$

in resemblance with (B.17), yet, here with function

$$V(z,\tau) = f_R\int_{-\infty}^{\tau} H(\tau-\tau')\left|\psi_0(z,\tau')\right|^2 d\tau' = f_R\frac{d_2}{\sigma^2 a^2}\int \frac{H(\tau-\tau')}{\cosh^2\frac{\tau'-\xi}{\sigma}}\,d\tau' \tag{B.26}$$

The evolution equations (B.18) are used and terms involving V are replaced in favor of an expression involving a derivative V_τ by appropriate partial integration:

$$\left[\frac{d_2}{\sigma a^2}\right]_z = -s\frac{d_2}{2\sigma^2}\int d\tau\,\frac{V_\tau(z,\tau)}{\cosh^2\frac{\tau-\xi}{\sigma}} \tag{B.27}$$

$$\nu_z = -\frac{a^2}{2\sigma}\int d\tau\,\frac{V_\tau(z,\tau)}{\cosh^2\frac{\tau-\xi}{\sigma}} \tag{B.28}$$

$$\xi_z = d_1 + s\frac{a^2}{2\sigma}\int d\tau\left(\frac{V(z,\tau)}{\cosh^2\frac{\tau-\xi}{\sigma}} - \frac{[\tau-\xi]V_\tau(z,\tau)}{\cosh^2\frac{\tau-\xi}{\sigma}}\right) \tag{B.29}$$

$$\theta_z = \frac{d_2}{2}\frac{1}{\sigma^2} + \frac{a^2}{2\sigma}\int d\tau\left(\frac{V(z,\tau)}{\cosh^2\frac{\tau-\xi}{\sigma}} - \frac{[\tau-\xi]\,V_\tau(z,\tau)}{\cosh^2\frac{\tau-\xi}{\sigma}}\right) \tag{B.30}$$

The function V depends on $\tau - \xi$, using the transformation $(\tau' - \xi) \to \tau'$, [2],

$$V(z,\tau) = f_R \frac{d_2}{\sigma^2 a^2} \int \frac{H(\tau - \xi - \tau')}{\cosh^2 \frac{\tau'}{\sigma}} \, d\tau'$$

Plug this into the evolution equations for soliton parameters and use parameter transformation $(\tau - \xi) \to \tau$:

$$\begin{aligned}
\left[\frac{d_2}{\sigma a^2}\right]_z &= -f_R \frac{s d_2^2}{2\sigma^4 a^2} \iint d\tau \, d\tau' \, \frac{H_\tau(\tau - \tau')}{\cosh^2 \frac{\tau}{\sigma} \cosh^2 \frac{\tau'}{\sigma}} \\
\nu_z &= -f_R \frac{d_2}{2\sigma^3} \iint d\tau \, d\tau' \, \frac{H_\tau(\tau - \tau')}{\cosh^2 \frac{\tau}{\sigma} \cosh^2 \frac{\tau'}{\sigma}} \\
\xi_z &= d_1 + f_R \frac{sd}{2\sigma^3} \iint d\tau \, d\tau' \, \frac{H(\tau - \tau') - \tau H_\tau(\tau - \tau')}{\cosh^2 \frac{\tau}{\sigma} \cosh^2 \frac{\tau'}{\sigma}} \\
\theta_z &= \frac{d_2}{2} \frac{1}{\sigma^2} + f_R \frac{d_2}{2\sigma^3} \iint d\tau \, d\tau' \, \frac{H(\tau - \tau') - \tau \, H_\tau(\tau - \tau')}{\cosh^2 \frac{\tau}{\sigma} \, \cosh^2 \frac{\tau'}{\sigma}}
\end{aligned}$$

Remark. All integrals are symmetrized with respect to τ and τ', e.g.:

$$\iint d\tau \, d\tau' \, \frac{\tau \, h_\tau(\tau - \tau')}{\cosh^2 \frac{\tau}{\sigma} \, \cosh^2 \frac{\tau'}{\sigma}} = \frac{1}{2} \iint d\tau \, d\tau' \, \frac{(\tau - \tau') \, h_\tau(\tau - \tau')}{\cosh^2 \frac{\tau}{\sigma} \, \cosh^2 \frac{\tau'}{\sigma}}$$

To see that, $h(\tau) = h_e(\tau) + h_o(\tau)$ is split into even and odd parts:

$$I_e := \iint d\tau \, d\tau' \, \frac{\tau h_e(\tau - \tau')}{\cosh^2 \frac{\tau}{\sigma} \cosh^2 \frac{\tau'}{\sigma}} = 0 = \iint d\tau \, d\tau' \, \frac{(\tau - \tau') h_e(\tau - \tau')}{\cosh^2 \frac{\tau}{\sigma} \cosh^2 \frac{\tau'}{\sigma}}$$

and for the odd part τ and τ' are exchanged in the first transformation step ($\tau \to \tau'$ and $\tau' \to \tau$):

$$I_o := \iint d\tau \, d\tau' \, \frac{\tau h_o(\tau - \tau')}{\cosh^2 \frac{\tau}{\sigma} \cosh^2 \frac{\tau'}{\sigma}} = \iint d\tau \, d\tau' \, \frac{\tau' h_o(\tau' - \tau)}{\cosh^2 \frac{\tau}{\sigma} \cosh^2 \frac{\tau'}{\sigma}} = \iint d\tau \, d\tau' \, \frac{-\tau' h_o(\tau - \tau')}{\cosh^2 \frac{\tau}{\sigma} \cosh^2 \frac{\tau'}{\sigma}}$$

so

$$2I_o := \iint d\tau \, d\tau' \, \frac{(\tau - \tau') \, h_o(\tau' - \tau)}{\cosh^2 \frac{\tau}{\sigma} \cosh^2 \frac{\tau'}{\sigma}}$$

and $I = I_e + I_o = \frac{1}{2} \iint d\tau \, d\tau' \, \frac{(\tau - \tau') h(\tau' - \tau)}{\cosh^2 \frac{\tau}{\sigma} \cosh^2 \frac{\tau'}{\sigma}}$.

The appearing double integrals can be simplified as follows:

$$\iint d\tau \, d\tau' \, \frac{H(\tau - \tau')}{\cosh^2 \frac{\tau}{\sigma} \cosh^2 \frac{\tau'}{\sigma}} = \frac{\sigma^4 \pi}{2} \int d\omega \, \frac{\omega^2 \hat{H}(\omega)}{\sinh^2(\frac{\pi}{2}\sigma\omega)} \tag{B.31a}$$

$$\iint d\tau \, d\tau' \, \frac{H_\tau(\tau - \tau')}{\cosh^2 \frac{\tau}{\sigma} \cosh^2 \frac{\tau'}{\sigma}} = \frac{i\sigma^4 \pi}{2} \int d\omega \, \frac{\omega^3 \hat{H}(\omega)}{\sinh^2 \frac{\pi}{2}\sigma\omega} \tag{B.31b}$$

$$\iint d\tau \, d\tau' \frac{(\tau - \tau') H_\tau(\tau - \tau')}{\cosh^2 \frac{\tau}{\sigma} \cosh^2 \frac{\tau'}{\sigma}} = -\frac{\sigma^4 \pi}{2} \int d\omega \, \frac{\omega^2 \left(\omega \hat{H}(\omega)\right)_\omega}{\sinh^2 \frac{\pi}{2}\sigma\omega} \tag{B.31c}$$

$$\iint d\tau \, d\tau' \frac{H(\tau - \tau') - \frac{1}{2}(\tau - \tau') H_\tau(\tau - \tau')}{\cosh^2 \frac{\tau}{\sigma} \cosh^2 \frac{\tau'}{\sigma}} = \frac{3\sigma^4 \pi}{4} \int d\omega \, \omega^2 \frac{\hat{H}(\omega) + \frac{1}{3}\omega \hat{H}_\omega(\omega)}{\sinh^2 \frac{\pi}{2}\sigma\omega} \tag{B.31d}$$

[2] Remember the right-arrow meens set $\tau'' := \tau' - \xi$ and $d\tau'' = d\tau'$, then replace τ'' again by τ' to keep a simple notation.

Proof of (B.31). First use the relation

$$\frac{1}{\cosh^2\frac{\tau}{\sigma}} = \frac{\sigma^2}{2}\int d\omega\,\frac{\omega e^{i\omega\tau}}{\sinh\frac{\pi}{2}\sigma\omega}$$

then introduce $\xi = \tau - \tau'$, $d\tau = d\xi$, and apply rules for Fourier transform ($\int H(\tau)e^{-i\omega\tau}d\tau = \hat{H}(\omega)$ or $\int \partial_\tau H(\tau)e^{-i\omega\tau}d\tau = i\omega\hat{H}(\omega)$) and definition of delta function ($2\pi\delta(\omega) = \int e^{i\omega\tau}d\tau$). Exemplary for (B.31a) this goes as follows:

$$\begin{aligned}
\iint d\tau\,d\tau'\,\frac{H(\tau-\tau')}{\cosh^2\frac{\tau}{\sigma}\cosh^2\frac{\tau'}{\sigma}} &= \frac{\sigma^4}{4}\iint d\tau\,d\tau'\iint d\omega\,d\omega'\,\frac{\omega\omega' H(\tau-\tau')e^{i\omega\tau}e^{i\omega'\tau'}}{\sinh(\frac{\pi}{2}\sigma\omega)\sinh(\frac{\pi}{2}\sigma\omega')}\\
&= \frac{\sigma^4}{4}\int d\tau'\iint d\omega\,d\omega'\,\frac{\omega\omega'\left(\int d\xi\,H(\xi)e^{i\omega\xi}\right)e^{i\omega\tau'}e^{i\omega'\tau'}}{\sinh(\frac{\pi}{2}\sigma\omega)\sinh(\frac{\pi}{2}\sigma\omega')}\\
&= \frac{\sigma^4}{4}\int d\tau'\iint d\omega\,d\omega'\,\frac{\omega\omega'\hat{H}(-\omega)e^{i(\omega+\omega')\tau'}}{\sinh(\frac{\pi}{2}\sigma\omega)\sinh(\frac{\pi}{2}\sigma\omega')}\\
&= 2\pi\frac{\sigma^4}{4}\int d\omega'\,\frac{(\omega')^2\hat{H}(\omega')}{\sinh^2(\frac{\pi}{2}\sigma\omega')} = \pi\frac{\sigma^4}{2}\int d\omega\,\frac{\omega^2\hat{H}(\omega)}{\sinh^2(\frac{\pi}{2}\sigma\omega)}
\end{aligned}$$

For (B.31c) the following was used

$$\mathcal{F}\left(\xi\cdot H_\xi(\xi)\right) = \mathcal{F}(\xi) * \mathcal{F}\left(H_\xi(\xi)\right) = \left(i\delta'(\omega)\right) * \left(i\omega\hat{H}(\omega)\right) = -\partial_\omega\left(\omega\hat{H}(\omega)\right)$$

□

Then the evolution equations read

$$\left[\frac{d_2}{\sigma a^2}\right]_z = -f_R\frac{\pi s d_2^2}{4a^2}i\int_{-\infty}^{\infty}d\omega\,\frac{\omega^3\hat{H}(\omega)}{\sinh^2\frac{\pi}{2}\sigma\omega} \tag{B.32a}$$

$$\nu_z = -f_R\frac{\pi d_2\sigma}{4}i\int_{-\infty}^{\infty}d\omega\,\frac{\omega^3\hat{H}(\omega)}{\sinh^2\frac{\pi}{2}\sigma\omega} \tag{B.32b}$$

$$\xi_z = d_1 + f_R\frac{3\pi s d_2\sigma}{8}\int_{-\infty}^{\infty}d\omega\,\omega^2\frac{\hat{H}(\omega)+\frac{1}{3}\omega\hat{H}_\omega(\omega)}{\sinh^2\frac{\pi}{2}\sigma\omega} \tag{B.32c}$$

$$\theta_z = \frac{d_2}{2}\frac{1}{\sigma^2} + f_R\frac{3\pi d_2\sigma}{8}\int_{-\infty}^{\infty}d\omega\,\omega^2\frac{\hat{H}(\omega)+\frac{1}{3}\omega\hat{H}_\omega(\omega)}{\sinh^2\frac{\pi}{2}\sigma\omega} \tag{B.32d}$$

Recall that $\hat{H}(\omega) = \hat{h}(\omega) - \hat{h}(0)$ and $\hat{H}_\omega(\omega) = \hat{h}_\omega(\omega)$. The appearing integrals

$$\mathcal{R}_1 = i\int_{-\infty}^{\infty}d\omega\,\frac{\omega^3\hat{H}(\omega)}{\sinh^2\frac{\pi}{2}\sigma\omega},\quad \mathcal{R}_2 = \int_{-\infty}^{\infty}d\omega\,\omega^2\frac{\hat{H}(\omega)+\frac{1}{3}\omega\hat{H}_\omega(\omega)}{\sinh^2\frac{\pi}{2}\sigma\omega} \tag{B.33}$$

take real values. They are tabulated for possible values of soliton duration σ, or soliton frequency ν if soliton duration can be expressed as $\sigma = \sigma(\nu)$.

C Scattering problem at a moving barrier

The "optical" scattering problem (3.46) resembles the one-dimensional quantum mechanical problem of a plane wave scattered at a potential barrier.

The scattering theory of quantum mechanics applies to a stationary potential barrier. A suitable parameter transformation (similar to a Galilei transformation) maps the scattering problem with a moving barrier to a problem with a static problem. The transformation is shown in Section C.1. Then a known solution of the quantum mechanical scattering problem for a static barrier with a hyperbolic secant shape typical for fundamental solitons can be used. The QM solution is shortly reviewed in Section C.2 and the translation into an optical formulation is given.

C.1 Scattering at a moving potential barrier

The one-particle Schrödinger equation for a wave function $\Psi(t,x)$ in one spatial dimension reads

$$i\frac{d\Psi}{dt} = -\frac{1}{2m}\frac{d^2\Psi}{dx^2} + V(x - x_0(t))\psi \tag{C.1}$$

where $\hbar$ is set to 1 for brevity of notation. The particle mass m is kept, it will be later associated with the GVD coefficient in the optical notation. The position of the potential V is moving with velocity $x_0'(t)$.

The forward and backward waves

$$\Psi = e^{\pm ikx - i\omega_k t} \quad \text{with} \quad \omega_k = \frac{k^2}{2m} \tag{C.2}$$

are a suitable solution for (C.1) far away from the barrier.

The desired solution is parametrized by the wave number k, and it has the asymptotic properties

$$\Psi_k(t,x) = \begin{cases} e^{ikx - i\omega_k t} + b(k)e^{-iKx - i\omega_K t} & \text{for} \quad x \to -\infty \\ a(k)e^{ikx - i\omega_k t} & \text{for} \quad x \to \infty \end{cases} \tag{C.3}$$

where $a(k)$ and $b(k)$ quantify transmission and reflection, respectively. The new wave vector of the reflected wave is

$$K = k - 2mx_0'(t). \tag{C.4}$$

It describes the change in momentum due to reflection by a moving barrier.

The scattering problem for a moving barrier can be solved by a suitable parameter transformation, relating it to the scattering at a static barrier. Equation (C.1) is solved by the

wave function

$$\Psi_{k+mx_0'(t)}(t,x) = \Phi(t,\xi)\cdot e^{i\omega_{mx_0'(t)}t - imx_0'(t)x}, \qquad \xi = x - x_0(t), \tag{C.5}$$

if $\Phi(t,\xi)$ is a solution to

$$i\frac{d\Phi}{dt} - \frac{1}{2m}\frac{d^2}{d\xi^2}\Phi + V(\xi)\Phi = 0, \tag{C.6}$$

with the asymptotic behavior

$$\Phi(t,\xi) = \begin{cases} e^{i[k\xi-\omega_k t]} + B(k)e^{i[-k\xi-\omega_k t]} & \text{for} \quad \xi \to -\infty \\ A(k)e^{i[k\xi-\omega_k t]} & \text{for} \quad \xi \to \infty \end{cases} \tag{C.7}$$

where

$$A(k) = a(k + mx_0'(t)), \qquad B(k) = b(k + mx_0'(t)). \tag{C.8}$$

The ansatz

$$\Phi(t,\xi) = \varphi(\xi)e^{-i\omega_k t} \tag{C.9}$$

yields the differential equation

$$\left[-\frac{1}{2m}\frac{d^2}{d\xi^2} + V(\xi)\right]\varphi(\xi) = \omega_k\varphi(\xi) \tag{C.10}$$

with the reduced asymptotic property

$$\varphi(\xi) = \begin{cases} e^{ik\xi} + B(k)e^{-ik\xi} & \text{for} \quad \xi \to -\infty \\ A(k)e^{ik\xi} & \text{for} \quad \xi \to \infty \end{cases} \tag{C.11}$$

This is the standard formulation of the scattering problem in quantum mechanics. Its solution for a soliton-like barrier V is reproduced in the next section.

C.2 Plane wave scattering at a static sech^2 -barrier

The classical (linear) Schrödinger equation (LSE) [50, 34] for the problem at hand

$$\frac{d^2}{dx^2}\varphi(x) + \left[k^2 - 2mV(x)\right]\varphi(x) = 0 \tag{C.12}$$

describes the scattering of a wave φ at a potential barrier V. Here a fundamental soliton constitutes the barrier, so V has a hyperbolic secant shape

$$V(x) = \frac{V_0}{\cosh^2(x/\ell)}\,. \tag{C.13}$$

The barrier height V_0 and width ℓ are both positive constants. An analytical solution for this problem is given in textbooks [50, 34], and is briefly recaptured here.

Firstly, the change of variable

$$\xi := \tanh\left(x/\ell\right) \tag{C.14}$$

transforms (C.12) to

$$\frac{d}{d\xi}\left[[1-\xi^2]\frac{d}{d\xi}\varphi(\xi)\right] + \left[\frac{[\ell k]^2}{1-\xi^2} - 2m\ell^2 V_0\right]\varphi(\xi) = 0. \tag{C.15}$$

Secondly, the following ansatz function[1] is defined for φ

$$\varphi(\xi) := 2^{i\varepsilon}\left[1-\xi^2\right]^{-i\frac{\varepsilon}{2}} f(\xi) \tag{C.16}$$

for which

$$\frac{d}{d\xi}\left[[1-\xi^2]\frac{d\varphi}{d\xi}\right] = 2^{i\varepsilon}\left[1-\xi^2\right]^{-i\frac{\varepsilon}{2}} \times \tag{C.17}$$

$$\left\{\left[1-\xi^2\right]f''(\xi) - 2\left[1-i\varepsilon\right]\xi f'(\xi) + \left[-\varepsilon^2\frac{\xi^2}{1-\xi^2} + i\varepsilon\right]f(\xi)\right\}. \tag{C.18}$$

With this (C.15) reads

$$\left[1-\xi^2\right]f''(\xi) - 2\left[1-i\varepsilon\right]\xi f'(\xi) + \left[\varepsilon^2 + i\varepsilon - 2m\ell^2 V_0\right]f(\xi) = 0, \quad \text{if} \quad \varepsilon^2 = [\ell k]^2. \tag{C.19}$$

Thirdly, the variable change

$$y := \frac{1}{2}\left[1-\xi\right] \tag{C.20}$$

results in

$$y[1-y]f''(y) + \{1 - i\varepsilon - 2[1-i\varepsilon]y\}\, f'(y) - \left[2m\ell^2 V_0 - \varepsilon^2 - i\varepsilon\right]f(y) = 0 \tag{C.21}$$

This is the scattering problem "in hypergeometric form" as it resembles the "standard" equation for hypergeometric functions

$$y[1-y]\, f''(y) + \{\mathfrak{c} - [\mathfrak{a}+\mathfrak{b}+1]y\}\; f'(y) - \mathfrak{a}\mathfrak{b}\, f(y) = 0$$

if

$$\mathfrak{c} = 1 - i\varepsilon\,, \quad \mathfrak{a}+\mathfrak{b}+1 = 2[1-i\varepsilon]\,, \quad \mathfrak{a}\cdot\mathfrak{b} = 2m\ell^2 V_0 - \varepsilon^2 - i\varepsilon\,.$$

Equation (C.21) is solved by the hypergeometric function

$$f(y) = {}_2F_1\left(\mathfrak{a},\mathfrak{b};\mathfrak{c};y\right) \tag{C.22}$$

with parameters

$$\mathfrak{a} = 1 - i\varepsilon + i\mathfrak{z}\,, \quad \mathfrak{b} = 1 - i\varepsilon - i\mathfrak{z}\,, \quad \mathfrak{c} = 1 - i\varepsilon \quad \text{and} \quad \mathfrak{z} = \frac{1}{2}\sqrt{8m\ell^2 V_0 - 1}\,. \tag{C.23}$$

Lastly, going back to the the original variable x yields a general solution to the scattering problem (C.12)

$$\varphi(x) = A\cdot 2^{i\varepsilon}\cosh^{i\varepsilon}\left(\tfrac{x}{\ell}\right){}_2F_1\left(\mathfrak{a},\mathfrak{b};\mathfrak{c};\tfrac{1}{2}\left[1-\tanh\tfrac{x}{\ell}\right]\right). \tag{C.24}$$

with parameters as in (C.23). The factor A is still free. It is defined by stating (asymptotic) boundary conditions the solution should satisfy, as is discussed in the next Section.

[1] Actually one makes the ansatz $\varphi(\xi) = \left(1-\xi^2\right)^{\nu} f(\xi)$ and later finds $2\nu = -i\varepsilon$ to be a convenient choice. Also the scaling factor $2^{i\varepsilon}$ is there for convenience.

C.2.1 Asymptotic behavior in the up-switching case

In the up-switching case it is $k > 0$. The solution (C.24) should obey boundary conditions

$$\varphi(x) = \begin{cases} e^{ikx} + Be^{-ikx} & \text{for} \quad x \to -\infty \\ Ae^{ikx} & \text{for} \quad x \to \infty \end{cases} \tag{C.25}$$

The factor $2^{i\varepsilon}\cosh^{i\varepsilon}\left(\frac{x}{\ell}\right) = [e^{-x/\ell} + e^{-x/\ell}]^{i\varepsilon}$ behaves in the limiting cases like

$$2^{i\varepsilon}\cosh^{i\varepsilon}\left(\tfrac{x}{\ell}\right) \simeq \begin{cases} e^{i\varepsilon\frac{x}{\ell}} = e^{ikx} & \text{for } x \to \infty \\ e^{-i\varepsilon\frac{x}{\ell}} = e^{-ikx} & \text{for } x \to -\infty \end{cases}$$

if we choose $\varepsilon = \ell k$. Also $y = \frac{1}{2}[1 - \tanh\frac{x}{\ell}] = \frac{1}{e^{2x/\ell}+1} \to 0$ if $x \to \infty$ and therefore ${}_2F_1\left(\mathscr{a}, \mathscr{b}; \mathscr{c}; y\right) \to 1$ in (C.24).

So for $x \to \infty$ the solution (C.24) behaves according to the boundary solution:

$$\varphi(x) = A \cdot e^{ikx} \qquad \text{for} \quad x \to \infty \tag{C.26}$$

if $\varepsilon = \ell k$.

To evaluate the solution (C.24) for $x \to -\infty$ the following relation for the hypergeometric function is used:

$$\begin{aligned} {}_2F_1\left(\mathscr{a}, \mathscr{b}; \mathscr{c}; y\right) = {} & \frac{\Gamma(\mathscr{c})\Gamma(\mathscr{c} - \mathscr{a} - \mathscr{b})}{\Gamma(\mathscr{c} - \mathscr{a})\Gamma(\mathscr{c} - \mathscr{b})}\, {}_2F_1\left(\mathscr{a}, \mathscr{b}; \mathscr{a} + \mathscr{b} + 1 - \mathscr{c}; 1 - y\right) \\ & + \frac{\Gamma(\mathscr{c})\Gamma(\mathscr{a} + \mathscr{b} - \mathscr{c})}{\Gamma(\mathscr{a})\Gamma(\mathscr{b})}(1 - y)^{\mathscr{c} - \mathscr{a} - \mathscr{b}} \\ & \times {}_2F_1\left(\mathscr{c} - \mathscr{a}, \mathscr{c} - \mathscr{b}; \mathscr{c} + 1 - \mathscr{a} - \mathscr{b}; 1 - y\right) \end{aligned} \tag{C.27}$$

where Γ is the Gamma function. Then (C.24) takes the form

$$\begin{aligned} \varphi(x) = A \cdot 2^{i\varepsilon}\cosh^{i\varepsilon}\left(\tfrac{x}{\ell}\right) \Big[& C_1 \cdot {}_2F_1\left(\mathscr{a}, \mathscr{b}; \mathscr{a} + \mathscr{b} + 1 - \mathscr{c}; \tfrac{e^{2x/\ell}}{e^{2x/\ell}+1}\right) \\ & + C_2 \cdot \left(\tfrac{e^{2x/\ell}}{e^{2x/\ell}+1}\right)^{i\varepsilon} {}_2F_1\left(\mathscr{a}, \mathscr{b}; \mathscr{a} + \mathscr{b} + 1 - \mathscr{c}; \tfrac{e^{2x/\ell}}{e^{2x/\ell}+1}\right)\Big] \end{aligned} \tag{C.28}$$

with

$$C_1 = \frac{\Gamma(1 - i\varepsilon)\Gamma(i\varepsilon)}{\Gamma\left(\frac{1}{2} + i\mathscr{s}\right)\Gamma\left(\frac{1}{2} - i\mathscr{s}\right)}, \qquad C_2 = \frac{\Gamma(1 - i\varepsilon)\Gamma(-i\varepsilon)}{\Gamma\left(\frac{1}{2} - i\varepsilon - i\mathscr{s}\right)\Gamma\left(\frac{1}{2} - i\varepsilon + i\mathscr{s}\right)}. \tag{C.29}$$

As $x \to -\infty$, $(1 - y) = 1 - \frac{1}{e^{2x/\ell}+1} = \frac{e^{2x/\ell}}{e^{2x/\ell}+1} \to 0$, and the hypergeometric functions in (C.28) both tend to 1. Asymptotically

$$(1 - y)^{i\varepsilon} \simeq e^{2i\varepsilon x/\ell} = e^{2ikx} \quad \text{as } x \to -\infty$$

using again $\varepsilon = \ell k$.

So for $x \to -\infty$ solution (C.28) is

$$\varphi(x) = A \cdot \left[C_1 e^{-ikx} + C_2 e^{ikx}\right] \tag{C.30}$$

By comparing to the boundary conditions (C.39) we get equations for the coefficients:

$$\{A \cdot C_2 = 1 \text{ and } A \cdot C_1 = B\} \quad \Rightarrow \quad \left\{A = \frac{1}{C_2} \text{ and } B = \frac{C_1}{C_2}\right\}.$$

resulting in

$$A = \frac{\Gamma\left(\frac{1}{2} - i\varepsilon - i\mathfrak{s}\right)\Gamma\left(\frac{1}{2} - i\varepsilon + i\mathfrak{s}\right)}{\Gamma\left(1 - i\varepsilon\right)\Gamma\left(-i\varepsilon\right)}, \qquad B = \frac{\Gamma\left(1 - i\varepsilon\right)\Gamma\left(i\varepsilon\right)}{\Gamma\left(\frac{1}{2} + i\mathfrak{s}\right)\Gamma\left(\frac{1}{2} - i\mathfrak{s}\right)} \cdot A\,. \tag{C.31}$$

Going back to the original solution $\Psi_k(t,x)$:

$$|\Psi_k(t,x)|^2 = T(\bar{k})\,|_2F_1\left(\mathfrak{a},\mathfrak{b};\mathfrak{c};y\right)|^2 \tag{C.32}$$

where

$$y = \frac{1}{2}\left[1 - \tanh\frac{x - x_0(t)}{\ell}\right], \qquad \bar{k} = k - mx_0'(t). \tag{C.33}$$

C.2.2 Asymptotic behavior in the down-switching case

In the down-switching case $k(\equiv -\Delta\Omega_b) < 0$. The solution (C.24) should have the following asymptotic property:

$$\varphi(x) = \begin{cases} Ae^{ikx} & \text{for} \quad x \to -\infty \\ e^{ikx} + Be^{-ikx} & \text{for} \quad x \to \infty \end{cases} \tag{C.34}$$

The down-switching case can be traced back to the up-switching case, by a simple parameter transformation $\bar{x} := -x$:

$$\varphi(\bar{x}) = \begin{cases} Ae^{-ik\bar{x}} & \text{for} \quad \bar{x} \to \infty \\ e^{-ik\bar{x}} + Be^{ik\bar{x}} & \text{for} \quad \bar{x} \to -\infty \end{cases}$$

Going back to variable x the solution reads

$$\varphi(x) = A \cdot 2^{i\varepsilon}\cosh^{i\varepsilon}\left(\tfrac{x}{\ell}\right)\,{}_2F_1\left(\mathfrak{a},\mathfrak{b};\mathfrak{c};y\right) \tag{C.35}$$

with new variables

$$y = \tfrac{1}{2}\left[1 - \tanh\tfrac{-x}{\ell}\right] = \tfrac{1}{2}\left[1 + \tanh\tfrac{x}{\ell}\right] \tag{C.36}$$

and A as in (C.31), and $\mathfrak{a}$, $\mathfrak{b}$, $\mathfrak{c}$ as in (C.23).

The transformation (C.5) to a barrier moving with velocity $x_0'(t)$ applied to this solution results in

$$|\Psi_k(t,x)|^2 = T(\bar{k})\,|_2F_1\left(\mathfrak{a},\mathfrak{b};\mathfrak{c};y\right)|^2 \tag{C.37}$$

where

$$y = \frac{1}{2}\left[1 + \tanh\frac{x - x_0(t)}{\ell}\right], \qquad \bar{k} = k - mx_0'(t). \tag{C.38}$$

Table C.1: Replacement rules that transform the quantum mechanical scattering problem (C.1) to the optical scattering problem (3.33).

Ψ^*	t	x	k	ω_k	m^{-1}	ℓ	$a^*(k)$	$b^*(k)$
ψ_{DW}	z	τ	Δ	κ	$\beta''(\omega_1)$	σ	$\mathfrak{t}(\Delta)$	$\mathfrak{r}(\Delta)$

The full solution has the asymptotic properties

$$\Psi_k(t,x) = \begin{cases} e^{ikx-i\omega_k t} + B(k)e^{-iKx-i\omega_K t} & \text{for} \quad x \to -\infty \\ A(k)e^{ikx-i\omega_k t} & \text{for} \quad x \to -\infty \end{cases} \tag{C.39}$$

where $A(k)$ and $B(k)$ quantify transmission and reflection, respectively. The wave vector of the reflected wave is again $K = k - 2mx_0'(t)$.

C.2.3 Transmission and reflection coefficients

The transmission coefficient $T = |A|^2$ is calculated from (C.31) using formulas

$$\Gamma(iy)\,\Gamma(-iy) = |\Gamma(iy)|^2 = \frac{\pi}{y\sinh(\pi y)}\,, \qquad y \in \mathbb{R} \tag{C.40}$$

$$\Gamma\left(\tfrac{1}{2}+iy\right)\Gamma\left(\tfrac{1}{2}-iy\right) = \left|\Gamma\left(\tfrac{1}{2}+iy\right)\right|^2 = \frac{\pi}{\cosh(\pi y)}\,, \tag{C.41}$$

$$\Gamma(1+iy)\,\Gamma(1-iy) = |\Gamma(1+iy)|^2 = \frac{\pi y}{\sinh(\pi y)}\,. \tag{C.42}$$

resulting in

$$T = |A|^2 = \frac{\left|\Gamma\left(\frac{1}{2}-i[\varepsilon-\mathfrak{z}]\right)\right|^2 \left|\Gamma\left(\frac{1}{2}-i[\varepsilon+\mathfrak{z}]\right)\right|^2}{|\Gamma(1-i\varepsilon)|^2\,|\Gamma(-i\varepsilon)|^2} = \frac{\sinh^2(\pi\varepsilon)}{\cosh\pi\,[\varepsilon+\mathfrak{z}]\,\cosh\pi\,[\varepsilon-\mathfrak{z}]}\,, \tag{C.43}$$

The denominator can be further transformed by the relation

$$\cosh\pi\,[\varepsilon+\mathfrak{z}]\cdot\cosh\pi\,[\varepsilon-\mathfrak{z}] = \cosh^2\pi\mathfrak{z} + \sinh^2\pi\varepsilon.$$

In cases where $8m\ell^2V_0 < 1$, set $\mathfrak{z} = \frac{1}{2}\sqrt{8m\ell^2V_0-1} = i\bar{\mathfrak{z}} \in i\mathbb{R}$, and use $\cosh i\pi\bar{\mathfrak{z}} = \cos\pi\bar{\mathfrak{z}}$. Thus

$$T = \frac{\sinh^2\pi\varepsilon}{\sinh^2\pi\varepsilon + \cosh^2\frac{\pi}{2}\sqrt{8m\ell^2V_0-1}} \qquad \text{if} \quad 8m\ell^2V_0 > 1 \tag{C.44a}$$

and

$$T = \frac{\sinh^2\pi\varepsilon}{\sinh^2\pi\varepsilon + \cos^2\frac{\pi}{2}\sqrt{1-8m\ell^2V_0}} \qquad \text{if} \quad 8m\ell^2V_0 < 1 \tag{C.44b}$$

and reflection coefficient $R = |B|^2 = 1 - T$.

Abbreviations

DW dispersive wave

FWHM full width at half maximum

GNLS generalized nonlinear Schrödinger

GVD group velocity dispersion

NLS nonlinear Schrödinger

ODE ordinary differential equation

PDE partial differential equation

SPT soliton perturbation theory

SSFS soliton self-frequency shift

XPM cross-phase modulation

ZDF zero dispersion frequency

Acknowledgements

I would like to thank Uwe Bandelow for the opportunity to work at an interesting topic as a part of his research group at Weierstrass-Institute for Applied Analysis and Stochastics. I am very grateful to S. Amiranashvili and U. Bandelow for their continuous and kind help during my PhD time. I thank C. Brée, T. Koprucki, M. Wolfrum, H.-J. Wünsche for discussions and support. My warm thanks go to all members of the "Laser Dynamics" research group at WIAS for a very friendly working environment.

Selbständigkeitserklärung

Ich erkläre, dass ich die Dissertation selbständig und nur unter Verwendung der von mir gemäß §7 Abs. 3 der Promotionsordnung der Mathematisch-Naturwissenschaftlichen Fakultät, veröffentlicht im Amtlichen Mitteilungsblatt der Humboldt-Universität zu Berlin Nr. 126/2014 am 18.11.2014 angegebenen Hilfsmittel angefertigt habe.

Berlin, den 23.01.2018

Sabrina Pickartz